Active surfaces for controllable activation of DNA-based molecular programming framework in microfluidics

Ievgen Kurylo

THESE DE DOCTORAT

presentée à
L´école doctorale Sciences pour l´ingénieur
Spécialité Micro et nano technologies, acoustique et télécommunications

intitulée

Surfaces actives pour l'activation contrôlable de la programmation moléculaire basée sur l'ADN en microfluidique

Par
Ievgen Kurylo

Soutenue publiquement le 27 juin 2018 devant le jury d´examen :

Director	L. Buchaillot	IEMN, Lille
Co-Encadrant	Y. Coffinier	IEMN, Lille
Co-Encadrant	A. Vlandas	IEMN, Lille
Examinateur	R. Boukherroub	IRI, Lille
Examinateur	J.- C. Galas	Université Pierre Et Marie Curie
Rapportrice	A. Galtayries	Chimie Paris
Rapportrice	V. Taly	Universite Paris Descartes
President	S. Ingebrandt	Rwth Aachen

Acknowledgments

I would like to thank my PhD supervisors Alexis Vlandas, Yannick Coffinier and Lionel Buchaillot. I would also like to thank the Region Haut de France and CNRS for the financial support.

Introduction

This work was done during three years at the Institute of electronics, microelectronics and nanotechnology (Villeneuve d'Ascq, France) in the BioMEMS research group. It was focused on novel research activity for the laboratory – molecular programming - and its interfacing with micro actuators fabricated in microfluidic chambers. While the molecular programming part was not previously present in the laboratory, the thesis relied heavily on the expertise of IEMN and BioMEMS in microfluidics and microfabrication.

The molecular programming research was inspired from living organisms in nature, which possess marvellous capabilities for information processing. For example, the living cell, as an elementary unit of the organism, makes during its lifetime complex computations such as finding food, adapting to changing conditions (metabolism), reproducing itself etc. All these activities can be considered as processing information. Recent studies show that this computation work is performed by connected chemical reactions, or chemical reaction networks (CRNs). It has to be noted, that since this biochemical reactions take place in cell spatially, diffusion processes are crucial for biocomputation.

From our point of view, it would be interesting to build artificial information-processing systems, which are based on such nature computing principles. This can be useful for several purposes:

Firstly, mimicking nature in this way will substantially increase our knowledge about the mechanisms behind information processing of living organisms (so-called «learning-by-doing» approach) and will be beneficial for the fundamental biology.

Next, by applying this knowledge one can potentially build novel types of biosensors or handle the materials self-assembly in a more efficient way.

Finally, such research can open a new ways for the non-conventional computing.

First successful attempts of elaboration of these synthetic information processing systems relying on inorganic-, organic- and bio- chemistry were already done in recent years in a relatively high amount. From our point of view, the most reliable approaches were based on deoxyribonucleic acid (DNA). Indeed, this biopolymer possesses the most predictable and programmable interactions among any known molecule. Due to this unique property (and taking into account commercial availability of synthetic DNA with any designed sequence), one can easily build complex DNA-based reaction networks which, as it will be discussed further, is essential for the artificial information-processing systems.

Despite the obvious progress in elaboration of such technologies, there is a lack of tools for interacting with them which substantially restricts their practical implementation. We believe that by overcoming this issue, one can boost the field of bioinspired computing. Filling this gap was the main motivation of doing the current research work.

One of the most recent examples of such DNA-based CRNs is the Polymerase/Exonuclease/Nickase (PEN) toolbox. We propose a novel method of interaction with this biochemical tool. It relies on application of DNA-based active surfaces. Upon application of electrochemical potential, it is possible to purposely change their properties in a way to give the needed instructions to the molecular system in solution, which is in contact with them. By varying the surface chemistry, one can manage to obtain such designed behaviour as triggering, inhibition or switching form the one state to another of the molecular system.

Our technological solution was purposely developed in microfluidics rather than in well-mixed tubes for two main reasons. Firstly, to minimise costs due to reduced solution volumes. Next, to facilitate observation of reaction-diffusion processes, which, as it will be discussed further, are crucial for information processing in living cell.

In chapter 1 we will discuss the necessary theoretical background, which is needed for a good understanding of the current research. In chapter 2, we will focus on the detailed description of the PEN toolbox functions on which this work relies. We will also discuss the other experimental techniques used in this study. In chapter 3, we will show how the PEN toolbox can be used in microfluidic channels, the materials issues that we had to solve to make it work and our first attempts of building an activator to give instructions to molecular circuit. In chapter 4, we will demonstrate the successful use of single shot activator and, finally, in chapter 5, we will show the preliminary concepts of using active surfaces as a promising tool for more reliable and reversible controllers of DNA-based CRNs.

Résumé

Les organismes vivants prennent des décisions en permanence à l'aide de réseau de réactions chimiques couplées (CRN) les unes aux autres. Cette capacité a inspirée de nombreux scientifiques qui cherchent aujourd'hui à construire des versions synthétiques de ces réseaux pour créer des systèmes dynamiques complexes.

Les molécules d'ADN constitue une solution idéale pour construire de tels CRNs du fait de la nature programmable et prévisibles de leurs interactions. Un des exemples les plus récents d'un système à base d'ADN est la PEN (Polymérase, Exonucléase et Nickase) toolbox. Le travail de recherche présenté dans ce manuscrit vise à développer des surface actives qui permettent d'interagir avec la PEN toolbox en environnement microfluidique afin de pouvoir utiliser pleinement le potentiel de tels systèmes moléculaires.

Dans un premier temps nous avons étudié l'utilisation de la PEN toolbox en microfluidique en explorant différents paramètres afin de faciliter l'adoption de cette approche de programmation moléculaire.

Nous discuterons ensuite de la réalisation de surfaces actives et de leur caractérisation. Celles-ci sont concues pour permettre l'immobilisation de brins d'ADN via une liaison thiol et leur largage en solution en rompant électro-chimiquement cette liaison. Nous discuterons également d'aspect technique permettant l'intégration aisée d'une telle stratégie dans des dispositifs microfluidiques. Nous démontrerons l'efficacité de cette approche dans un cas simple d'activation puis d'autocatalyse programmé à l'aide de la PEN toolbox.

Par la suite, montrerons qu'il est possible de contrôler spatio-temporellement le largage d'instructions à base d'ADN. Pour ce faire, nous nous appuierons sur une version plus évoluée de l'auto-catalyseur présenté précédemment. Nous mettrons en évidence qu'il est possible d'initier de façon contrôlée des phénomènes de réaction-diffusion dans des canaux microfluidiques.

Pour finir, nous ouvrirons des perspectives pour la conception de surface actives permettant un niveau de contrôle encore plus grand des systèmes moléculaire via la réalisation de motifs statiques de greffage d'ADN ou l'utilisation d'actionneurs électriques réutilisables.

PhD thesis

Active surfaces for controllable activation of DNA-based molecular programming framework in microfluidics

Abstract

Living organisms perform complex information processing tasks with a help of intertwined chemical reaction networks (CRNs) and diffusion processes. These biological phenomena inspired scientists to design from the bottom-up dynamical systems with complex spatiotemporal behaviour.

DNA provides a perfect solution for building these synthetic CRNs due to its highly predictable and programmable interactions. One of the most recent examples of such DNA-based systems is Polymerase/Exonuclease/Nickase (PEN) toolbox. Our research work focused on designing active surfaces with the aim to provide a convenient way to interact in microfluidics with the PEN toolbox (as an example of DNA-based CRNs) and explore the full potential of these novel biochemistry tools.

First of all, we will study the step by step assembly and optimisation of the PEN toolbox parameters, which can be useful for the research groups aiming to use this technology in their laboratories for the first time.

Next, we will discuss the elaboration and characterisation of active surfaces, which provide loading and controllable release of DNA input, based on formation and electrochemical cleavage of gold-thiol bound. We will also provide a technological solution to integrate these surfaces and the PEN toolbox in microfluidics. We will show controllable triggering of basic activation and autocatalysis PEN toolbox modules.

We will further apply our method for spatiotemporal control of autocatalytic CRNs, which have higher stability then simple autocatalytic module while still providing an exponential signal amplification contrary to the activation module. This approach allows us to investigate and optimise the parameters of our technology.

Finally, we will discuss the elaboration of active surfaces with irreversibly bound DNA, which provides a higher level of the PEN toolbox spatiotemporal behaviour, based on electrical polarisation and tuning the shape of surface-attached DNA patterns.

Introduction

This work was done during three years at the Institute of electronics, microelectronics and nanotechnology (Villeneuve d'Ascq, France) at the BioMEMS research group. It was focused on such a novel research activity for the laboratory such as molecular programming.

The idea of the project was inspired from the living nature, which poses marvellous capabilities for information processing. For example, the living cell, as an elementary unit of the organism, during its living time makes complex computation work such as finding food, adapting to changing conditions (metabolism), reproducing itself etc.

From our point of view, it would be interesting to build artificially information-processing systems, which are based on nature computing principles. This can be useful from the following points of view. Firstly, mimicking nature in this way will substantially increase our knowledge about the mechanisms, behind information processing of living organisms (so-called «learning-by-doing» approach) and will be beneficial for the fundamental biology. Next, by applying this knowledge one can potentially build novel types of biosensors or handle the materials self-assembly in a more efficient way. Finally, such research can open a new ways for the non-conventional computing.

First successful attempts of elaboration of these synthetic information processing systems applying inorganic-, organic- and biochemistry were already done in recent years in a relatively high amount. From our point of view, the most reliable approaches were realised, based on deoxyribonucleic acid (DNA). Indeed, this biopolymer poses the most predictable and programmable interactions among any known molecule. Due to this unique property (and taking into account commercial availability of synthetic DNA with any designed sequence), one can easily build complex DNA-based reaction networks which, as it will be discussed further, is essential for the artificial information-processing systems.

Despite the obvious progress in elaboration of such technologies, there is a lack of interaction tools for them, which substantially limit their practical implementation. We belief, that by overcoming this issue, one can boost the field of bioinspired computing. Briefly, this was the main motivation of doing the current research work.

One of the most recent examples of such DNA-based systems is Polymerase/Exonuclease/Nickase (PEN) toolbox. We propose the novel method of interaction with this biochemical tool. It is based on application of DNA-based active surfaces. Upon application of electrochemical potential, it is possible to purposely change their properties in a

way to give the needed instructions to the molecular system in solution, which is in contact with them. By varying the surface chemistry, one can manage to obtain such designed behaviour as triggering, inhibition or switching form the one state to another of the molecular system.

Our technological solution was purposely developed in microfluidics rather than in well-mixed tubes for two main reasons. Firstly, to minimise costs due to reduced solution volumes. Next, to facilitate observation of reaction-diffusion processes, which, as it will be discussed further, are crucial for information processing in living cell.

In chapter 1 we will discuss the necessary theoretical background, which is needed for understanding of the current research. In chapter 2, we will focus on the detailed description of the PEN toolbox function on which this work relies but also the other experimental techniques used in this study. In chapter 3, we will show how the PEN toolbox can be used in microfluidic channels, the materials issues that we had to solve to make it work and our first attempt of building an activator to give instructions to molecular circuit. In chapter 4, we will demonstrate the successful use of single shot activator and, finally, in chapter 5, we will show the preliminary concepts of using active surfaces as a promising tool for more reliable and reversible controllers of DNA-based CRNs.

Contents

Chapter 1

Overview

1.1 Mimicking of information processing in living organisms

Various dynamic processes of living cell such as division, movement, proliferation, motility, reaction on environmental stimuli or signaling pathways are all possible due to sets of interconnected chemical reactions and are regulated by them [1]. These reactions are linked to each other in complex cascading systems, known as chemical reactions networks, or CRNs. By using the concept of CRNs one can explain numerous complex dynamical *in vivo* behaviours such as oscillation, logic and feedback control, bistability, memory *etc*. [2 3 4 5 6]

Additionally, it is important to recognize the central role played by diffusion processes in controlling complex information-processing events in living cell besides CRNs. For this reason, the concept of "reaction-diffusion (RD) systems" has emerged. Such systems combine spatially distributed chemical reactions with the diffusion of chemical species. RD systems are based on spontaneous processes, and lead to formation of complex patterns or self-organisation of structures on molecular level.

Interestingly, RD systems can explain not only biochemical processes occurring in simple cell, such as division [7], but also functions seen in multicellular systems, like messenger waves of calcium ions in heart, blood coagulation [8], collective cells decisions [9] *etc*. or even pattern formation at organism level [10]. Moreover, various examples of similar processes in the non-living world are known [11] (fig. 1.1).

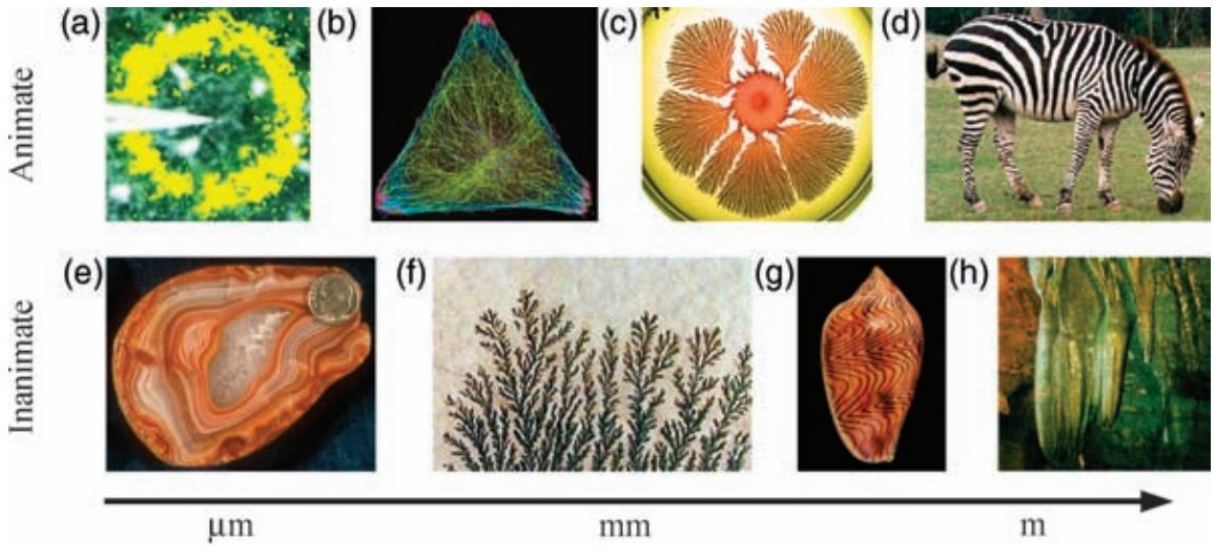

Figure 1.1. Variety of RD systems in micro- and macroworld in both living and non-living nature: (a) calcium waves in cell; (b) fluorescently labelled microtubules in a cell; (c) growth of bacterial colony; (d) RD-based patterns on a zebra; (e) Brazilian agate mineral; (f) dendritic formations on limestone; (g) RD patterns on sea shell Amoria undulate; (h) cave stalactites. Figure was taken from [11].

1.1.1 Reaction-diffusion

The theory of RD systems was introduced in 1952 by Alan Turing [12], who aimed to answer the question how such complex heterogeneous system like a living embryo can appear from the homogeneous zygote. The central idea of his concept, which explained formation of biological patterns, was that chemical species do not only diffuse, but also interact with each other forming feedback loop regulation. Turing stated that for this purpose it is sufficient to have a combination of known physical elements. The model comprises 2 species, an activator and an inhibitor, which interact with each other and diffuse in continuous a continuous medium. The activator is involved in an autocatalytic self-production reaction and, at the same time, produces inhibitor molecules, which block activator production. Since activator and inhibitor are different chemical species, they have different diffusion coefficients. It has to be noted that the mandatory condition for Turing patterns formations is that inhibitor species diffuse significantly faster than activator. Because of this difference in diffusion coefficients of the chemical species involved in the process, zones appear where either inhibitor or activator dominates. As a result,

periodic waves of concentration of inhibitor and activator species are formed that lead to the emergence of complex spatial patterns (fig. 1.2 c).

Biological patterns can also appear on morphogen gradient mechanism (fig. 1.2 a b) [13]. It might be seen as a particular case of RD model with no reaction part but introducing "boundary conditions".

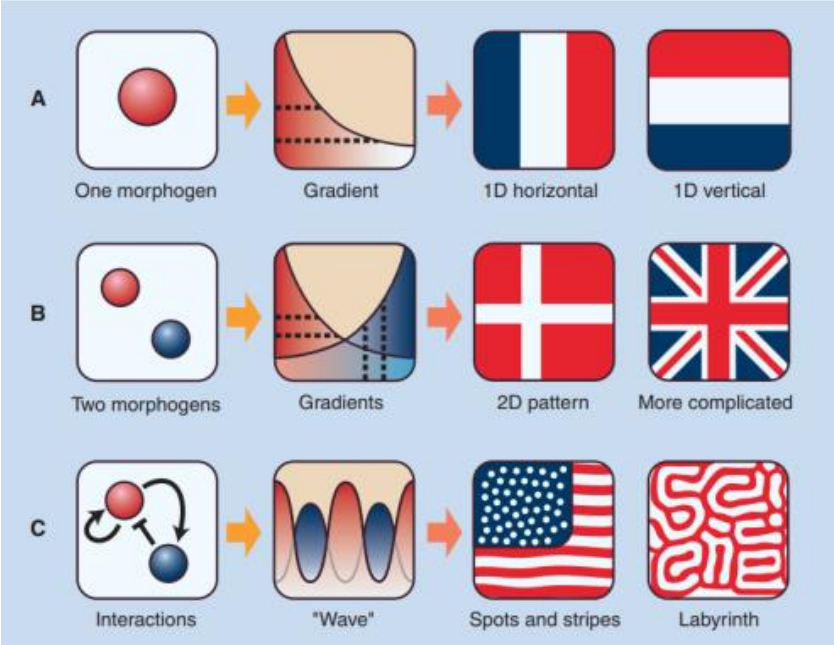

Figure 1.2. Different mechanisms of patterns formation. Morphogen gradient model (a and b) and Turing RD model (c). Figure is taken from [14].

Artificial RD systems, based on CRNs with complex dynamical behaviour, are needed in order to improve our knowledge of cellular processes and, on the other hand, to mimic natural CRNs for real-life applications such as the design of novel biosensors, smart autonomous systems, unconventional computation *etc.* [15]

1.1.2 CRNs motifs

Despite the tremendous complexity and multiplicity of CRNs, some basic processes such as activation or inhibition are common to all of them. It has been showed that for complex dynamical networks including both natural and artificial systems it is feasible to distinguish elementary blocks, network motifs, which contain either positive or negative feedback loops [16].

Thus, their emergence in such networks is much more common than random connections (fig. 1.3)

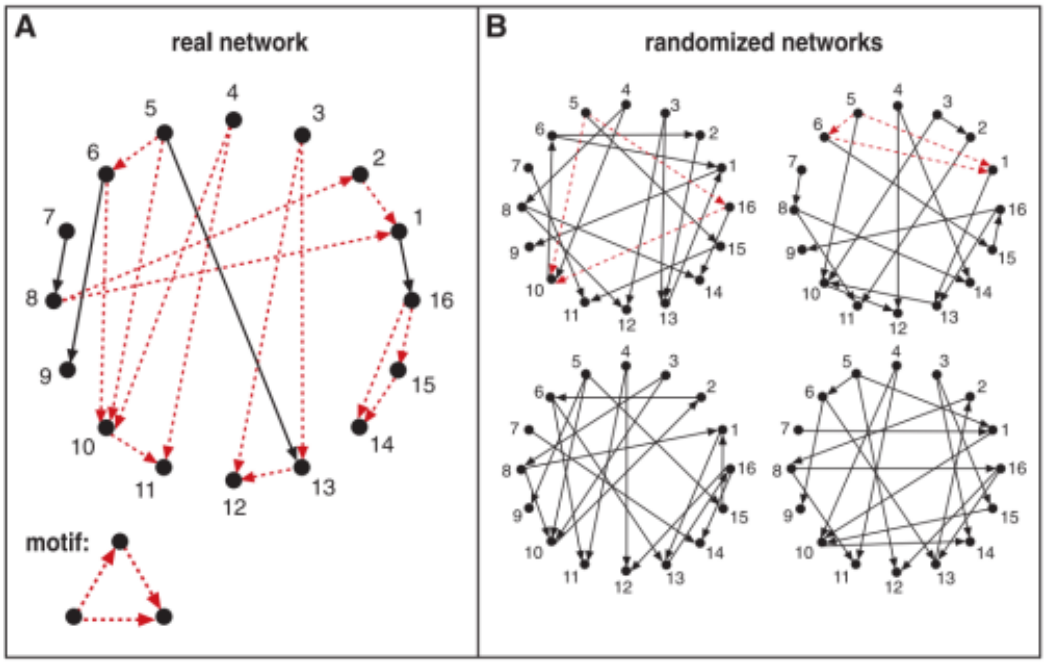

Figure 1.3. Primitive motifs as basic elements of complex networks. Repeatable 3 nods motif, described on the dawn left part emerges substantially often in *E. coli* transcription network (A) than in randomized simulations of similar network (B). Figure was taken from [16]

Structures of the minimal network motifs, which permit a realization of arguably the two most important dynamical functionalities, bistability and oscillations, were proposed in [17]. Authors proposed the chemical reactions schemes, which corresponded to these motifs, and developed mathematical modelling of their reaction rates (fig. 1.4).

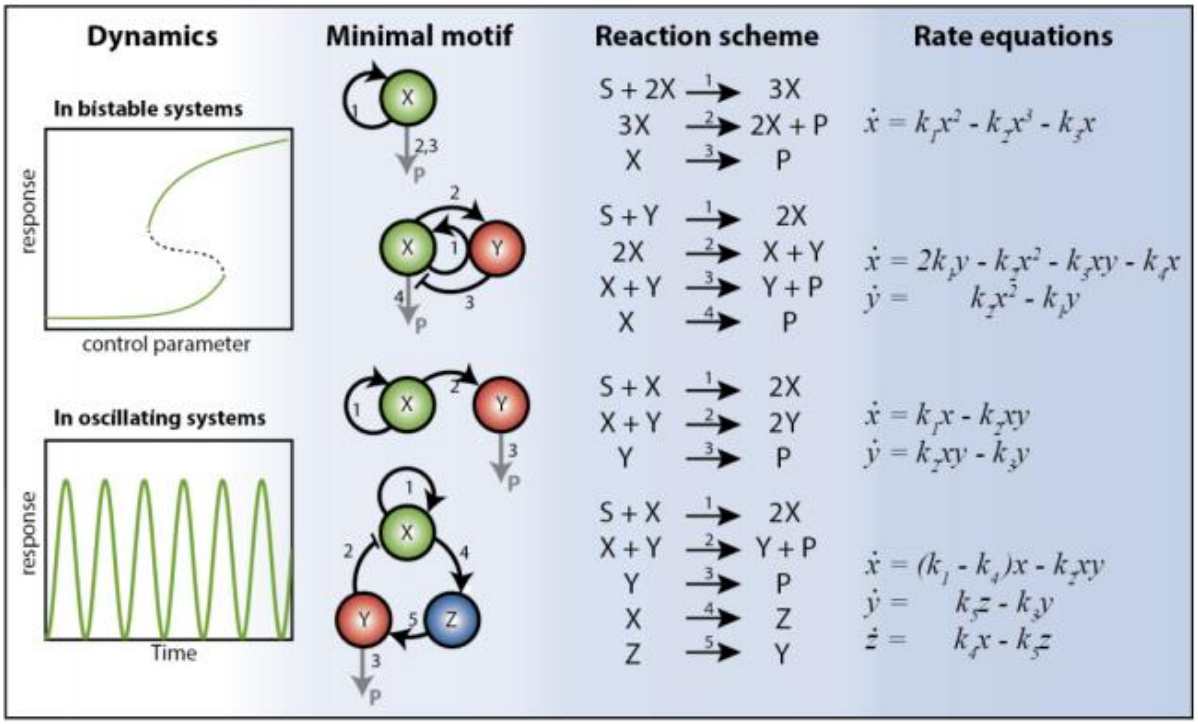

Figure 1.4. Network motifs, permitting bistability and oscillation behaviours, their corresponding formal chemical reactions equations with their reaction rates formulas. Figure was reproduced from [18].

In this context, the main challenge is to understand how simple chemical reactions can program complex behaviour and try to artificially reconstruct natural CRNs. Thus, we can highlight several conditions that must be fulfilled in order to achieve these objectives. First, it is necessary to identify network motifs, which are responsible for certain dynamical behaviours. Second, network motifs must be modular, *i.e.* output of one motif can interact as an input for another (cascadability). Third, reaction rates within and between motifs should be tuneable.

1.1.3 Inorganic systems with complex dynamics

Existence of complex dynamic behaviours driven by CRNs are to a certain extent counter logical and, from the first point of view, contradicts the second low of thermodynamic, which states that total entropy of an isolated system can only increase. Indeed, the intuitively understandable principle of chemical reaction is that one or several reagents are transforming in one or several products with the total decrease of the system free energy as the driving force

of the whole process. It can be either reversible or mostly irreversible, but always occurs until reaching an equilibrium, which means the end of the process.

From this perspective, it is not surprising that when the first oscillation chemical reaction was discovered by luck in 1921 by William Bray [19], it was not recognized as such and was globally rejected by scientific community. Bray studied the catalytic decay of hydrogen peroxide (H_2O_2) in the presence of iodate anion and noticed that the concentration profile of iodine (I_2), the intermediate product of the reaction, was periodically decreasing and increasing with time. The mechanism of the process is as follows. First, the reduction of iodate to iodine by hydrogen peroxide takes place:

$$5\ H_2O_2 + 2\ IO_3^- + 2\ H^+ \rightarrow I_2 + 5\ O_2 + 6\ H_2O$$

And, after that, oxidation of iodine back to iodate:

$$5\ H_2O_2 + I_2 \rightarrow 2\ IO_3^- + 2\ H^+ + 4\ H_2O$$

Depending on the ratio of concentrations of iodate anion to iodine, either the first or the second reaction dominates. It has to be noticed, that the whole process is possible because the value of redox potential of hydrogen peroxide enables these two reactions.

The same resistance was faced in 1951 by Boris Belousov who studied inorganic analogues of the Krebs cycle. One of his experiments was an oxidation of citric acid by potassium bromate in acidic medium in presence of a catalyst – cerium ions Ce^{+3}. He mentioned that the colour of the solution was periodically changing from colourless to yellow and back, which was caused by cyclic transformation of cerium species. His results faced massive scepticism, since the existence of chemical oscillations was considered impossible. Belousov finally published his results, 8 years after his discovery, in a non-reviewed journal [20].

Ananatol Zhabotinsky and co-workers [21] [22] investigated different variants of Belousov's reaction and proposed the first mathematical model of it. In particular, they found that another organic acid, malonic acid, can be used instead of citric acid and the cerium-based catalyst can be replaced by ferroin, which provides a better contrast of colour change from red to blue:

$$3CH_2(COOH)_2 + 4BrO_3^- \ 4Br^- + 9CO_2 + 6H_2O$$

In 1969, Zhabotinsky's team discovered that, in a thin layer of reaction mixture, waves of concentration changes could appear which can be seen in presence of an indicator. This pattern emergence (fig. 1.5) is a clear illustration of links between CRNs with complex dynamics and diffusion processes.

Figure 1.5. Patterns, produced by the B-Z reaction, starting from initially homogeneous solution in Petri dish after perturbation with silver thread. Figure was taken from https://debanupf.wordpress.com/author/debanupf/

In the following years, chemical reactions of this kind were called Belousov-Zhabotinsky (B-Z). According to the modern understanding[23], B-Z reaction comprises 80 elementary reactions between 26 components (fig. 1.6).

		rate constant
	1. Inorganic Subset	
1	$HOBr + Br^- + H^+ \rightarrow Br_2 + H_2O$	2.3E+9 M^{-2} s^{-1}
2	$Br_2 + H_2O \rightarrow HOBr + Br^- + H^+$	2.0 s^{-1}
3	$Br^- + HBrO_2 + H^+ \rightarrow 2HOBr$	2.0E+6 M^{-2} s^{-1}
4	$2HOBr \rightarrow Br^- + HBrO_2 + H^+$	2.0E−5 M^{-1} s^{-1}
5	$Br^- + BrO_3^- + 2H^+ \rightarrow HOBr + HBrO_2$	2.0 M^{-3} s^{-1}
6	$HOBr + HBrO_2 \rightarrow Br^- + BrO_3^- + 2H^+$	3.3 M^{-1} s^{-1}
7	$2HBrO_2 \rightarrow BrO_3^- + HOBr + H^+$	3.0E+3 M^{-1} s^{-1}
8	$BrO_3^- + HOBr + H^+ \rightarrow 2HBrO_2$	7.5E−9 M^{-2} s^{-1}
9	$BrO_3^- + HBrO_2 + H^+ \rightarrow Br_2O_4 + H_2O$	33.0 M^{-2} s^{-1}
10	$Br_2O_4 + H_2O \rightarrow BrO_3^- + HBrO_2 + H^+$	2200 s^{-1}
11	$Br_2O_4 \rightarrow 2BrO_2^\bullet$	7.4E+4 s^{-1}
12	$2BrO_2^\bullet \rightarrow Br_2O_4$	1.4E+9 M^{-1} s^{-1}
13	$Ce^{3+} + BrO_2^\bullet + H^+ \rightarrow HBrO_2 + Ce^{4+}$	6.2E+4 M^{-2} s^{-1}
14	$HBrO_2 + Ce^{4+} \rightarrow Ce^{3+} + BrO_2^\bullet + H^+$	7.0E+3 M^{-1} s^{-1}
	2. Reactions Involving Organic Species	
	a. Reactions Not Consuming or Producing Radicals	
15	$MA \rightarrow ENOL$	3.0E−3 s^{-1}
16	$ENOL \rightarrow MA$	200.0 s^{-1}
17	$ENOL + Br_2 \rightarrow BrMA + Br^- + H^+$	1.91E+6 M^{-1} s^{-1}
18	$MA + HOBr \rightarrow BrMA + H_2O$	8.2 M^{-1} s^{-1}
19	$BrMA + HOBr \rightarrow Br_2MA + H_2O$	0.1 M^{-1} s^{-1}
20	$TTA + HOBr \rightarrow BrTTA + H_2O$	5.0 M^{-1} s^{-1}
21	$BrO_2MA + H_2O \rightarrow HBrO_2 + TTA$	1.0 s^{-1}
22	$BrO_2MA \rightarrow HOBr + MOA$	1.0 s^{-1}
23	$BrO_2TTA \rightarrow HBrO_2 + MOA$	1.0 s^{-1}
24	$BrTTA \rightarrow Br^- + MOA + H^+$	1.0 s^{-1}
	b. Reactions Producing Radicals	
25	$Ce^{4+} + BrMA \rightarrow Ce^{3+} + BrMA^\bullet + H^+$	0.09 M^{-1} s^{-1}
26	$Ce^{4+} + MA \rightarrow Ce^{3+} + MA^\bullet + H^+$	0.23 M^{-1} s^{-1}
27	$Ce^{4+} + TTA \rightarrow Ce^{3+} + TTA^\bullet + H^+$	0.66 M^{-1} s^{-1}
28	$HOBr + MOA \rightarrow Br^\bullet + OA + {}^\bullet COOH$	140.0 M^{-1} s^{-1}
29	$Ce^{4+} + MOA + H_2O \rightarrow Ce^{3+} + OA + {}^\bullet COOH + H^+$	10.0 M^{-1} s^{-1}
30	$HOBr + OA \rightarrow Br^\bullet + {}^\bullet COOH + CO_2 + H_2O$	140.0 M^{-1} s^{-1}
31	$Ce^{4+} + OA \rightarrow Ce^{3+} + {}^\bullet COOH + CO_2 + H^+$	10.0 M^{-1} s^{-1}
32	$BrO_3^- + OA + H^+ \rightarrow BrO_2^\bullet + {}^\bullet COOH + CO_2 + H_2O$	1.6E−5 M^{-2} s^{-1}
	c. Reactions Consuming Radicals	
33	$2Br^\bullet \rightarrow Br_2$	1.0E+8 M^{-1} s^{-1}
34	$Br^\bullet + BrMA^\bullet \rightarrow Br_2MA$	1.0E+9 M^{-1} s^{-1}
35	$2BrMA^\bullet + H_2O \rightarrow BrMA + BrTTA$	1.0E+8 M^{-1} s^{-1}
36	$BrMA^\bullet + MA^\bullet + H_2O \rightarrow MA + BrTTA$	1.0E+9 M^{-1} s^{-1}
37	$BrMA^\bullet + TTA^\bullet + H_2O \rightarrow TTA + BrTTA$	1.0E+9 M^{-1} s^{-1}
38	$BrMA^\bullet + Ce^{4+} + H_2O \rightarrow Ce^{3+} + BrTTA + H^+$	1.0E+7 M^{-1} s^{-1}
39	$BrMA^\bullet + BrO_2^\bullet + H_2O \rightarrow HBrO_2 + BrTTA$	5.0E+9 M^{-1} s^{-1}
40	$BrMA^\bullet + {}^\bullet COOH \rightarrow BrMA + CO_2$	5.0E+8 M^{-1} s^{-1}
41	$2MA^\bullet + H_2O \rightarrow MA + TTA$	3.2E+9 M^{-1} s^{-1}
42	$MA^\bullet + TTA^\bullet + H_2O \rightarrow 2TTA$	1.0E+9 M^{-1} s^{-1}
43	$MA^\bullet + {}^\bullet COOH \rightarrow MA + CO_2$	2.0E+9 M^{-1} s^{-1}
44	$MA^\bullet + Br^\bullet \rightarrow BrMA$	1.0E+9 M^{-1} s^{-1}
45	$MA^\bullet + Ce^{3+} + H^+ \rightarrow MA + Ce^{4+}$	1.7E+4 M^{-2} s^{-1}
46	$MA^\bullet + BrO_2^\bullet \rightarrow BrO_2MA$	5.0E+9 M^{-1} s^{-1}
47	$2TTA^\bullet \rightarrow TTA + MOA$	1.0E+9 M^{-1} s^{-1}
48	$TTA^\bullet + {}^\bullet COOH \rightarrow TTA + CO_2$	2.0E+9 M^{-1} s^{-1}
49	$TTA^\bullet + Br^\bullet \rightarrow BrTTA$	1.0E+9 M^{-1} s^{-1}
50	$TTA^\bullet + Ce^{3+} + H^+ \rightarrow TTA + Ce^{4+}$	1.7E+4 M^{-2} s^{-1}
51	$TTA^\bullet + BrO_2^\bullet \rightarrow BrO_2TTA$	5.0E+9 M^{-1} s^{-1}
52	$2{}^\bullet COOH \rightarrow OA$	1.2E+9 M^{-1} s^{-1}
53	$^\bullet COOH + Ce^{4+} \rightarrow Ce^{3+} + CO_2 + H^+$	1.0E+7 M^{-1} s^{-1}
54	$^\bullet COOH + Br^\bullet \rightarrow Br^- + CO_2 + H^+$	1.0E+9 M^{-1} s^{-1}
55	$^\bullet COOH + BrO_2^\bullet \rightarrow HBrO_2 + CO_2$	5.0E+9 M^{-1} s^{-1}
	d. Reactions Preserving Radicals	
56	$MA^\bullet + Br_2 \rightarrow BrMA + Br^\bullet$	1.5E+8 M^{-1} s^{-1}
57	$MA^\bullet + HOBr \rightarrow TTA + Br^\bullet$	1.0E+7 M^{-1} s^{-1}
58	$MA^\bullet + BrO_3^- + H^+ \rightarrow TTA + BrO_2^\bullet$	40.0 M^{-2} s^{-1}
59	$MA^\bullet + TTA \rightarrow MA + TTA^\bullet$	1.0E+5 M^{-1} s^{-1}
60	$TTA^\bullet + MA \rightarrow TTA + MA^\bullet$	1.0E+5 M^{-1} s^{-1}
61	$MA^\bullet + BrMA \rightarrow MA + BrMA^\bullet$	1.0E+5 M^{-1} s^{-1}
62	$BrMA^\bullet + MA \rightarrow BrMA + MA^\bullet$	5.0E+2 M^{-1} s^{-1}
63	$TTA^\bullet + BrMA \rightarrow TTA + BrMA^\bullet$	2.0E+5 M^{-1} s^{-1}
64	$BrMA^\bullet + TTA \rightarrow BrMA + TTA^\bullet$	5.0E+3 M^{-1} s^{-1}
65	$TTA^\bullet + Br_2 \rightarrow BrTTA + Br^\bullet$	1.0E+8 M^{-1} s^{-1}
66	$TTA^\bullet + HOBr \rightarrow MOA + Br^\bullet + H_2O$	1.0E+7 M^{-1} s^{-1}
67	$TTA^\bullet + BrO_3^- + H^+ \rightarrow MOA + BrO_2^\bullet + H_2O$	40.0 M^{-2} s^{-1}
68	$BrMA^\bullet + Br_2 \rightarrow Br_2MA + Br^\bullet$	1.0E+6 M^{-1} s^{-1}
69	$BrMA^\bullet + HOBr \rightarrow BrTTA + Br^\bullet$	1.0E+5 M^{-1} s^{-1}
70	$BrMA^\bullet + BrO_3^- + H^+ \rightarrow BrO_2^\bullet + BrTTA$	40.0 M^{-2} s^{-1}
71	$^\bullet COOH + BrMA \rightarrow Br^- + MA^\bullet + CO_2 + H^+$	1.0E+7 M^{-1} s^{-1}
72	$^\bullet COOH + Br_2 \rightarrow Br^- + Br^\bullet + CO_2 + H^+$	1.5E+8 M^{-1} s^{-1}
73	$^\bullet COOH + HOBr \rightarrow Br^\bullet + CO_2 + H_2O$	2.0E+7 M^{-1} s^{-1}
74	$^\bullet COOH + BrO_2^\bullet + H^+ \rightarrow BrO_2^\bullet + CO_2 + H_2O$	2.1E+3 M^{-2} s^{-1}
75	$Br^\bullet + MA \rightarrow Br^- + MA^\bullet + H^+$	1.0E+5 M^{-1} s^{-1}
76	$Br^\bullet + TTA \rightarrow Br^- + TTA^\bullet + H^+$	1.0E+6 M^{-1} s^{-1}
77	$Br^\bullet + BrMA \rightarrow Br^- + BrMA^\bullet + H^+$	5.0E+6 M^{-1} s^{-1}
78	$Br^\bullet + MOA + H_2O \rightarrow Br^- + OA + {}^\bullet COOH + H^+$	2.0E+3 M^{-1} s^{-1}
79	$Br^\bullet + OA \rightarrow Br^- + {}^\bullet COOH + CO_2 + H^+$	2.0E+3 M^{-1} s^{-1}
80	$BrO_2^\bullet + OA \rightarrow HBrO_2 + {}^\bullet COOH + CO_2$	1.0E+2 M^{-1} s^{-1}

Figure 1.6. Complete mechanism of B-Z reaction. Figure was taken from [23].

Two important events in a mechanism of B-Z reaction should be mentioned: autocatalytic reaction and feedback loop. Importantly, same processes are in the basics of CRNs in living cell as well as in gene regulatory networks [24 25].

1.1.4 Dissipative systems

At nearly same time with discovery of B-Z reaction, Ilya Prigogine, developed a concept of dissipative structures [26], which is crucial for understanding and reconstruction of CRNs. Dissipative structure is a system which is functioning far from thermodynamic equilibrium A system is called dissipative if it is open and is functioning far from thermodynamic equilibrium and has dynamically repeated steady state. The B-Z reaction is an example of dissipative structures. All living organisms belongs to dissipative structures as well [27]. Prigogine underlines that non-equilibrium serves as a source of order and may cause complex self-organized systems. Thus, thanks to continuous flow of matter and energy from external environment, dissipative structures can keep themselves far from equilibrium steady state and, furthermore, react on increasing flow of energy by appearance of new steady states.

Prigogine also developed a thermodynamic theory of dissipative structures [26]. He received a Nobel Prize for his work in 1977 and inspired elaboration of chemical and biochemical reaction networks, emulating real life processes and performing designed dynamical behaviour. The key factors for elaboration of such networks are non-linear kinetics and functioning of system far from thermodynamic equilibrium. Thus, kinetic of energy consumption by system defines it dynamical behaviour.

Thus, we can highlight one more necessary condition for artificial elaboration of nature-like complex CRNs: system must be in out-of-equilibrium, dissipative, conditions in order to possess a dynamic behaviour.

Except implementation of such systems with inorganic chemistry, few of which were mentioned above, there exist several approaches, based on synthetic organic chemistry, which possesses much bigger number of chemical compounds and known reactions types in its arsenal.

The simplest method for making a dissipative system is to deal with continuous flow reactors [28] . In this case, chemical fuel is permanently provided from an external medium and waste degradation occurs through continuous removal of reaction mixture (fig. 1.7). Although application of this method permits to model such complex dynamical behaviors as oscillations and bistability, it leads to obvious inconveniences in their practical implementation.

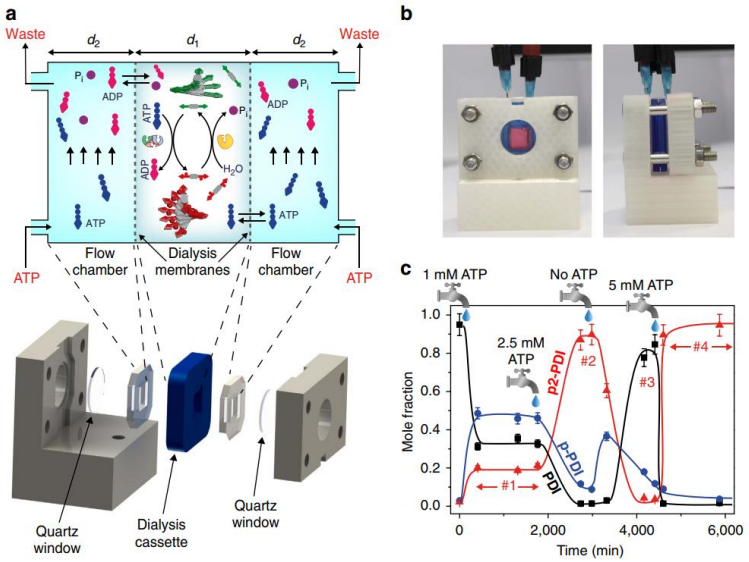

Figure 1.7. Continuous flow system to maintain dissipative system. Figure was taken from [29].

A more elegant and convenient approach relies on internally produced source of chemical fuel. Using it, in recent years a range of dissipative systems was created in which an additional chemical reaction inside the system serves as a driving force for designed process. For example, a cyclic self-assembly and decay of vesicles, made by surfactant molecules as an elementary building blocks, driven by chemical energy supply *via* enzymatic hydrolysis of ATP molecules (fig. 1.8 a) was demonstrated [30] . By controlling the rate of this hydrolysis, it was possible to tune the system lifetime. A similar approach was developed in [31] by producing self-assembled transient hydrogels, fuelled by chemical reaction of carboxylic groups from the gelator (the hydrogel building block) and a strong methylation agent, dimethyl sulphate (fig. 1.8 b). Again, the system lifetime was adjusted by controlling the kinetic of the "fuel" reaction.

Another example of a synthetic dissipative systems is unidirectional molecular motors with energy supply through the synthesis and decay of Fmoc chloride [32] (fig. 1.8 c) or palladium redox cycle (fig. 1.8 d).

It is important to notice that in order to maintain system in an out of equilibrium state the synthesis and degradation of chemical fuel cannot be just one reversible process. On the contrary, they are involved in another chemical reaction, resulting a conversion of fuel from high to low energy state and liberation of energy, which finally consuming by system and permit it to perform designed dynamical behaviour.

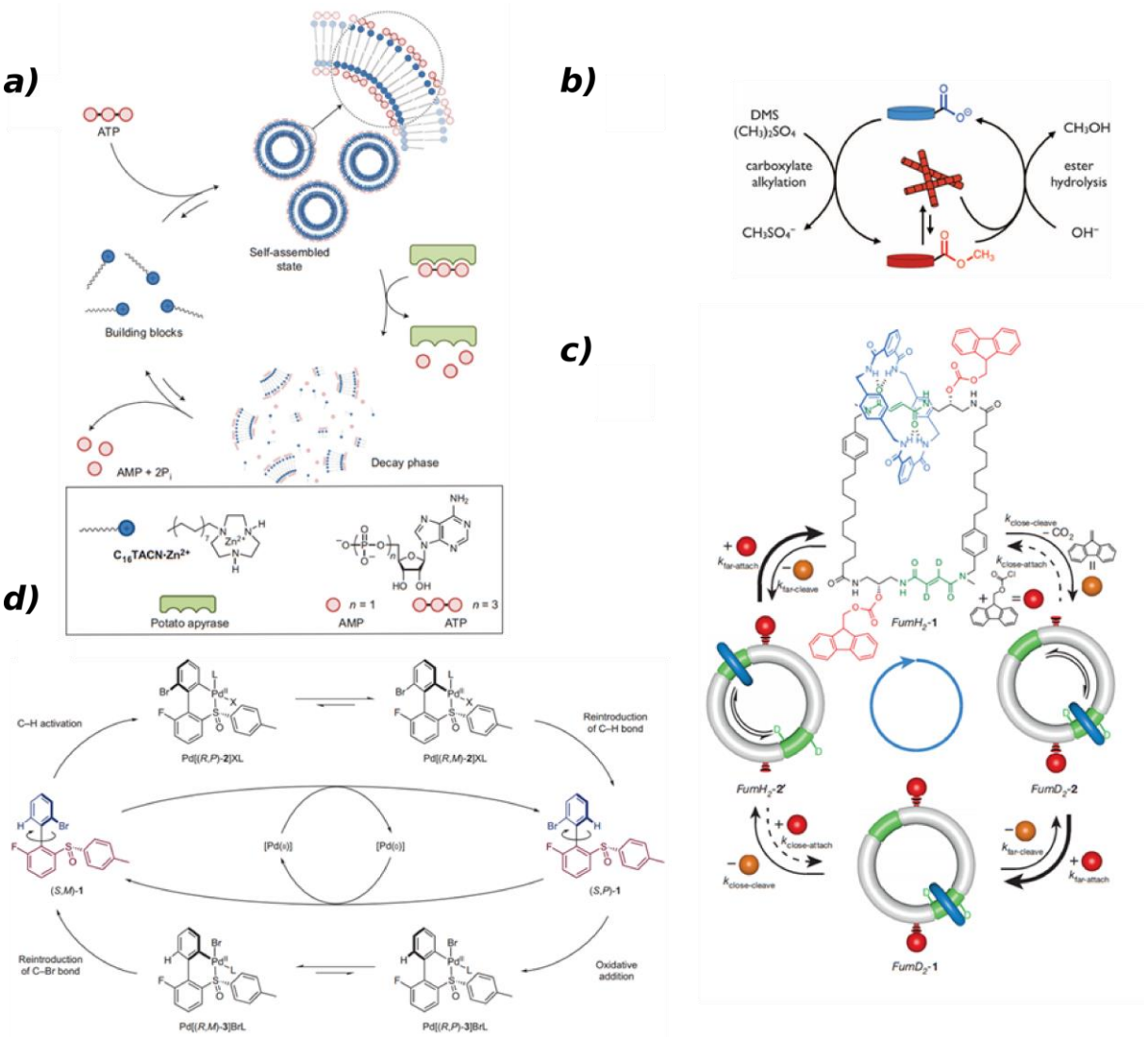

Figure 1.8. Synthetic dissipative systems, fuelled by energy of internal chemical reaction. Figures were taken from (a), [32] (d), [33] (c), [31] (b).

Thus, there is a substantial progress in elaboration of dissipative systems by both inorganic and organic chemistry. However, such approaches lack of modularity and facility of tuning reaction rates, and cannot be, consequently, scaled up. In addition, aggressive chemical medium and/or high temperatures in certain cases make them hardly biocompatible. All this drawbacks substantially limit their future development and potential applications. Thus, novel approaches are needed. In living world, CRNs are driven by biochemistry. And, by mimicking nature, was done a substantial progress in this field. In particular, use of DNA opened a numerous ways for making synthetic CRNs. Furthermore, due to its remarkable properties, DNA founds countless other applications, in particular, in nanotechnology and information

processing, which we will briefly overview further. But first, we will discuss what makes DNA such a unique biomolecule.

1.2 DNA as the basis for molecular engineering

DNA, deoxyribonucleic acid, is a biopolymer, made from nucleotides. Each nucleotide comprises one of four nitrogen-containing nucleobases, cytosine (C), guanine (G), adenine (A), or thymine (T), sugar molecule (deoxyribose) and a phosphate group. The nucleotides are joined to one another in a chain by covalent bonds between the sugar of one nucleotide and the phosphate of another.

Each of nucleobases can form hydrogen bonds with all others and itself, but the favourable base pairing, called complementarity, discovered by Watson and Crick [34] is following: A pairs with T and C pairs with G and as a result of such pairing, two separate polynucleotide strands can attach, or hybridize, together and form the double-helix DNA molecule (fig. 1.9). This makes DNA the molecule with "the most predictable and programmable interactions of any natural or synthetic molecule" [35] . Complementarity permits DNA molecule to recognize a proper strand in a mixture with many others. Moreover, a big number of hybridization events can take place simultaneously in parallel. Due to the ability to generate unique sequences from these 4 nucleotides in each DNA molecule, DNA possesses an incredible capacity for high density information storage : 215 million gigabytes can be stored in only 1 g DNA [36]. This property permits DNA to carry genetic information in living organisms and all the instructions necessary to build such enormously complex system as a human body are contained in a few tens DNA molecules! Finally, both synthesis and sequencing of DNA are well-mastered routing procedures, which take place nowadays in fully automated devices, which dramatically facilitates research work with DNA.

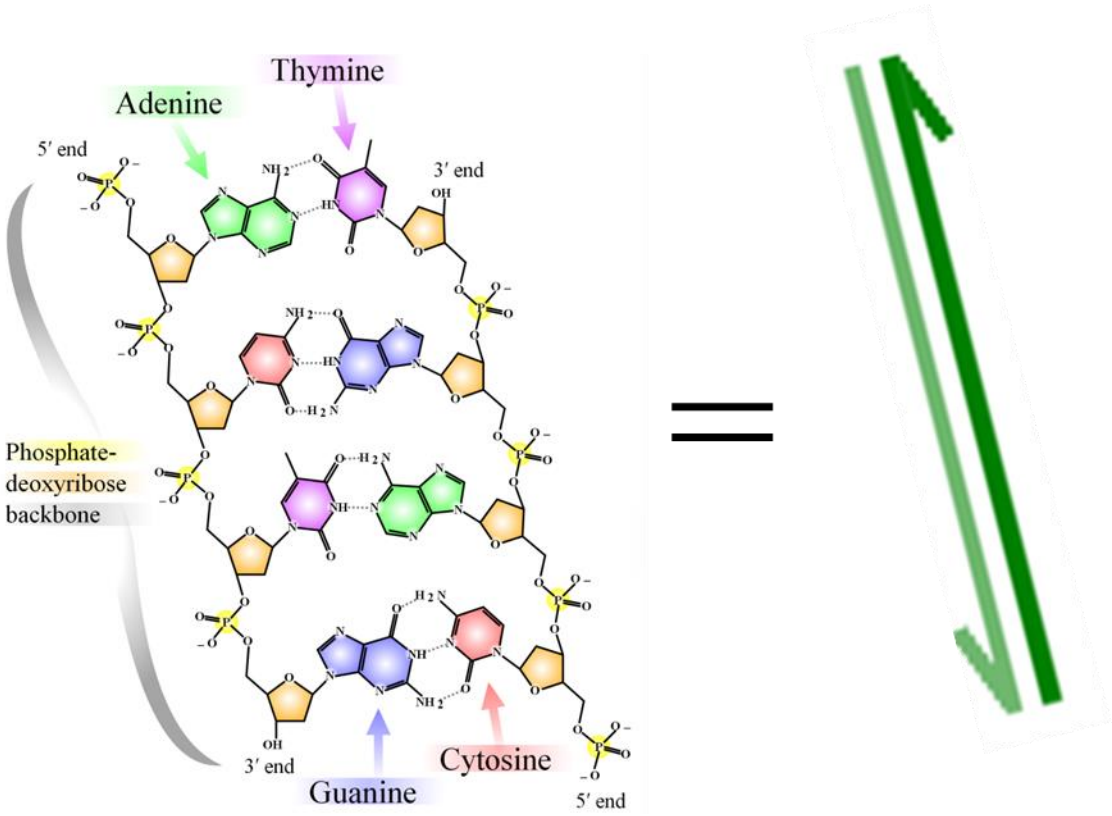

Figure 1.9. DNA structure: double-stranded DNA molecule showing base pairing (Left) and representation style, which will be used in most cases in this study (Right). The arrowhead indicates the 5' to 3' direction in single-stranded DNA molecule. Figure was taken with modifications from Wikipedia.

1.2.1 DNA computing

Using DNA for computation can be traced back to the seminal paper by Adleman [37] which illustrated the power of the massively parallel processing of information permitted by DNA by solving a seven-point Hamiltonian path problem, which is known to be one of NP-complete problems. Problem is called NP, when there is no such an algorithm to solve it, complexity of which will polynomially increase with increasing of complexity of the problem. In other words, if n – complexity of the problem (for instance, number of components, to which it should be applied), there is no known algorithm to solve it in $a \cdot n$ time. Otherwise, problem is called P. Instead, time to solve the problem increase exponentially: a^n. Particularity of NP-complete problems is that, finding a polynomial algorithm to one of them will automatically mean resolving in polynomial time all the others. One can understand the impotency of Adleman's discovery by knowing a fact, that the majority of cryptography behind modern e-

communication (including banking operations) is based on RSA mechanism (one of the authors of which was Adleman), in core of which is NP problem of decomposing numbers by primes.

The key point of the Adleman's experiment is illustrated in (fig 1.10 b and 1.10 c). Let the elementary volume of the reaction medium contain three molecules - encoding accordingly two different edges $u_{i,j}$, $u_{j,k}$ and a vertex v_j, common to them. Then there will be a connection of these molecules into one long chain $u_{i,k}$, which encodes the path from vertex i to vertex k. The resulting chain will be able to connect to another suitable chain that encodes the vertex, or another path fragment on the graph.

The experiment of Adleman took 7 days, out of which the most time was taken by the filtration procedure in step 4.

Despite the evident importance and breakthrough nature of Adleman's work, his computational method has some substantial limitations such as requiring highly time-consuming operations, being conducted under permanent operator control and inability to scale up due to progressively increasing amount of DNA molecules needed to perform the experiment (for instance, for the graph with 200 vertexes one would need DNA with total mass superior than mass of the Earth).

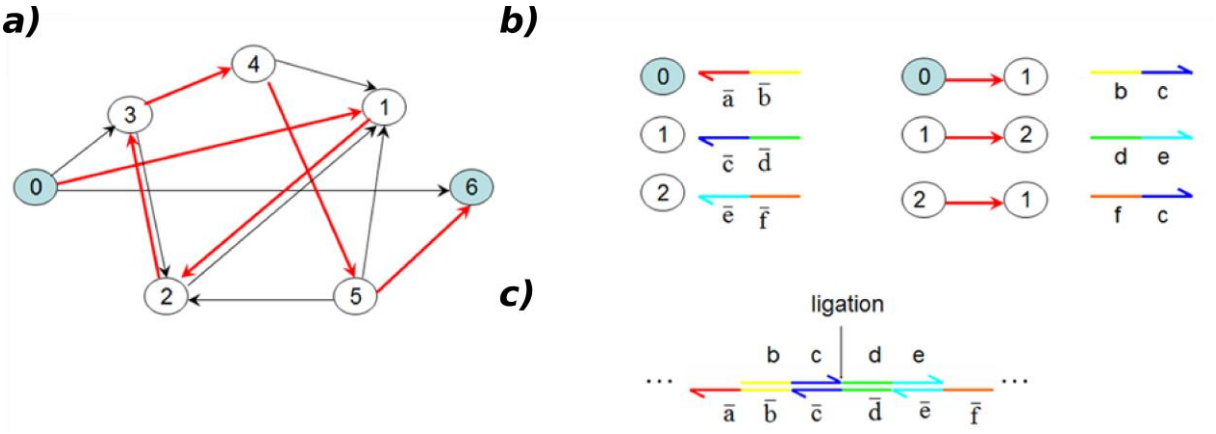

Figure 1.10. Principle of Adleman's experiment. (a) Scheme of graph, Hamiltonian path showed in red; (b) encoding of vertex end edges with DNA; (c) ligation procedure, needed for encoded the path.

Since Adleman's work, numerous other approaches for information processing using DNA, including elaboration of dissipative CRNs, emerged. These discoveries were made within the field of DNA nanotechnology. For this reason, we will review them in parallel with brief discussion of this discipline.

1.2.2 DNA nanotechnology

As was mentioned above, unique properties of DNA, such as predictable hybridization, well-mastered synthesis and sequencing and finally, stability of branched DNA permit to implement a wide range of DNA nanotechnology. This field can be divided in two groups – structural and dynamic. Structural DNA nanotechnology studies, generally speaking, "bottom-up" self-assembly of DNA structures. Dynamic DNA nanotechnology, in turn, deals with time-progressive DNA interactions.

The structural DNA nanotechnology field aims to construct different shapes and structures with high precision. In other words, this branch of DNA nanoscience develops approaches to place DNA molecule of interest in a specific place of the whole structure.

A central concept in structural DNA nanotechnology is sticky-ended cohesion, which describes how assembly through hybridization of two or more double-stranded DNA molecules, which have complementary single-stranded fragments (fig. 1.11), takes place. In case of several branched DNA with sticky ends it is possible to assemble complex 2D or even 3D structures, such as, for instance, cubes [38] with designed and predictable geometry. The most important examples of such kind of structures are DNA lattices and DNA origami.

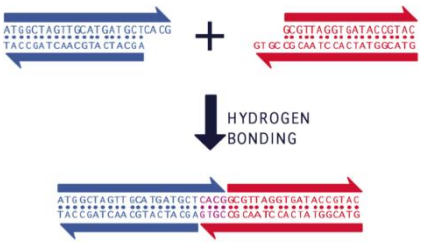

Figure 1.11. The principle of sticky-ended cohesion. Two double stranded DNA molecules forming agglomerate due to the presence of partially complementary parts (sticky ends) in theirs structures. Figure is taken from [39].

1.2.3 DNA tiles

DNA tiles (fig 1.12 a) are self-assembled from single-stranded DNA formations with a help of sticky-ended adhesion. They can form DNA lattices (fig 1.12 b), regular structures with repeated fragments.

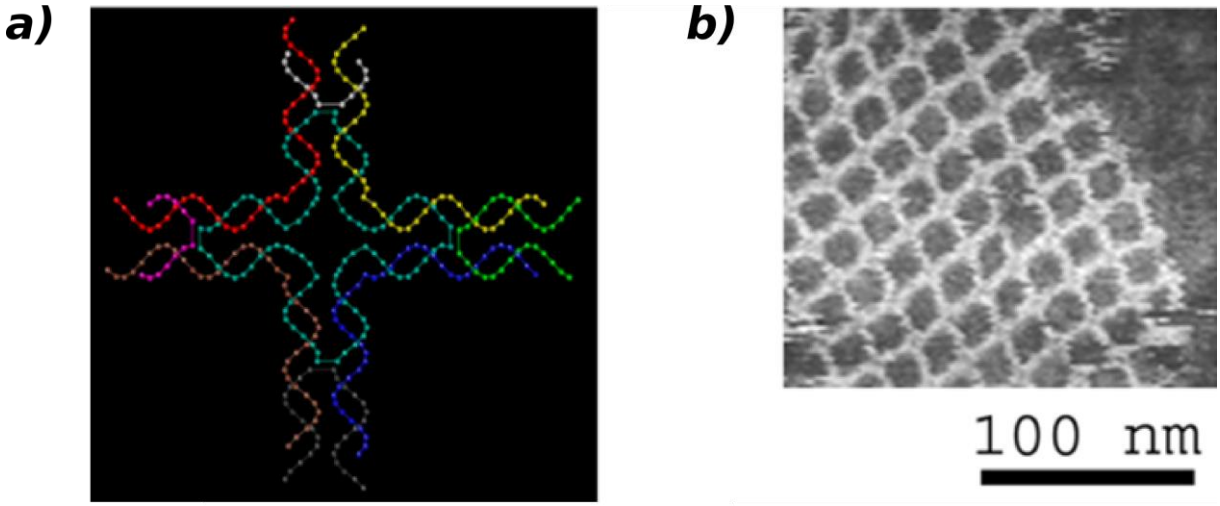

Figure 1.12. (a) Schematic representation of a simple DNA tile, formed by 4 orthogonal branched double-stranded DNA molecules as an elementary "building" block of DNA lattice, imaged on (b). (b) AFM image of self-assembled DNA lattice. Figure was taken from [40].

DNA tiles can be used for computation. The theoretical background for this was founded by mathematician H. Wang in 1961 [41] by introducing a tiling theory, the principle of which is the following: If one has square shape tiles, each edge of which is coloured, it is possible to realize a Turing machine if tiles are assembled in a following way. Edges, which have the same colour, must be oriented one towards another. Moreover, neither rotation nor reflection of tiles is allowed (fig. 1.13).

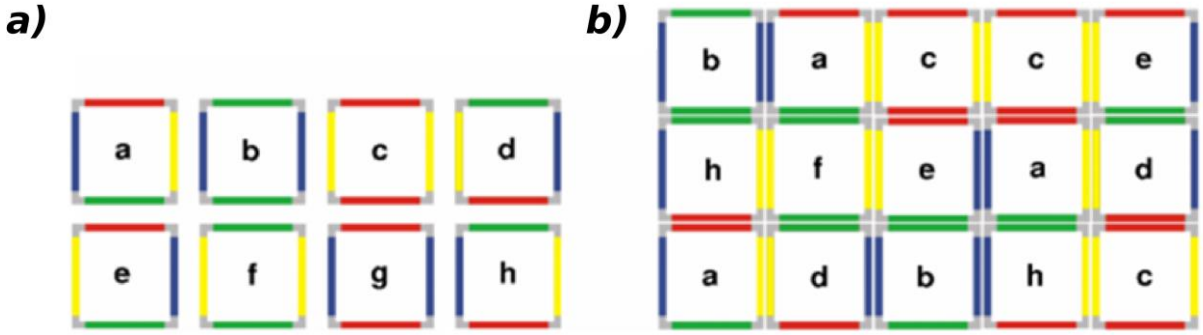

Figure 1.13. Wang tiles, with a help of which plane can be aperiodically covered (a) and a small part of such plane. Image was taken from [42].

E. Winfree [43] has developed the Wang theory and applied it to DNA tiles self-assembly. He demonstrated that such systems are capable to emulate Wang tiles in which connection DNA

"sticky ends" are an equivalent of the edges of Wang tiles. In a similar fashion as Wang tiles can be assembled by same colour rule, DNA tiles are assembled by complementarity rule and, thus, fill the plane in the same strictly specific way. Thus, Winfree extended the Wang tiles assembly by adding a physical mechanism of DNA molecular assembly and stated that one can perform computation using self-assembly of DNA tiles.

In 2000 Mao *et al.* [44] performed the first experimental computation using self-assembly of DNA tiles. They obtained a four steps logical operation, cumulative XOR, the principle of which is the following: If there are two binary inputs, after applying XOR, we will receive an output equal 0 if they both are the same (*i.e.* either 00 or 11) and an output equal 1 if they are different (*i.e.* either 01 or 10). The calculation result, y_i, defines as a result of XOR operation, applied to y_{i-1} and x_i: $y_i = y_{i-1} \mathrm{XOR} x_i$.

8 tiles were designed, each consisting of 4 DNA strands, which formed 3 domains and comprising sticky ends (fig. 1.14 a b). Two tiles, C1 and C2, served as corners and to set a direction of self-assembly. Each of the 6 remaining tiles encoded input and output data. There were two x tiles, corresponded to input values 1 and 0 and four y tiles: two for y=0 (one if x=0 and second if x=1) and two for y=1 (one if x=0 and second if x=1). The order of self-assembly is defined by the lengths of sticky-ends.

Results of the calculations were obtained as an assembly of ten tiles. y_i values were found as a numbers (0 or 1), encoded in tiles in C1 line. The reading of these results was performed with a help of reporter DNA strand, which binds to the final assembly. Next, ligation procedure was performed by adding two DNA ligation enzymes. Depending on the value of tile (0 or 1) they contained a six nucleotides restriction site for one of two ligation enzymes. By doing so, it was possible to find the value of each tile and then to associate output with input.

The principles of tiles design, encoding them, results of computation as tiles self-assembly and reporting strategy demonstrated in fig. 1.14.

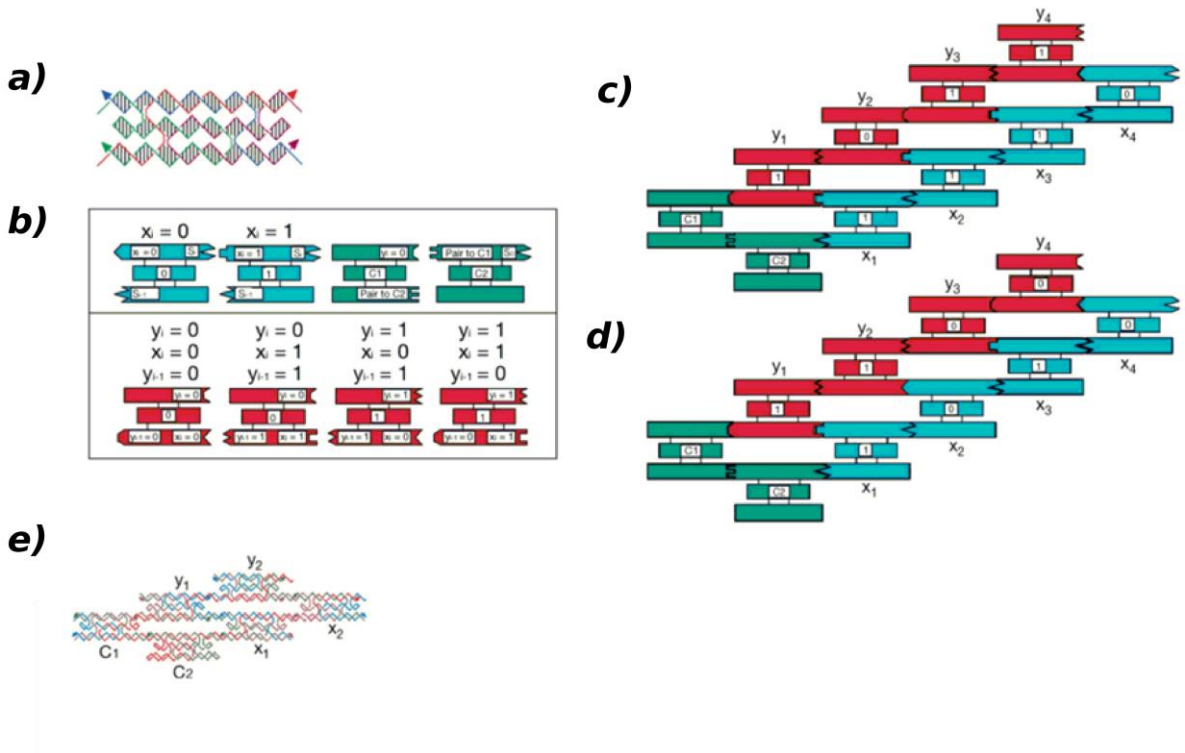

Figure 1.14. Implementation of XOR logic gate with DNA tales. a) 4 single-stranded DNA molecules form a tale with 3 domains; b) encoding calculation parts with tales; c) and d) two calculations results with different input values; e) reporting DNA strand, attached to the calculation result.

Since then, computation using self-assembly of DNA tiles was developed by different research groups which obtained results such as arithmetic computation [45], computation a finite field GF(2(n)) (one of the most commonly used systems in cryptography) [46] *etc*. Computational systems, based on DNA tiles self-assembly, do not require any biochemical reactions, unlike for instance, Adleman's approach, and therefore are more autonomous and need less external control. For the same reason they are substantially faster, since one does not need to wait until all reactions with a set of DNA molecules have been completed.

1.2.4 DNA origami

DNA lattices are limited to produce either small aperiodic structures or bigger formations with periodically repeated patterns. Another strategy to obtain more complex aperiodic structures had to be developed: DNA origami. It relies on the bottom-up self-assembly of small synthetic DNA molecules (typically 20-60 bases long) around a one long DNA strand, which is in most cases a circular genomic DNA from bacteriophage M13 that contains around 7000 bases. This

long DNA strand serves as a scaffold and is folded during self-assembly of shorter strands, so called "staples", around it and reaches eventually the designed shape.

The first steps in DNA origami can be traced back to a seminal paper of Yan et al. [47]. The authors applied the known principle of DNA tiles self-assembly in order to form a lattice, which was formed around a scaffold viral DNA strand with a help of number of small synthetic DNA strands assembled to it. Depending on small synthetic DNA sequences, scaffold DNA strand was folded in programmable shapes simulating the barcode image.

However, DNA origami attracted a massive scientific interest only after the paper [48], where the authors applied the same approach of folding the scaffold viral DNA with a help of small synthetic strands and made a number of different shapes, such as, for instance, smiley face. In 2009 Shih and co-authors [49] made a breakthrough in assembly of nanoscale 3D objects, based on DNA origami. They assembled DNA in a honeycomb lattice and used it to construct complex 3D objects. An interesting example of such discoveries is a box with 4 zepto liters volume, which can be opened and closed on demand and potentially used in medicine for drug delivery [50] (fig. 1.15).

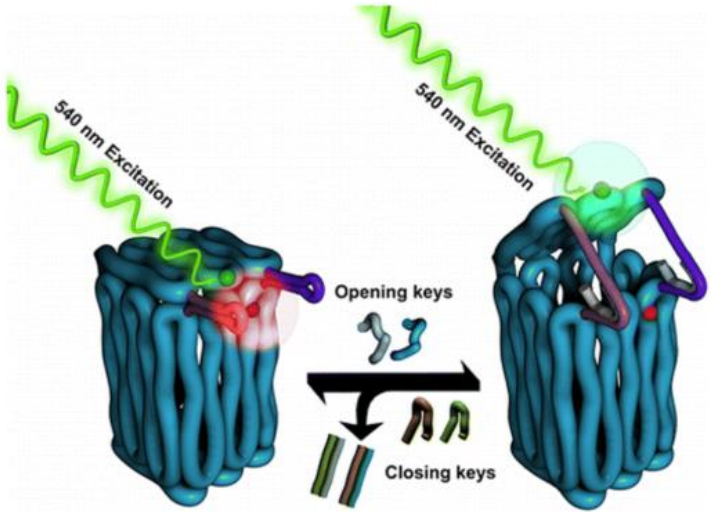

Figure 1.15. 3D box, made from DNA origami, can be controllably open and closed. Figure was taken from [50].

DNA origami was used for a huge variety of applications, such as nanofabrication with gold or silver nanoparticles [51 52] or proteins [53 54], manufacturing of biosensors [55 56], drug delivery systems [57 58] *etc.*

In 2014 nanorobots, based on DNA origami, were used to perform *in vivo* computation [59]**.** These robots were capable of dynamically interacting with each other inside a living animal (*Blaberus discoidalis*). As an example of computation in this work, various logic gates were

emulated: NOT, AND, OR, XOR and NAND. The authors proposed a hypothetical model, based on these logic gates, which can potentially permit simultaneous drug delivery, and be capable to respond on stimuli.

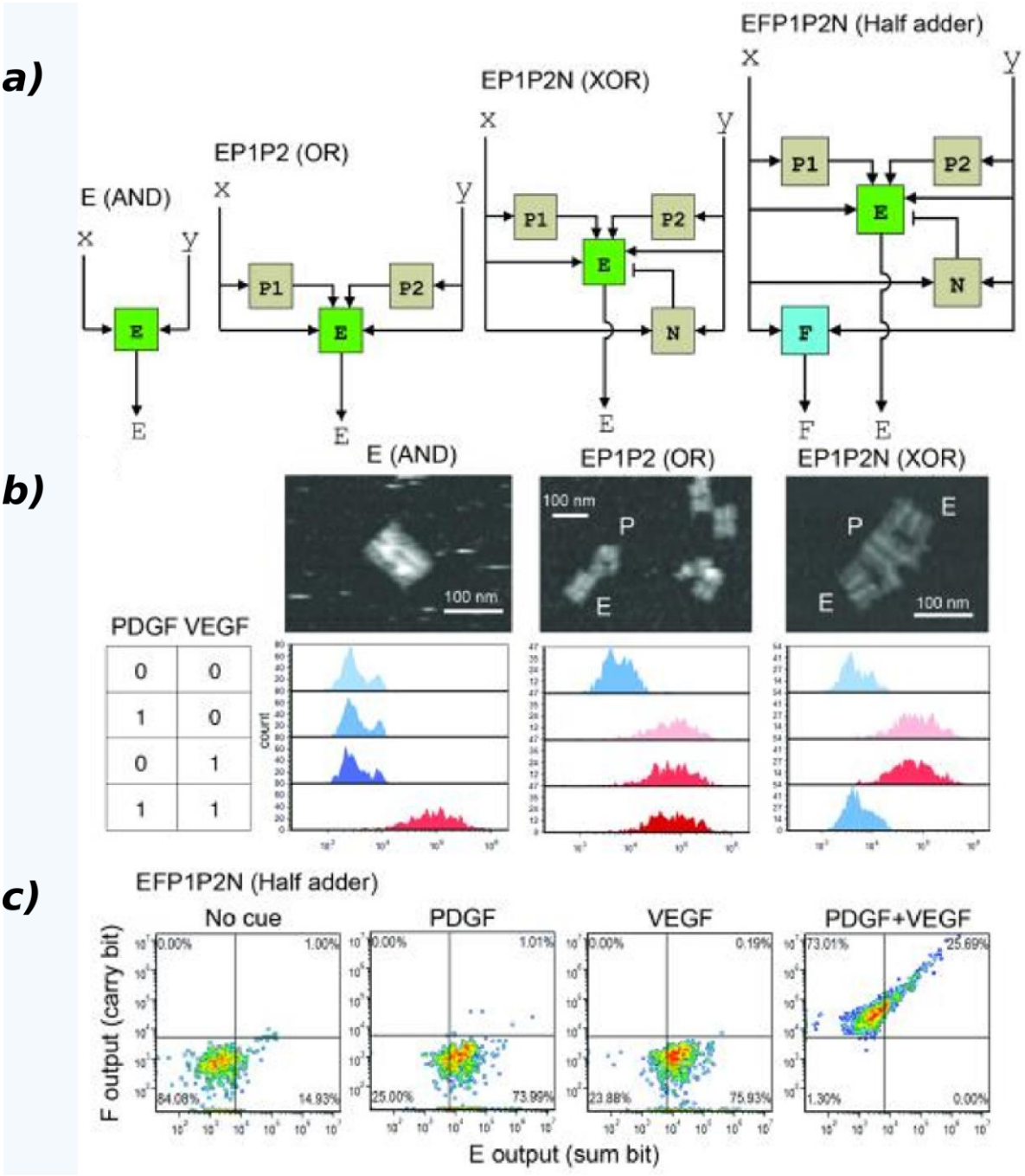

Figure. 1.16. Robot, based on DNA origami, able to emulate AND, OR and XOR logic gates in a living animal. Figure was taken from [59].

1.2.5 Dynamic DNA nanotechnology

Dynamic DNA nanotechnology studies time-progressive DNA interactions. We will mostly limit the overview of this field to the discussion of techniques, based on DNA strands displacement, because of their major importance in information processing approaches, including elaboration of CRNs with complex dynamics.

DNA strands displacement is a process in which single-stranded DNA substitutes one or several DNA from a double-stranded complex and forms a new double-stranded DNA. This process occurs due to the gain of free energy by the system because of the higher affinity between new the components of the double-stranded DNA. It is usually initiated from reversible hybridization of complementary single-stranded segments, which are called toeholds. (However, strands displacement reactions with no free toehold domain are also possible [60]. In this case, reaction rate is substantially lower: two orders of magnitude compared to the reaction mediated by 5 bp long toehold). After hybridization of toehold segments, an irreversible branch migration process occurs followed by dissociation of new strand(s) and formation of new double-stranded DNA. The whole process is showed in figure 1.17 a.

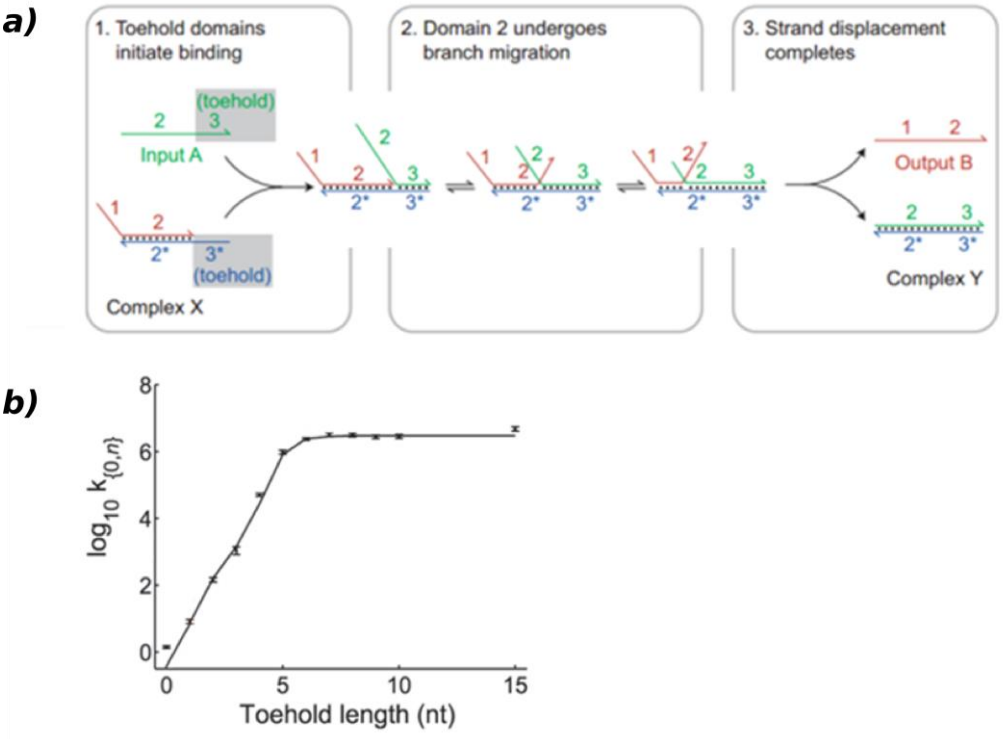

Figure 1.17. Strands displacement toehold. (a) Basic principle: binding of two single-stranded toehold domains followed by branch migration. (b) Strands displacement reaction rate as a function of toehold

length (nucleotides) for a DNA sequence with a roughly equal number of all four nucleotides. Figures were taken from [61] (a) and [62] (b).

The concept of toehold mediated strands displacement was introduced in 2000 by Yurke *et al.* [63], who developed DNA tweezers (fig. 1.18): a molecular machine capable of reversible change between "on" and "off" states. DNA was used both as a building material and as a fuel to control its motion.

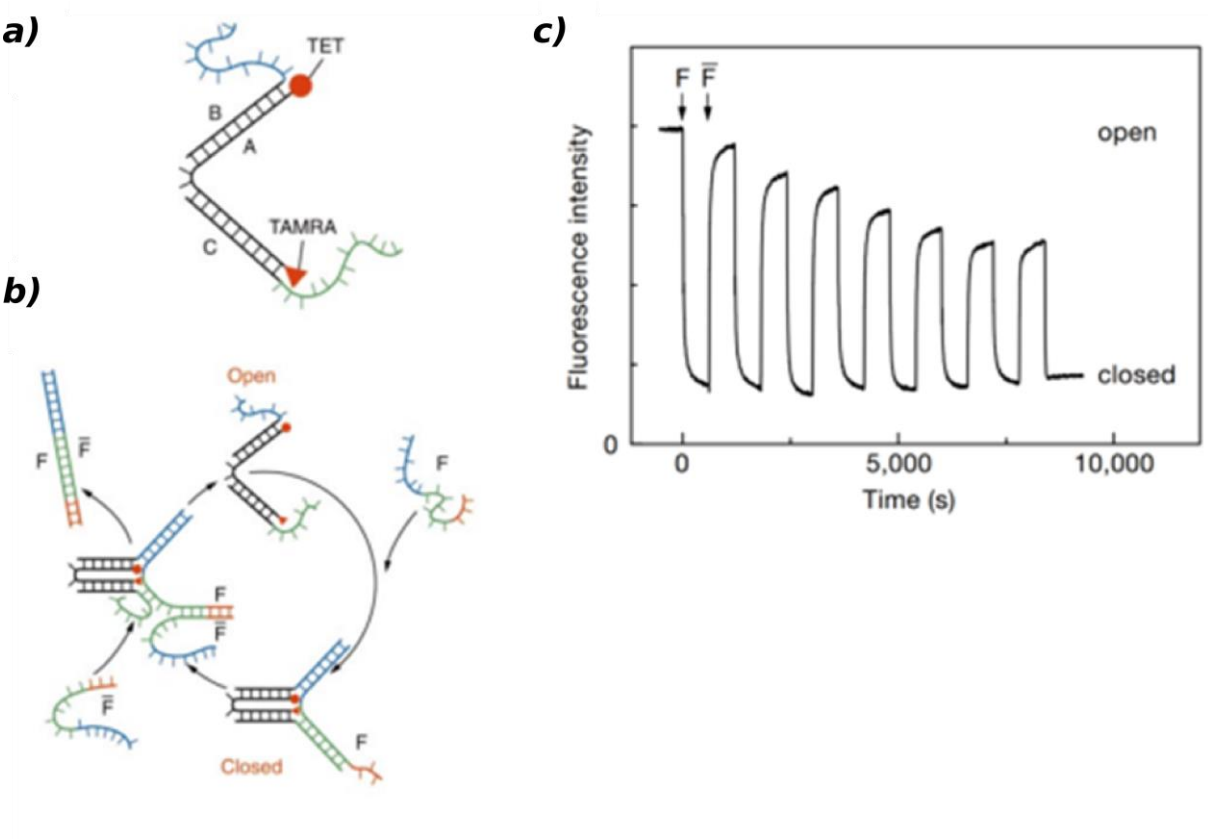

Figure 1.18. Molecular tweezers, based on strands displacement toehold: (a) open tweezers configuration as an assembly of 3 single-stranded DNA molecules, A, B and C; (b) process of reversible closing, driven by two additional single-stranded DNA, F and $\overline{F}$. Toehold domain coloured in red; (c) fluorescence detection: tweezers opening provoke increase of the distance between fluorophore and quencher and fluorescence signal rise up. Closing of tweezers, in its turn, results opposite process and signal declines. This cycle can be repeated several times. Figure was taken from [63].

Winfree *et al.* demonstrated that reaction rate constant can be tuned over a factor 10^6 by changing a toehold length (fig. 1.17 b) [62]. Additionally, authors for the first time applied toehold exchange to construct a DNA autocatalytic reaction.

These results opened a way for various computation techniques, based on strands displacement, such as elaboration of digital logic circuits and implementation of CRNs with complex dynamical behaviour.

1.2.5 Implementation of logic gates

Elaboration of logic gates, based on DNA strands displacement, was pioneered by Winfree and co-workers who introduced a system [64], capable for implementation of AND, OR, and NOT logic gates (fig. 1.18). Their system was modular in a sense that output of one gate can be an input for another, which opened a way for further complexification. Moreover, since the function of logic gates was defined exclusively by nucleotide pairing rules, this system worked with both DNA and RNA inputs.

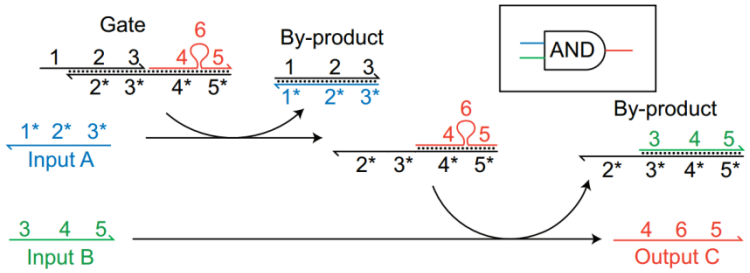

Figure 1.18. Principle of AND logic gate, realized with DNA strands displacement in [64]. The result of AND gate calculation is either output C (if both inputs A and B are present in solution) or absence of output C (otherwise). Figure was taken from [61].

Authors made a proof of biocompatibility of their technology by showing no interference on gate functioning under conditions close to those *in vivo* (presence of mouse brain total RNA in relatively high concentration). Binary inputs and outputs value, 0 and 1, were encoded as low and high concentration profiles respectively. The ability of signal restoration, feedback and cascading were demonstrated. However, the biggest circuit experimentally implemented comprised only 11 gates.

In later work [65] Winfree's research group optimized logic gate design by introducing "seesaw" network (fig. 1.19). Authors stated that it permits the elaboration of circuits with thousands of distinct gates. This approach was further scaled up [66] and applied for mimicking neural network (computation four-neuron Hopfield associative memory) [67].

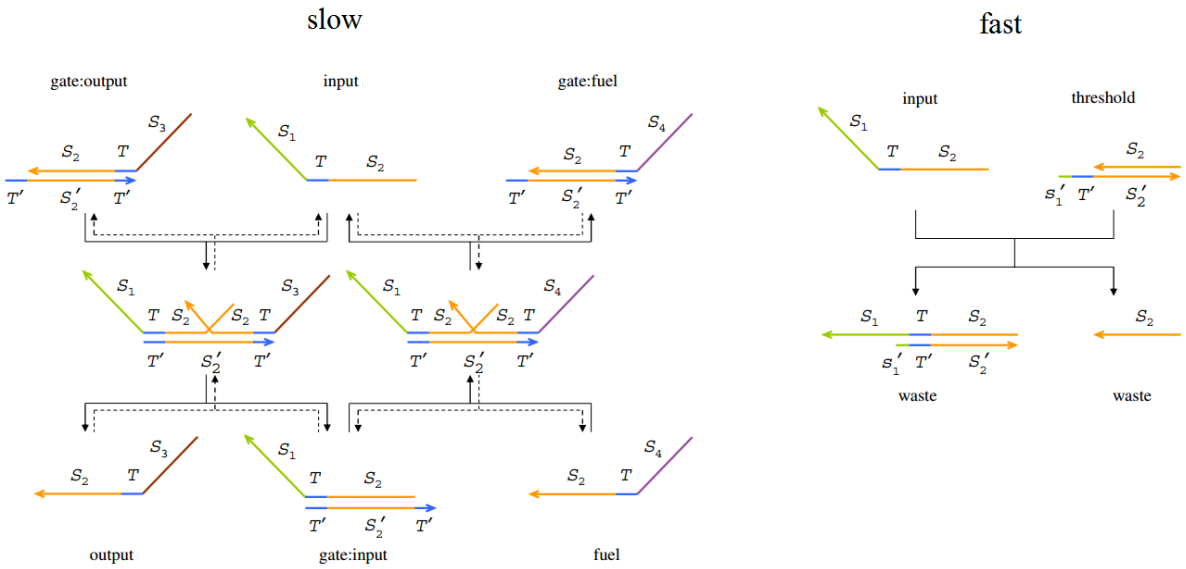

Figure 1.19. Principle of "seesaw" network. Gate strand can equivalently bind to both input and output and to "fuel" strand. Reaction driven force is high concentration of fuel and irreversible consumption reaction with "threshold" strand, which designed to have 5 nucleotides longer binding site and, consequently, faster reaction rate. Figure was taken with modifications from [65].

A sequential computing operation was recently reported, implemented by DNA-based logic gates in water-in-oil microdroplets. Each gate was made in a separate droplet. Computation was performed by adding input-DNA to one droplet with subsequent mixing it with another droplet, after producing of output (fig. 1.20). In this way, the authors obtained more controllable behaviour of single logic gate and avoided a crosstalk between DNA strands in different gates. More precisely, were implemented OR and NOT gates and their connection in NOR logic gate. NOR operation takes around 90 minutes in total. Authors suggested several ways to improve this value, for instance, by decreasing the droplets volume.

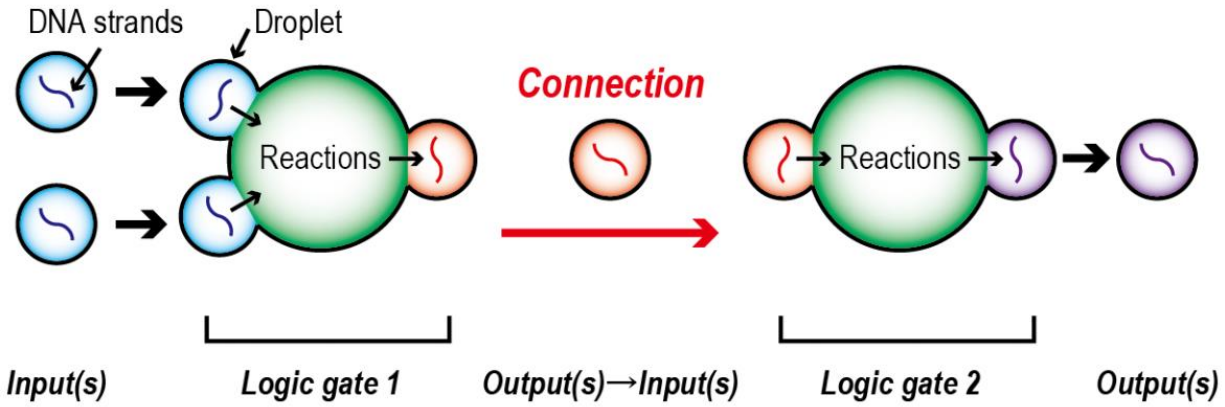

Figure 1.20. Elaboration DNA logic gates in droplets.

There were various other successful attempts of nucleic acid-based logic gates implementation [68] [69]. Furthermore, there exist some other DNA (RNA) computation methods, such as implementation of finite automata or logic programs [70] [71]. This technology is used mostly in medicine for both diagnostic and therapy.

In this way, computation of digital logic gates, using nucleic acids permits setting up large reliable circuits. However, this approach does not utilize the possibility of tuning kinetic of chemical reactions, which are essentially analogue (concentrations of reactants and products are continually changing by time). By doing so, it is possible to obtain more complex behaviours, such as oscillations, formation of patterns, bistability, chaos *etc*., and, consequently, perform more complex information processing.

1.3 Nucleic acid-based molecular circuits with programmable complex dynamical behaviour

1.3.1 Genelet network

In 2006 Erik Winfree and co-workers developed a cell-free molecular framework, capable to perform designed dynamical behaviour [72]. This molecular circuit, "genelet", was constructed by emulating gene transcription network (fig. 1.21). It is based on two main ideas: First, if within gene transcription network one would encode a part of promoter sequence in DNA single strand, then, by controlling hybridization and dehybridization of this strand with genetic DNA, it is possible to control the whole transcription process through activation and deactivation of RNA polymerase. The second principle is DNA strands displacement, which was described previously.

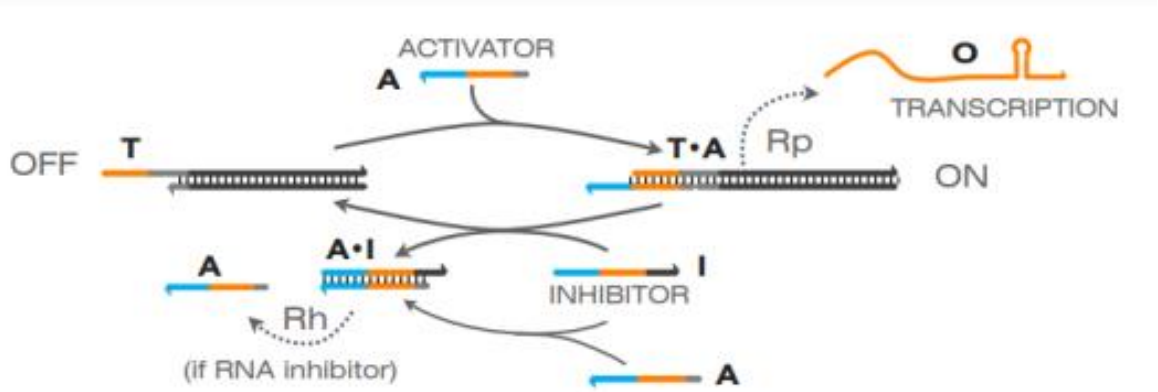

Figure 1.21. Schematic representation of genelet network. Taken from [73].

The genelet network contains double stranded DNA template, named genelet, which emulate the genetic DNA. Based on this template RNA strand can be produced through the interaction with T7 RNA polymerase enzyme (RNAP). However, this reaction cannot occur since DNA template does not contain the whole promoter sequence (specific sequence of base-pairs in double stranded DNA which activates RNAP). In order to enable this process, another DNA strand, named activator, has to be present in the system. Its role is to bind to DNA template double-helix thus forming the promoter site which makes possible the reaction with RNAP. The system also contains an inhibitor, either DNA or RNA single strand. Its role is to attach to the activator and then, through the strands displacement mechanism, to inhibit the production of RNA output.

The system can be either activated or inhibited by adding a new RNA strand. In the first case scenario, which is activation, this new RNA strand, RNA activator (rA), breaks double-helix DNA of activator-inhibitor pair and binds to inhibitor by strands-displacement mechanism. The released activator, in its turn, attaches to template double-helix and RNAP starts to produce RNA output.

When suppression scenario is realizing, RNA inhibitor (rI) serves for direct blocking of DNA activator. Finally, genelet network contains the second enzyme, Ribonuclease H (RNA H). It is a non-sequence specific endonuclease, specifically used for RNA degradation. RNA H in the presence of DNA/RNA duplex does not react with DNA strand and system remains out of equilibrium due to continues degradation of RNA strands.

Activating and inhibiting domains can be connected to each other in order to form more complex networks with designed behavior. Using this feature, such complex system behaviors as bistable switch [72] and 3 design of oscillator [73] were obtained.

Despite the obvious progress made by genelet network, it has substantial limitations. The main of which is an occurrence of non-designed side reactions (partial degradation and either “abortive” or mixed transcription) and impact of their products on system behavior with dynamical influence on reaction rates. This drawback makes system dynamic difficult to predict and complicates modelling.

Soloveichik *et al.* proposed an approach to realize wide range of formal CRNs with DNA strands displacement [74]. This approach comprises 3 basic modules (see fig. 1.22): unimolecular (if formal reaction of CRN of interest has only 1 input specie), bimolecular (if their number is 2) and “buffering” module (which needed for regulation of reaction rates).

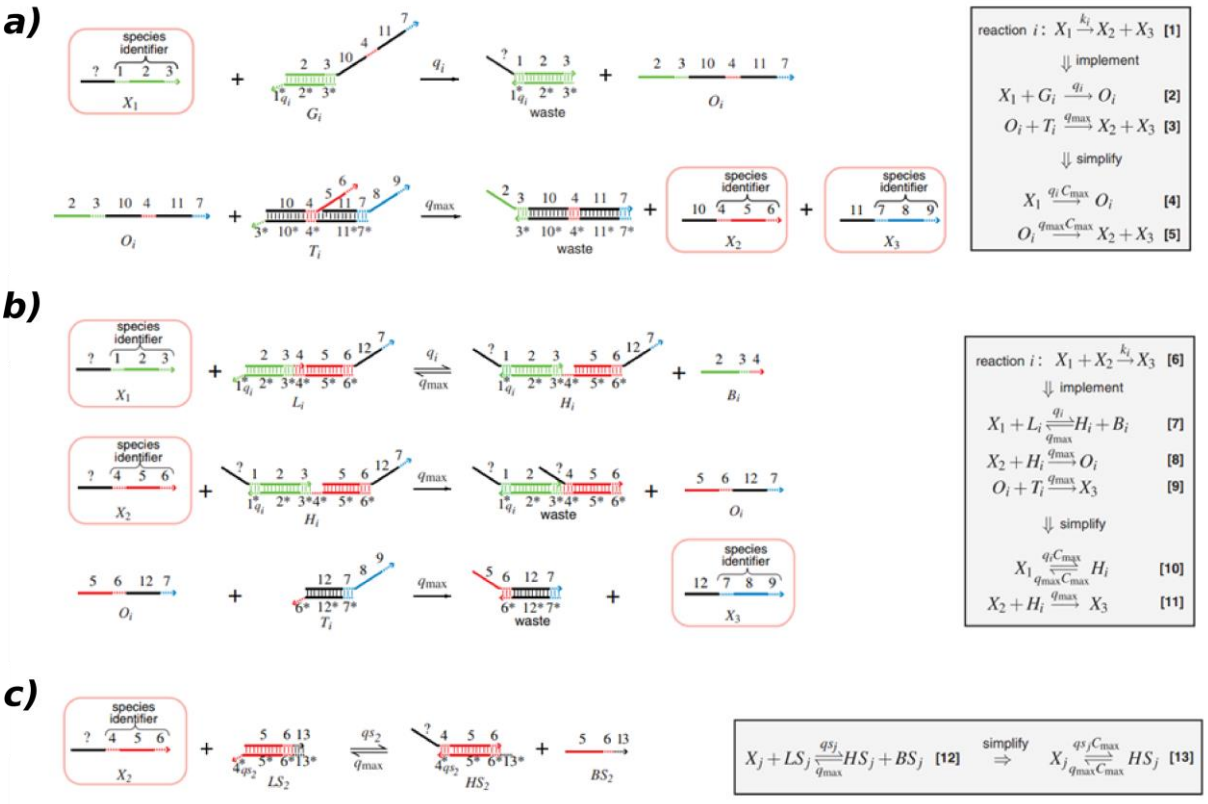

Figure 1.22. Basic modules of system to implementation of formal CRNs in nucleic acid based chemistry: unimolecular (A), bimolecular (B) and buffering module (C). DNA analogues of specie in formal CRN are in red rectangles. Schematic representation of reactions depicted in grey rectangles. Figure is taken with modifications from [74].

By combination of these basic modules were realized CRNs with complex dynamical behaviours: oscillations (Lotka-Volterra oscillator and limit cycle oscillator), chaos and also logic gates based digital circuit, 2-bit pulse counter.

1.3.2 PEN toolbox

Another approach dealing with the elaboration of molecular circuits, named PEN toolbox, was developed by Yannick Rondelez and co-workers (fig. 1.23) [75]. It was inspired by gene regulatory networks. There are similar kinds of DNA molecules as in genelet network: a template (for producing single-stranded DNA output, from single-stranded input DNA), an activator (input DNA, which activates the production of new DNA from template) and an inhibitor (single-stranded DNA, which deactivates template). The enzymatic reactions were driven by 3 enzymes – polymerase, exonuclease and nickase (PEN). For more detailed mechanism of PEN toolbox see section 2.4.

System behavior was accurately described with a set of kinetic and thermodynamic parameters and it was demonstrated that this parameters are easy to tune. This approach has achieved substantial progress by correcting the balance between production and degradation molecular events and leading to an oscillative system with living time up to 30 hours. Later, by using PEN toolbox, a bistable memory circuit was made [76]. The PEN toolbox operates with shorter (*i.e.* cheaper to synthesize) oligonucleotides (around 20 bases long templates *vs* more than 100 for genelet network).

As genelet, the PEN toolbox, is modular in a sense that different topologies can be constructed by varying network nods and their interconnections. Authors realized a network motif, with pursuit-and-evasion (predator-prey) dynamics [77].

The basic principle of PEN toolbox with predator-prey dynamics is the following (fig. 1.23 c): Input ("prey") affinity to templates ("grass" and "predator") was settled by tuning their secondary structure. By doing so, prey binds to grass template and initiate its own autocatalytic production. When certain level of prey concentration is reached, predator template functioning, resulting in an increase of its own concentration and to a decrease concentration of the prey. By continuing the degradation of predator and prey (but not grass), high prey and predator concentration levels changing each other, leading to oscillations.

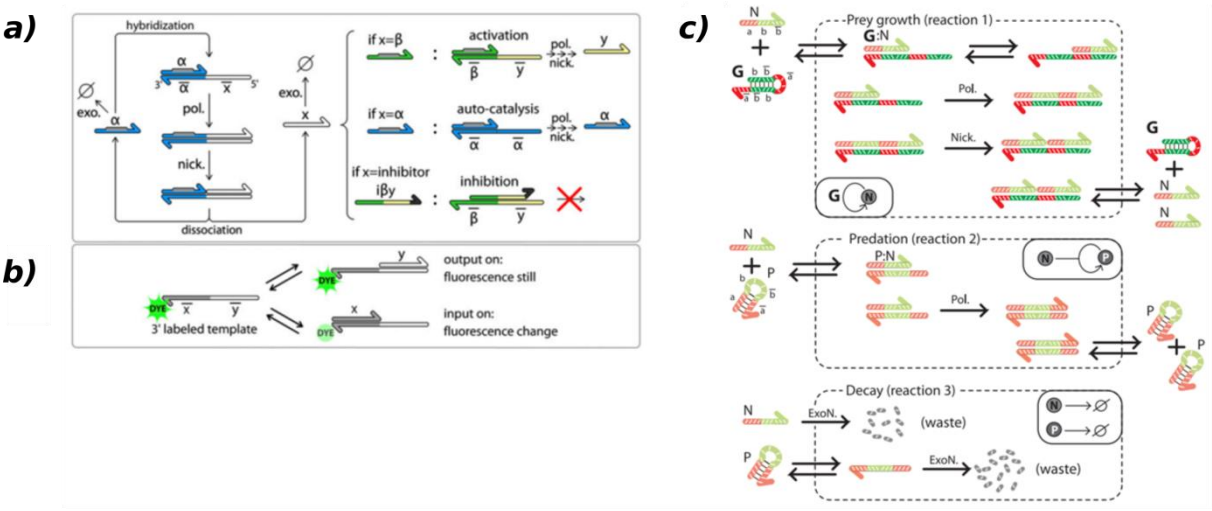

Figure 1.23. Basic principles of PEN toolbox reactions (a), reporting strategy (b) and implementation of predator- prey oscillation network (c). Figures a and b were taken from [76] and c from [77].

1.3.2 Displacillator network

Very recently it was reported by Erik Winfree and coworkers the creation of a new DNA-based CRN, capable for implementation of oscillation (and potentially other complex dynamic behaviors) [78]. Their system, called Displacillator, is enzyme-free and totally based on DNA strands displacement reactions. Authors proposed a principle of implementation CRN pattern by DNA. As an example, it was chosen rock-paper-scissors oscillator CRN, which consists of 3 connected autocatalytic reactions. In that case, the output from one reaction serves as an input of another (fig. 1.24)

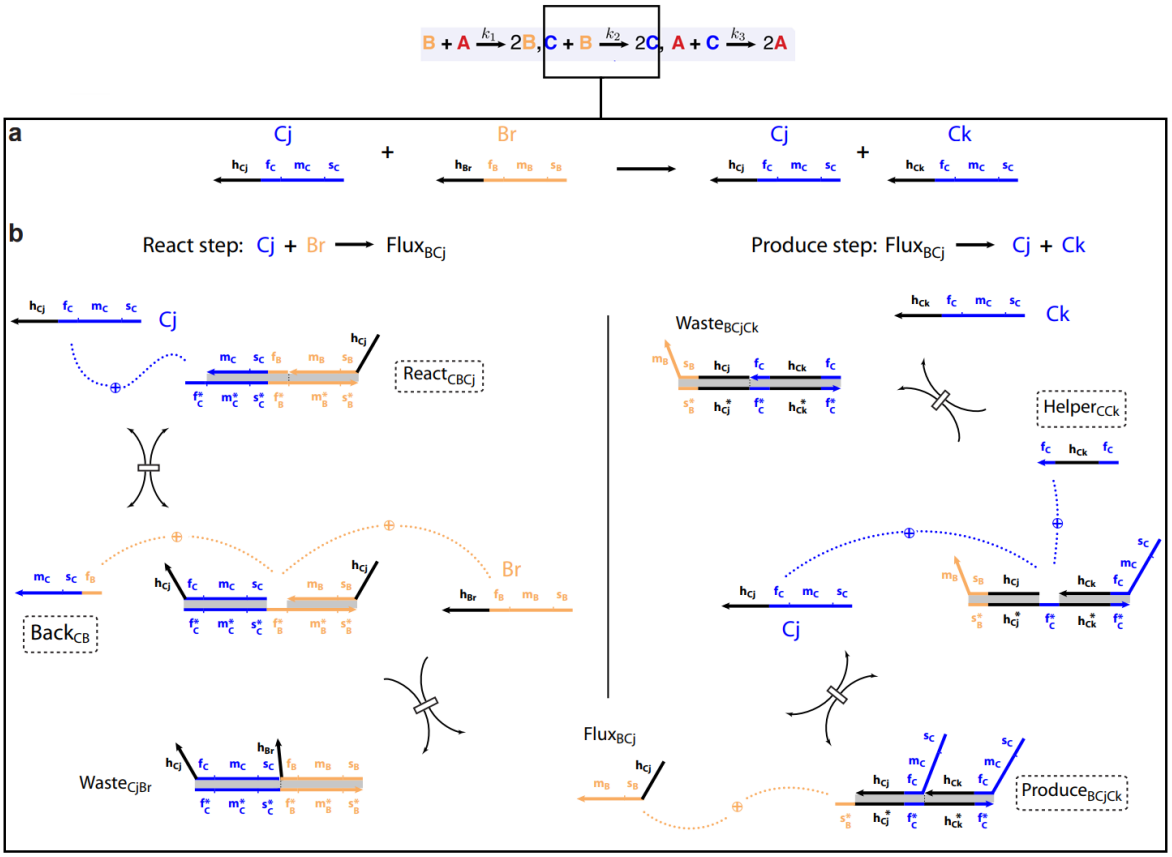

Figure 1.24. Rock-paper-scissors oscillator scheme (up) and its implementation with CRN, based on DNA strands-displacement (down) (only one autocatalytic reaction from 3 is represented on picture). Figure is taken with modifications from [78].

We will discuss the principle of Displacillator, by taking one of the autocatalytic reactions, C+B = 2C, as an example.

Species C, as A and B, are encoded by 2 single-stranded DNA molecules each and called "signal". Each of them consists of 4 domains, 3 of which are the same for both C species and identically react with reported DNA strand (not showed in fig. 1.24), resulting the identical fluorescence signal. The fourth domain (named "historical") determines the order on which species react.

On the first step one of the C strands attaches to auxiliary double-stranded DNA complex, named "React", by strands displacement toehold mechanism. It makes possible assembly of B strand to the resulting assembly and releasing "Flux" DNA single strand. New double-stranded complex no longer participates to the reaction. "Flux" attaches to the second auxiliary double-stranded DNA complex, named "Produce", and release first output C strand. Double-stranded assembly, formed after "Flux" strand attachment, reacts with the third

auxiliary DNA strand, named “Helper”, and provides release of the second C species. Another reaction product, new double-stranded DNA, is no longer participating in reaction.

Strands displacement reactions occur one after another because of subsequent opening of toehold domains on auxiliary double-stranded complexes or liberation of new DNA strands (in case of “Flux”).

As a summary, C and B “signal“ species do not interact directly with each other, but instead, react with 3 auxiliary DNA species (2 double-stranded complexes and 1 DNA single strand), resulting in the release of two C species and the consumption of one B species. The two other autocatalytic reactions, within this network, function in exactly the same way. Since no direct interaction between signal species occurs, elementary reactions of given network can be implemented independently, *i.e.* system is modular and can be used for realization of wide range of CRNs.

The oscillator, realized within this system, does not require enzymes and, consequently, does not produce any “black box” products, however, sustained oscillations were not achieved and the oscillation period was around 202 hours (for example, this time is 1.7 h for oscillator with PEN toolbox or 3 hours for the “genelet” based oscillator). The authors suggest that dynamic behaviour can be improved by, for instance, continuous supply of auxiliary species and removing the waste products.

In this way, biochemical approaches, relying on DNA, permit elaboration of CRNs with complex dynamics and overcome limitations of the dissipative systems realized with a help of organic and inorganic chemistry. Moreover, DNA-based molecular circuits are known to be able to explore RD phenomena, which permits them to solve more complex information processing tasks and which will be discussed next.

1.4 RD systems, based on DNA molecular circuits

Zadorin et al. [79] have introduced a fully programmable RD systems based on PEN DNA toolbox autocatalytic reaction. Authors showed tunability of all parameters mandatory for the creation of arbitrary spatiotemporal patterns. DNA appears as an attractive choice for this. By tuning concentration and sequences of DNA species, they programmed their diffusion coefficients and the reaction rates. The reaction topology was programmed by combination of DNA hybridization with enzymatic reactions within PEN DNA toolbox. Choice of different enzymes

and theirs concentrations also allowed to modify propagation velocity (however in non-specific way). Furthermore, the proposed system is modular *i.e.* can be used to generate predictable and complex spatiotemporal patterns. The system was kept out of equilibrium by constant synthesis and degradation of DNA strands and consuming reaction fuel, dNTPs. It has generated millimetre scale reaction fronts which propagate with uniform and sequence specific velocity (fig. 1.25 a), typically around 100 μm min^{-1}. It has been demonstrated that fronts of different species collide without changing the propagation velocity (fig. 1.25 b). Finally, the diffusion coefficients of given species was successfully decreased without changing the reaction rates by attaching to DNA species hydrodynamic drag *via* streptavidin-biotin irreversible interaction (fig. 1.25 c).

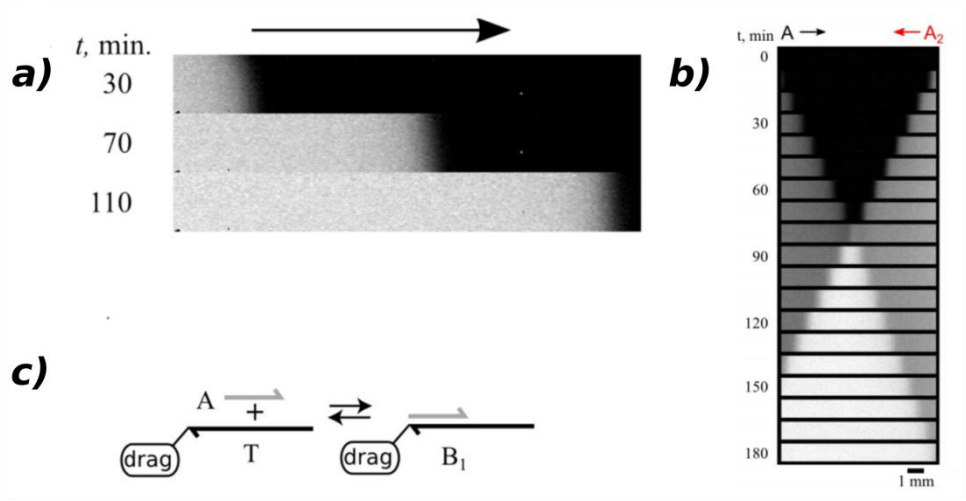

Figure 1.25. Generation of RD fronts, based on PEN toolbox: (a) single front propagation with uniform velocity; (b) two fronts, based on system with orthogonal sequences collide with no interaction; (c) attachment of hydrodynamic drag by biotin-streptavidin linkage as a diffusion controlling strategy. Figure was taken with modifications from [79].

In 2013, RD phenomena as spirals and travailing waves were demonstrated based on PEN-toolbox network with predator prey behaviour [80] (fig. 1.26 a b). This work was further continued by the same group [81] by introducing the methods of controlling the initial and boundary conditions with the help of microfluidics. This approach was applied for finding the shortest path in a maze with pursuit-and-evasion DNA wave (fig. 1.26 c). The advantage this approach compared to inorganic chemistry based analogues, is that reaction output can further interact with another node of CRNs due to modularity of the PEN toolbox.

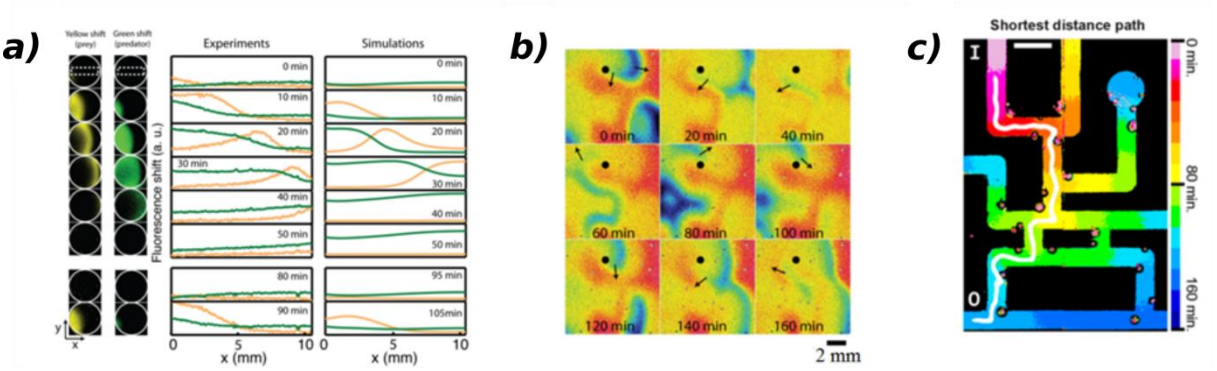

Figure 1.26. RD experiments using PEN toolbox with predator-prey dynamics: (a) pursuit-and-evasion travelling waves (experimental results and simulations); (b) spirals of prey species. (c) computation of shortest distance path, based on RD pulse of prey species. Figures were taken from [80] (a and b) and [81] (c).

In the work done by Zadorin et al. [82] the *in vitro* formation of patterns on RD mechanism was demonstrated. A RD French flag system, based on PEN DNA toolbox was thus created. To do so, authors used two orthogonal molecular networks (fig. 1.27 a). Each of them consists of an autocatalytic node and a repressor. DNA strands, produced by autocatalytic reaction can hybridize to the repressor and be elongated. This process led to its deactivation. Two mechanisms were applied to create French flag patterns. First, with an initial gradient of repressors to 2 reaction networks. Second strategy was to create an initial gradient of repressor from one network and autocatalytic template from another. Concentration gradients of species were exponential and were created by Taylor dispersion. The reactions were performed in 1-dimension glass capillaries. The resulting pattern consists of 3 concentration zones with sharp boundaries.

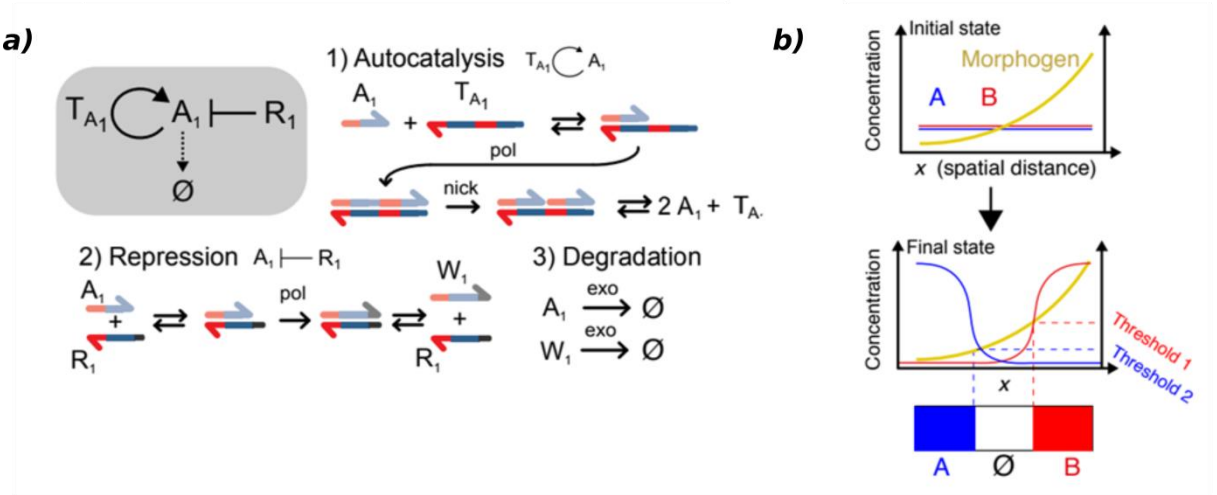

Figure 1.27. PEN-toolbox-based molecular circuit (a) and "French flag" concentration pattern (b), which was created with it. Figure is taken with modifications from [82].

Enzymes-free DNA-based CRNs were also recently utilized to explore the potential of RD [60]. DNA strands displacement reactions were applied in combination with diffusion in agarose hydrogel in order to create stable patterns (fig. 1.28). The stability of patterns was achieved due to continuous release and consumption of DNA species (output). These two reactions (fig. 1.28 a) were balanced in a way to compensate diffusive homogenization of patterns. Moreover, it was done a scaling of proposed approach by introducing second system, with orthogonal sequence and demonstrated simultaneous formation of two stable non-interacting patterns (fig. 1.28 c).

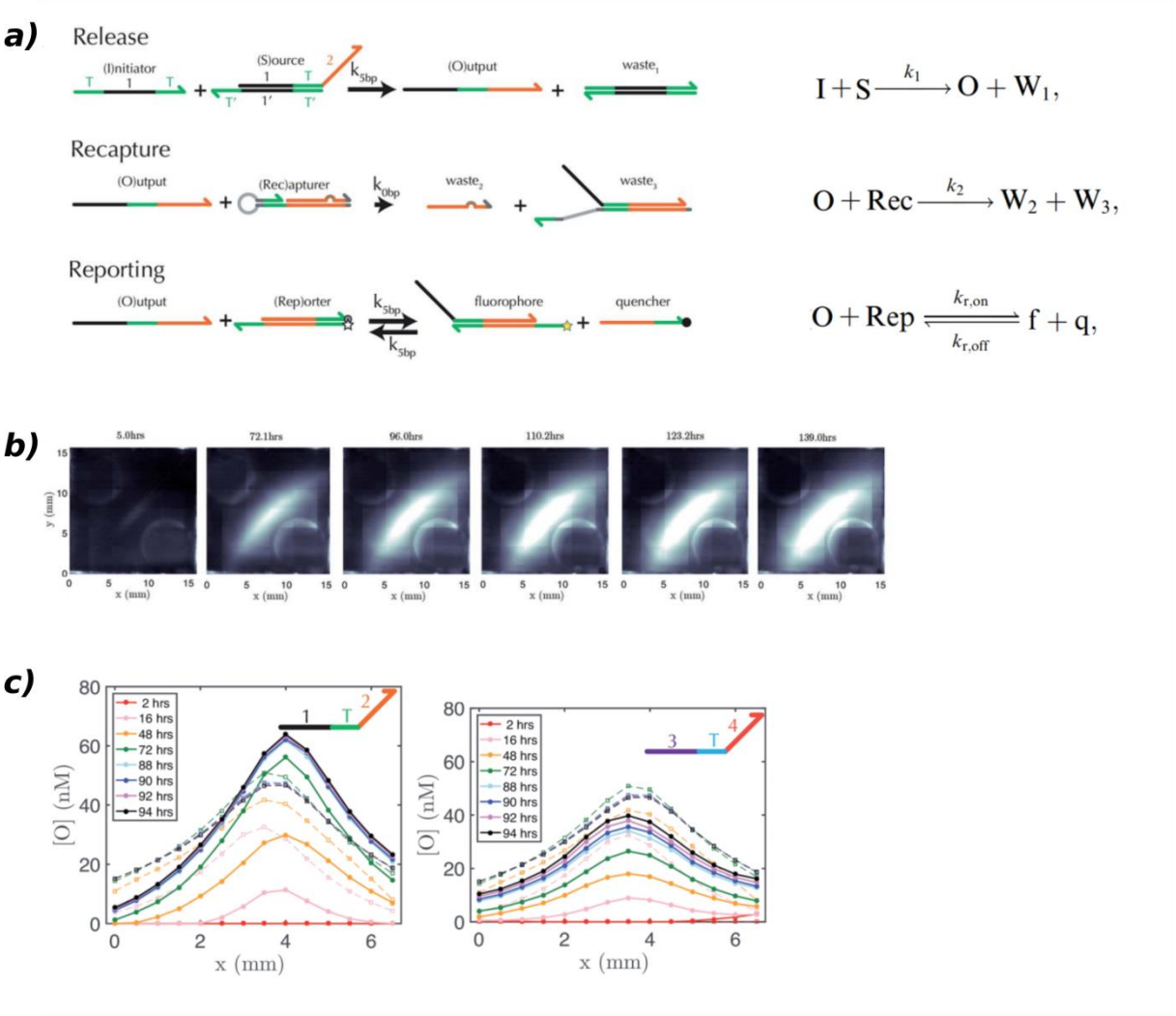

Figure 1.28. Stable two-dimensional DNA RD patterns: (a) strands displacement reactions enabling patterns formation and reporting strategy (left) and their principle schemes (right). Note, that arrows length on the left part represent relative values of reaction rates; (b) fluorescence images of progressive patterns formation from 5 hours (left) to 139 hours (right); (c) simultaneous formations of patterns in two systems with orthogonal sequences. Figure was taken with modifications from [60].

1.5 Conclusion

This chapter presents an overview of CRNs and their artificial analogues. We have shown that a certain number of fully synthetic with rich dynamics DNA based CRNs in vitro were created and that they, furthermore, enable complex spatiotemporal behaviour due to RD. These technologies will help us to better understand the basic principles of functioning living organisms and eventually even to answer the ambitious question about the origin of life. Moreover, one can imagine several potential uses where they could be applied. Among them, we can list the development of new type of biosensors, molecular diagnostics, therapy or controllable self-assembly of smart materials.

Created by computer scientists and biochemists, and as a result employing the typical analytical operations of the trade such as pipetting, these promising technologies lack the methods of real time interaction and control, which limits their applicability. Furthermore, it is clear that such methods must be compatible with RD systems in order to control their spatiotemporal behavior and fully exploit the potential of this field.

The aim of this thesis work was to attempt to provide technological means to solve these problems by relying on a combination of microfluidics, surface- and electrochemistry, which provide both time and spatial control of RD systems, based on biochemical CRNs and allow keeping a reasonably small size of the working devices, and, consequently, their cost.

Chapter 2

Methods

2.1 Introduction

In this chapter, we will introduce the different techniques that we used over the course of the present study as well as essential theoretical background needed in order to design our experiments and interpreted the obtained data.

A first section will be dedicated to the description of electrochemical methods applied to characterize and confirm surface functionalization and DNA grafting used in the following chapters. In particular, we will demonstrate how to use them in order to make optimized active DNA-gold surfaces and estimate the density of their coverage. In addition, electrochemistry will be used for controllable cleavage of Au-S bond, which is essential for the elaboration of surface-attached DNA-activator. Next, we will discuss the basic theoretical principles behind fluorescence phenomenon and, particularly, fluorescence quenching. We will also show how it can be applied in order to monitor DNA hybridization events in both, sequence specific and non-specific ways. Next, we will briefly introduce fluorescence microscopy analytical method, as it was the main technique applied to conduct experiments in microfluidic channels.

Finally, a detailed description of the PEN toolbox will be provided. We will discuss the step-by-step implementation and characterization achieved in our laboratory, from the elementary modules, activation and autocatalysis, to the complex dynamical circuits, such as oscillator and invention module.

In this project/study, we used electrochemical methods for two main purposes. First, in order to perform qualitative and quantitative characterization of DNA-gold surfaces. Second, we used electrochemistry for controllable cleavage of Au-S bond, essential for elaboration of surface-attached DNA activator, which will be in details discussed in subsequent chapters.

2.2 Electrochemical methods

Electrochemical science can be broadly divided in two parts according to the aspects, which are investigating [83]. From the one hand, electrochemistry studies ionic aspects, *i.e.* the objects of research are ions of an electrolyte in liquid phase (liquid, dissolved, or melted electrolyte) under conditions of applying an electric current. From the other hand, electrochemistry studies electrodics aspects, *i.e.* it concerns the region between an electronic and ionic conductor and the handover of electricity across it.

Usually, in electrochemistry, a three-electrode cell is used. It includes a polarizable working (or indicator) electrode (WE), an auxiliary (or counter) electrode (through which electric current flows) and finally a reference electrode, which is necessary for monitoring the potential of the working electrode. However, two electrodes based electrochemical cell can be used as well in cases when it is not necessary to maintain strictly constant the potential of the working electrode.

Electrochemical process (electrolysis) is carried out for a comparatively short time (from several seconds to several minutes) on working stationary electrode, which can be made of platinum, graphite (or other carbon based conductive materials), mercury or gold. Solution is not mixed and contains so much excess of the background electrolyte that the ionic strength practically does not depend on the concentration of the electrochemically active substance studied.

The reference electrode is usually a saturated calomel or silver chloride electrode that remains unpolarized during the measurements. Its potential is maintained constant regardless of the small values of current passing through the cell. The counter electrode is usually made of platinum or graphite materials.

2.2.1 Electrochemical characterization of DNA-covered gold surfaces

In order to proof the attachment of DNA-thiol on gold surface we used cyclic voltammetry and chronocoulometry.

Cyclic voltammetry (CV) is an electrochemical method, in which the potential is permanently changing. It belongs to the so-called potentiodynamic electrochemical methods. Changing of potential between the electrodes happens in a following way: initially potential

increases up to reaching a certain value (defined by operator), and after that linearly decreases in a reverse direction until reaching the initial value and forms a cycle. The cycle can be repeated many times and the scan rate can be modulated. Electrical current is recorded as a respond on changing potential. Current in CV is usually limited by the diffusion of the redox molecule to the surface of the working electrode. To satisfy this condition, the electrolyte is not stirred and microelectrodes are usually used. This allows to study on the same time oxidized and reduced form of the redox molecule of interest.

CV can be used to characterize surface chemistry of the working electrode and all events taking place in the surrounding environment, in particular, it's a very accurate method to assess DNA-gold self-assembled monolayers (SAM) [84]. DNA molecules attached on gold surface lead to negative surface charges thus repulsing negatively charged redox species (fig. 2.1). Consequently, redox reaction on working electrode will be prevented. This will have a strong impact on the CV curve shape. In addition, this impact depends on surface coverage and on the concentration of the redox marker.

We applied this method in order to obtain preliminary verifications of DNA attachment to the gold surface. Figure 2.1 illustrates results of CV experiment obtained from bare and DNA covered gold electrode in presence of 10 mM redox marker, potassium ferrocyanide $K_3[Fe(CN)_6]$. On the working electrode surface, the following reaction can take place:

$$[Fe(CN)_6]^{3-} + e^- \rightleftharpoons [Fe(CN)_6]^{4-}$$

When bare gold electrode was used, the characteristic peaks for this redox couple were observed at ~0.15 V (cathodic current) and 0.3 V (anodic current) (fig. 2.1). However, they subsequently disappeared when DNA covered gold electrode is used instead. These results confirmed the successful DNA attachment on gold WE. We will discuss in details the surface functionalization and its characterization in section 3.2.

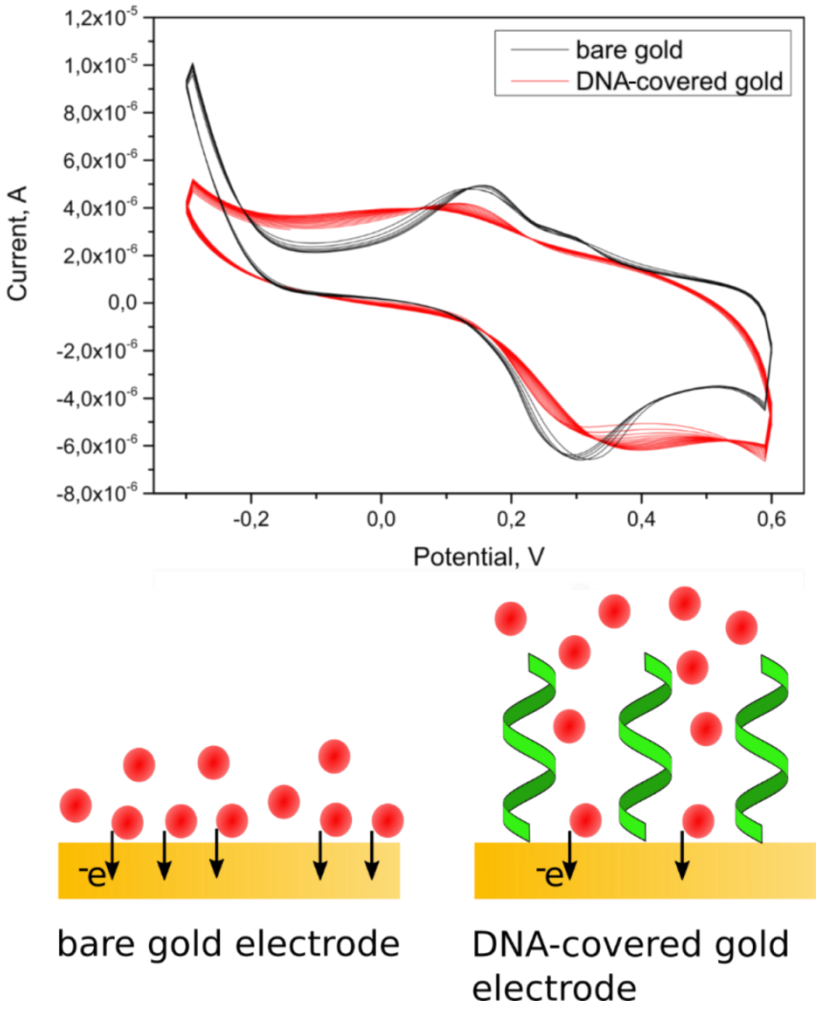

Figure 2.1. (up) Cyclic voltammetry curves, obtained using gold working electrode before and after DNA functionalization. Scan rate 0.1 V/s in 10 mM $K_3[Fe(CN)_6]$ and 10 mM KCl. Ag/AgCl counter electrode. (down) Schematic representation of principle of evolution of CV signal between bare and DNA-covered gold surfaces.

The principle of chronocoulometry (CC) is very similar to chronoamperometry (CA). In both techniques, the potential is instantaneously changed and maintained constant during the step time. In other words, these techniques are potential-controlled. The only difference is that, in CC, it is monitoring a resulting cumulative charge as a function of polarization time after applying the potential to the working electrode and not based on the measurement of current. However, the data obtained in CA can be converted in CC data through integration of the current values.

The solution usually contains a redox active substance such as ferrocyanide, ruthenium hexaaminochloride *etc*. By applying the potential, the electrolysis of this compound is initiated.

This process can occur in one direction (single potential step experiment) or be reversible due to application of a reverse potential (double potential step experiment).

Changing the current (and, consequently, the charge) after applying a potential, $\boldsymbol{E}$, follows the Nernst equation:

$$\boldsymbol{E} = \boldsymbol{E}^{\circ} + \frac{0{,}059}{\boldsymbol{n}} \log \frac{\boldsymbol{C_0^s}}{\boldsymbol{C_R^s}}$$

where E° is the formal redox potential for a given redox reaction, n is the number of electrons in the redox process, $\boldsymbol{C_0^s}$ and $\boldsymbol{C_R^s}$ are the concentrations of oxidized and reduced forms present on the working electrode surface, respectively. Applying the potential leads to the conversion between these two forms and the subsequent flow of electrons, *i.e.* electrical current.

CC can be successfully applied for studying molecules, which are adsorbed on the working electrode surface. The particularity of it is that electrolysis time in CC depends on distance between redox molecule and working electrode. While it is adsorbed on working electrode surface, electrolysis happened instantaneously after applying the potential. This charge is time independent. In another hand, redox species in solution must diffuse to the working electrode surface to be electrolysed and this process takes time. That is why, charges in CC, due to electrochemical conversion of adsorbed and dissolved redox molecules are distinguishable. Total charge is defined by three components: charge of adsorbed molecules, $\boldsymbol{Q_{ads}}$, charge of diffused molecules, $\boldsymbol{Q_{diff}}$, and charge of the electrical double layer, $\boldsymbol{Q_{dl}}$.

$\boldsymbol{Q_{total}} = \boldsymbol{Q_{ads}} + \boldsymbol{Q_{diff}} + \boldsymbol{Q_{dl}}$

These components are illustrated in fig. 2.2. One can see that the slope of the curve is defined by the diffusion component, while height is defined by the adsorption and the electrical double layer components. Thus, the intercept is a sum of $\boldsymbol{Q_{ads}}$ and $\boldsymbol{Q_{dl}}$. By subtracting $\boldsymbol{Q_{dl}}$ from intercept, $\boldsymbol{Q_{ads}}$ can be found. In order to observe a double layer change, CC experiments are usually conducted in supporting electrolyte without redox species. In this case $\boldsymbol{Q_{ads}} + \boldsymbol{Q_{diff}} = 0$ and $\boldsymbol{Q_{total}} = \boldsymbol{Q_{dl}}$.

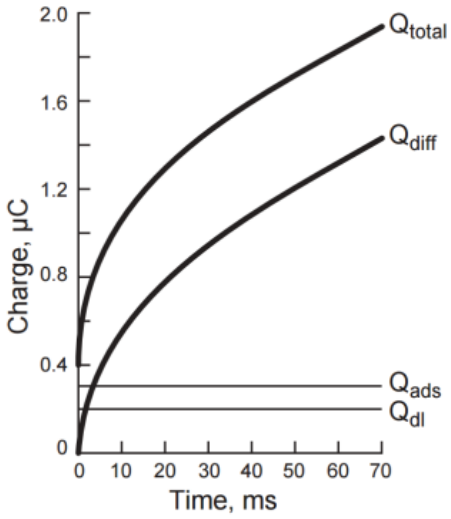

Figure 2.2. Charge as a function of the polarization time for total charge (Q_{total}) and individual components. Figure was taken from http://www.currentseparations.com/issues/20-4/20-4e.pdf.

Tarlov *et. al.* have demonstrated that thanks to CC measurements, one can determine the DNA surface coverage [85]. Since DNA molecules in solution are negatively charged due to the presence of phosphate groups, it can be associated with positive ions in order to compensate negative charge. Thus, the higher cationic charge is, the stronger the interaction with DNA is. Amount of DNA molecules on working electrode surface is defined by the amount of adsorbed redox species.

Anson equation describes the total charge as a function of polarisation time:

$\boldsymbol{Q = 2nFAC_0\sqrt{\frac{D_0 t}{\pi}} + Q_{dl} + nFA\Gamma_0}$. Where $\boldsymbol{n}$ is the number of electrons per molecule for reduction, $\boldsymbol{F}$ the Faraday constant (C/mol), $\boldsymbol{A}$ the electrode area (cm^2), $\boldsymbol{Do}$ the diffusion coefficient (cm^2/s), $\boldsymbol{C_0}$ the bulk concentration (mol/cm^3), $\boldsymbol{Q_{dl}}$ the capacitive charge ($\boldsymbol{C}$), and $\boldsymbol{nFA\Gamma_0}$ the charge from the reduction of $\boldsymbol{\Gamma_0}$ (mol/cm^2) of adsorbed redox marker.

At $\boldsymbol{t}$ = 0: $\boldsymbol{Q = Q_{dl} + nFA\Gamma_0}$. In absence of redox marker and $\boldsymbol{t}$ = 0: $\boldsymbol{Q = Q_{dl}}$. Consequently, difference between $\boldsymbol{Q}$ values at $\boldsymbol{t}$ = 0 for two identical chronocoulometric experiments with and without redox marker will be equal to $\boldsymbol{nFA\Gamma_0}$ **.**

When redox molecule is taken in excess, and that all DNA charges are compensated, the surface density, $\boldsymbol{\Gamma_{DNA}}$ ($molecules/cm^2$), can be defined as: $\boldsymbol{\Gamma_{DNA} = \Gamma_0(z/m)N_A}$, where $\boldsymbol{m}$ is the number of bases in adsorbed DNA molecule, $\boldsymbol{z}$ is the charge of the redox molecule, and $\boldsymbol{N_A}$ is the Avogadro's number.

We applied this approach as an alternative method for the determination of the thiol-conjugated DNA density on active surfaces.

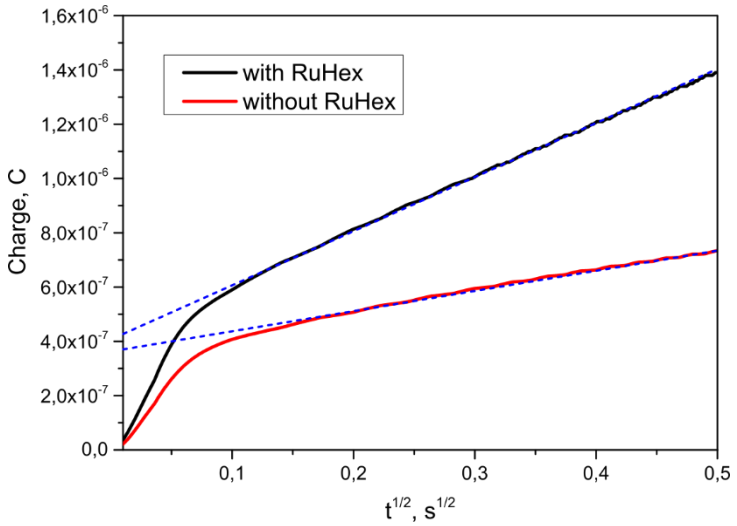

Figure 2.3. Chronocoulometric response curves for DNA covering gold surface in absence (red curve) and in presence (black curve) of 50μM of RuHex.

From fig. 2.3, we have obtained: $\boldsymbol{nFA\Gamma_0}$ = $4.3\cdot10^{-7} - 3.7\cdot10^{-7} = 6\cdot10^{-8}$ (C). For the redox reaction, which was taken place in the experiment, $[Ru(NH_3)_6]^{3+} + e^- \leftrightarrow [Ru(NH_3)_6]^{2+}$, $\boldsymbol{n}$ = 1. Electrode surface area, $\boldsymbol{A}$, was equal 0.2 cm^2. Consequently, $\boldsymbol{\Gamma_0} = 6\cdot10^{-8}/\boldsymbol{nFA} = 6\cdot10^{-8}/1\cdot96485\cdot0.2 = 3.1\cdot10^{-12}$ mol/cm^2. The DNA surface density was calculated by introducing the formula:

$\boldsymbol{\Gamma_{DNA}} = \boldsymbol{\Gamma_0(z/m)N_A} = 3.1\cdot10^{-12}\cdot(3/11)\cdot6.02\cdot10^{23} \approx \mathbf{10^{12}}$ (molecules/cm^2).

Obtained value which is in line with previously reported values for DNA-thiol SAM on gold [86].

2.2.2 Electrochemical desorption of DNA from the gold surfaces

With the goal to construct DNA activators, we aimed to realise controllable surface release of these molecules. For this purpose, we applied cyclic voltammetry and chronoamperometry techniques.

The redox reaction on DNA-gold SAM can occur in absence of any external marker due to oxidation and reduction of nucleotides, especially of dGMP and dAMP [87]. This particularity was applied in order to perform preliminary estimations of the potential value needed to release the attached DNA molecule from gold surface (fig. 2.4).

Desorption of thiolated DNA is taking place due to the following electrochemical reaction: ***Au-S-X*** + $^{-}$***e*** = ***Au*** + $^{-}$***S-X***, where ***X*** represents the DNA part of the molecule, attached to the thiol linker.

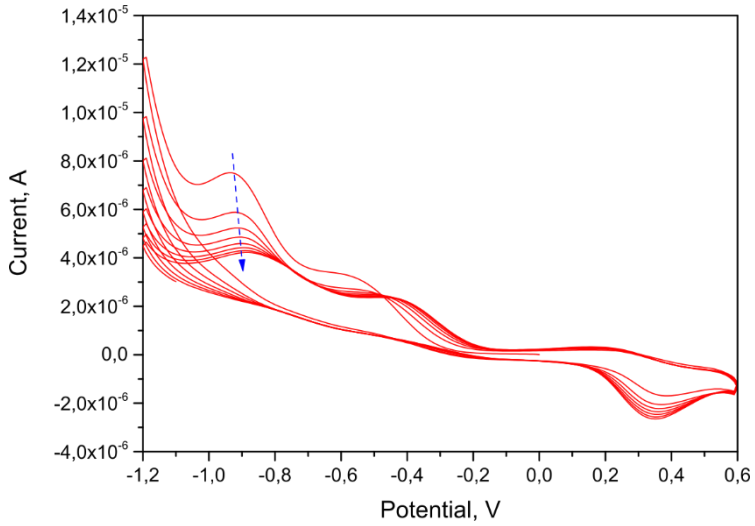

Figure 2.4. Cyclic voltammetry desorption of DNA-gold SAM from the working electrode surface. Scan rate 0.1 V/s in 10 mM KCl.

These data indicate a damping of the peak at ~ -0.9 V *vs* Ag/AgCl, corresponded to the attached DNA with each subsequent scan (9). Consequently, a potential value of -1.2 V *vs* Ag/AgCl was enough for the electrochemical desorption of DNA from the gold surface. It has to be noticed that the desorption potential will be accurately tuned due to the applied conditions (see section 3.2.1).

Chronoamperometry (CA) is an electrochemical method, which studies the dependence of current, flowing through the electrochemical cell, to the polarization time at a certain value of potential of the polarised electrode. This potential can be maintained, for example, with the help of a potentiostat and changed sequentially. Thus, the current will be measured as a response on potential stepping.

The value of current, obtained from CA, is mainly determined by the speed of the diffusion transfer of substances participating in the electrochemical process or by the kinetics of the electrochemical reaction.

CA is mainly used to study the kinetics and mechanism of electrode reactions, as well as to determine the amount of electricity in electrolysis.

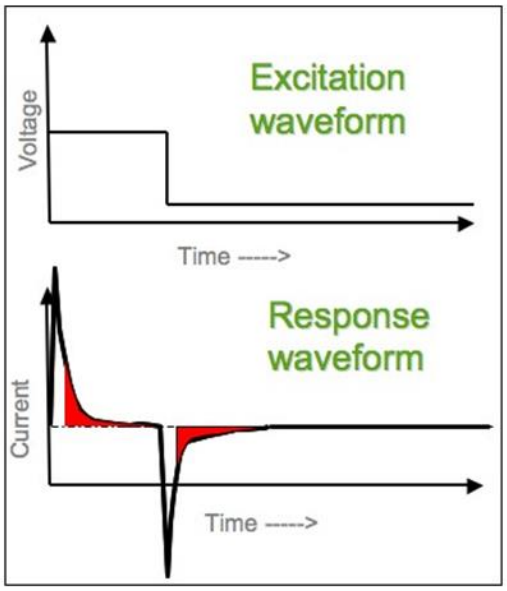

Figure 2.5. Stepping of the potential in CA (up) and electrical current profile as function of polarisation time under applied voltage values (down). Figure was taken from [88].

We have applied CA for the routine desorption of attached DNA from gold electrode surface (fig. 2.6).

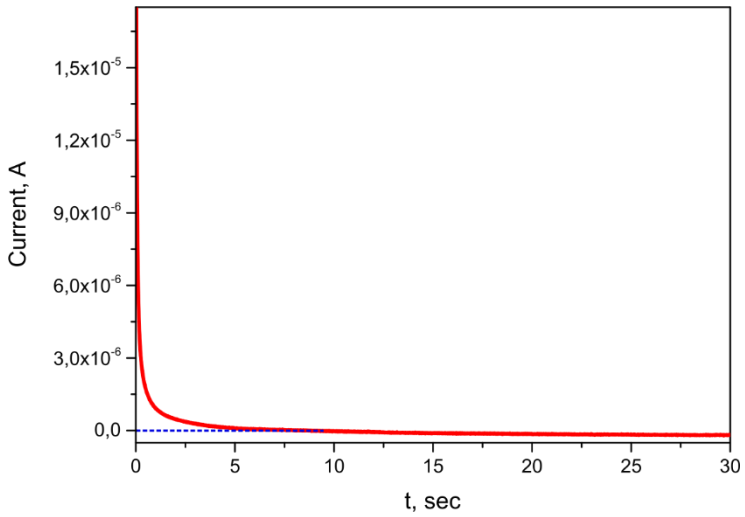

Figure 2.6. Release of DNA-thiol from gold surface at -2V (*vs* Au) in function of time measured by chronoamperometry.

From these data, we can see that DNA desorption occurs very fast, since current reaches 0 value within 5-6 seconds. Consequently, this time supposed to be sufficient for the complete desorption under given conditions. However, in order to maximize the desorption rate in

experiments, described in further chapters, we have usually performed CA during 20-30 seconds.

2.3 Fluorescence phenomenon

Fluorescence measurement was also used within this study to monitor our experiments. In this section, we will briefly discuss the elementary theoretical principles, which are behind the fluorescence phenomenon. Then, we will see afterwards the instrumental method to observe and measure it, that we applied for the majority of our experiments.

The basic principle of fluorescence is presented in fig. 2.7. Briefly, electrons from atom or molecule are capable to absorb light energy (photons) that is followed by the change their own energy state (excitation state). After a short time period (nanoseconds), electrons return to their initial energy state with emission of photon (relaxation). This emission is called fluorescence. Light absorption level and subsequent emission depend on energy levels of electrons in the considered molecule. Light absorption-emission ratio (quantum yield) cannot be 100% efficiently process, since a part of the photon energy is lost. Therefore, the energy of emitted photons is lower than the energy of the absorbed photons. Practically it means, that emitted light has longer wavelength ($\boldsymbol{E \sim \frac{1}{\lambda}}$) than the excitation light. What is more, the longer distance between these two wavelengths (which is called Stokes shift) for a given fluorophore, the more suitable for analytical application it is. From the point of view of chemical structure, fluorescence is possible in molecules, thanks to π-conjugated system (mainly aromatic and heterocyclic structures) which allows electron delocalization. They often contain as well (fig. 2.9).

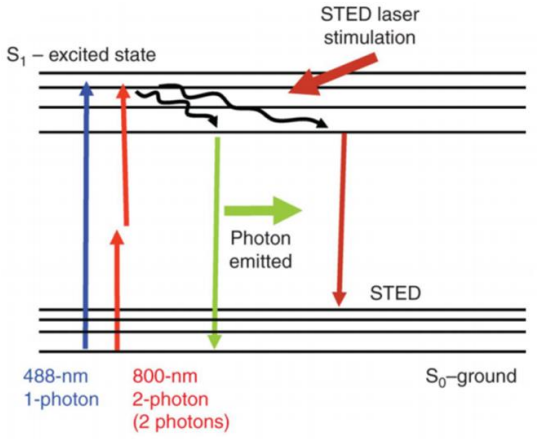

Figure 2.7. Basic principle of the fluorescence phenomenon. Transition from the ground to the excited state requires absorption of one photon at 488 nm or simultaneously absorption of two photons at 800 nm. Reverse transition due to relaxation, emits light at higher wavelength (lower energy).

2.3.1 Fluorescence quenching

Emitted fluorescence can be quenched by several mechanisms. In the present study, we used quenching by fluorophore molecules as well as by gold surface and by DNA bases. Behind all these processes for distance <10 nm is a phenomenon, called Förster resonance energy transfer (FRET) [89]. Its principle is as follows. After excitation of the "donor" fluorophore molecule, the received energy can be transferred to an "acceptor" without emission of a photon (non-radiative decay) when the excitation spectrum of the acceptor overlaps the emission spectrum of the donor. The role of acceptor can play by d-metal atoms such as gold [90]. Distance between the donor and acceptor is crucial for fluorescence quenching [91]. For this reason in normal fluorescence dye solution, no quenching is taking place (although excitation and emission spectra might substantially overlaps), since the distance between the molecules is not close enough. In contrast, when two fluorophore molecules of the same or different kinds with overlapping excitation and emission spectra are connected *via* alkyl or another linker, the shorter distance between them became sufficient to allow quenching.

Figure 2.8 describes the working principle of non-selective monitoring of PEN toolbox, based on Eva Green fluorescence dye. Its excitation and emission spectra have overlapping region between ~490 and 530 nm. Consequently, FRET is possible. Molecular structure of Eva Green is represented in fig. 2.9 a. One can see that its molecule consists of two acridine rings,

connected with a short linker. These structures can reversibly bind to each other due to the π-π stacking. In this case, inactive, self-quenched, Eva Green state is formed. When double-stranded DNA is present in solution, π-π stacking between DNA and acridine rings became more energetically beneficial than internal coupling. As a result, active dye form became more stable and leads to the enhancement/recovery of the fluorescence intensity.

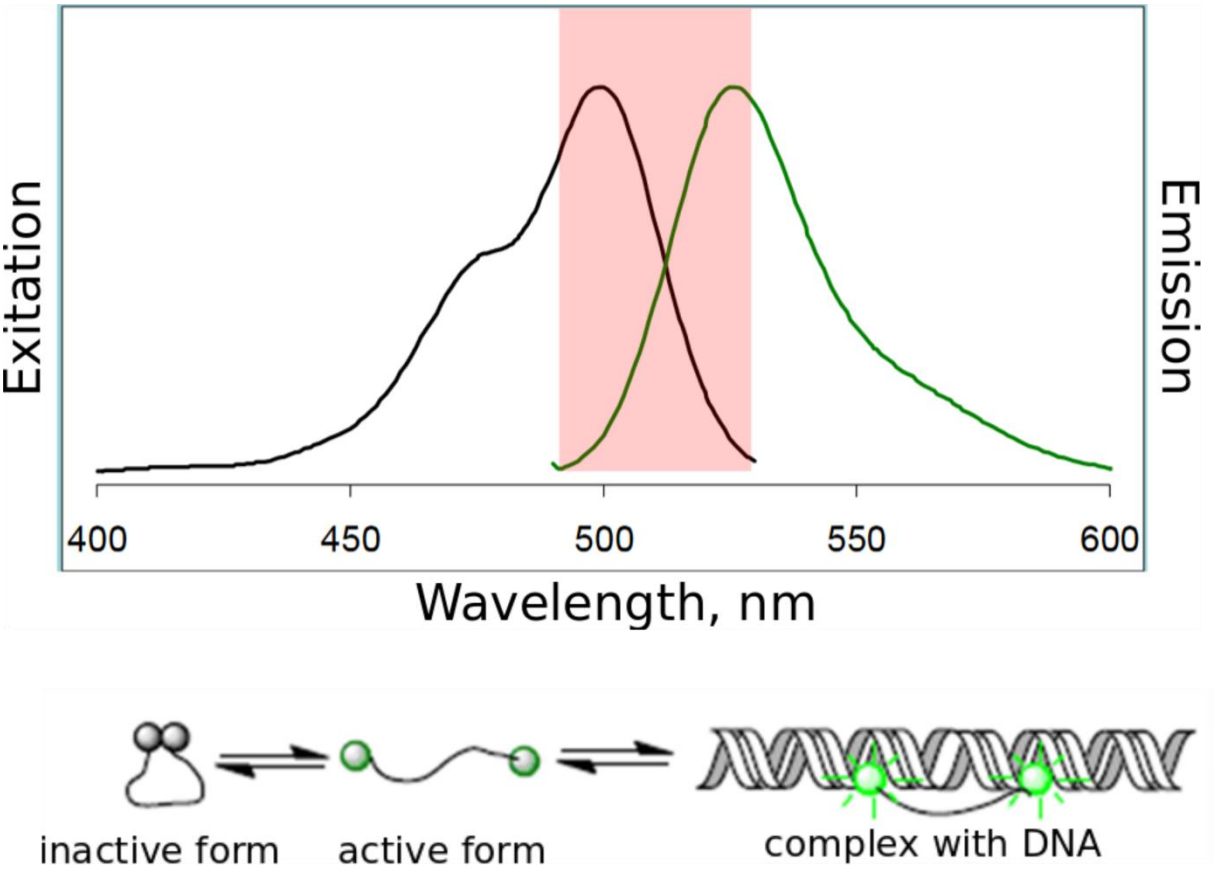

Figure 2.8. Principle of functioning of the Eva Green fluorescence dye. Overlapping between the emission and excitation spectra (marked in red colour) allows self-quenching (up). In absence of DNA, Eva Green is dynamically quenched due to the equilibrium between active and inactive forms. Binding to DNA, will stabilize the active dye form, leading to the enhancement of the fluorescence signal.

Finally, quenching can take place due to the charge transfer between nucleobases and attached fluorophore [92]. The fluorescence shifts upon attachment to the complementary strand and this quenching method can be applied for monitoring DNA hybridization. By attaching the fluorophore at the end of specific sequence, it is therefore possible to detect one complementary strand to this sequence when present in solution. This is useful to obtain a sequence specific monitoring strategy by contrast to Eva Green, which only monitors the total amounts of double strand DNA.

Thus, the intensity recovery can be either positive (terminal G-C bp) or negative (terminal A-T bp) and not all the fluorophores shows any fluorescence changing upon the hybridisation event [93]. We used in this study DY-530 fluorophore (fig. 2.9 d), which is well suitable to this purpose [94].

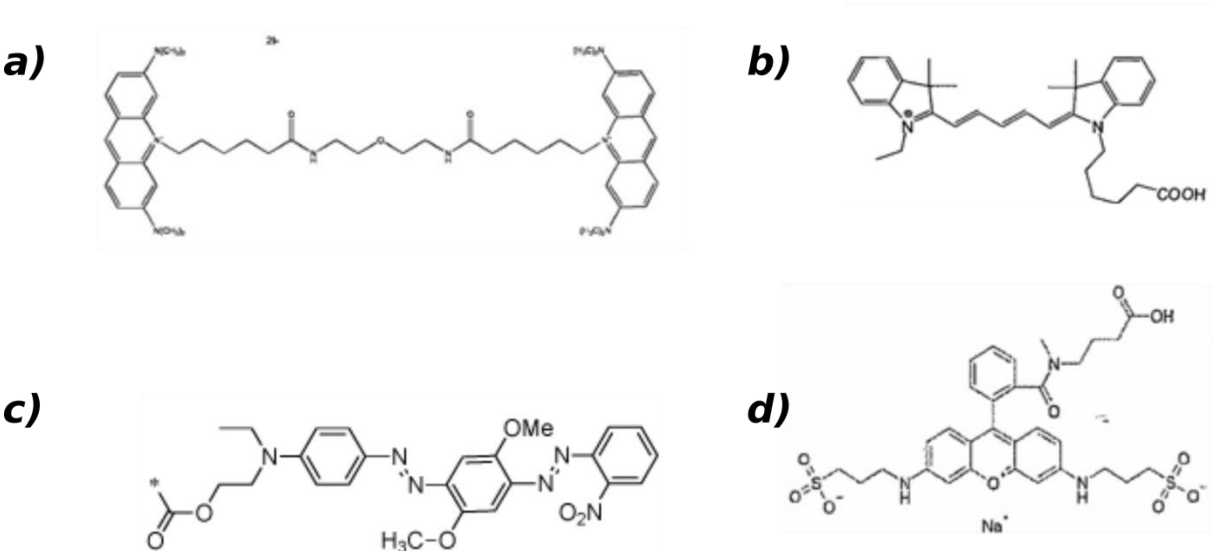

Figure 2.9. Chemical structures of fluorophores and quenchers, used in the present study. (a) Eva Green, (b) Cy-5, (c) BHQ-2, (d) DY-530.

2.4 PEN DNA Toolbox

PEN DNA toolbox relies on a combination of short DNA strands and set of enzymes to create dynamical system, which can be used for information processing. In this section, we will discuss in more details its main components and principles of functioning.

First of all, PEN toolbox is composed by 3 enzymes: polymerase, exonuclease and nickase, each of which has a having very specific function. As an example, different domains of exonuclease ttRecJ used in the present study are illustrated in fig. 2.10. One can see that this kind of biomolecules is fairly complex with a quaternary folding with 4 subunits giving enzymatic activity. In this way, ttRecJ can selectively recognize single-stranded DNA in a non-sequence specific manner and decompose it from 5’ end to 3’ end.

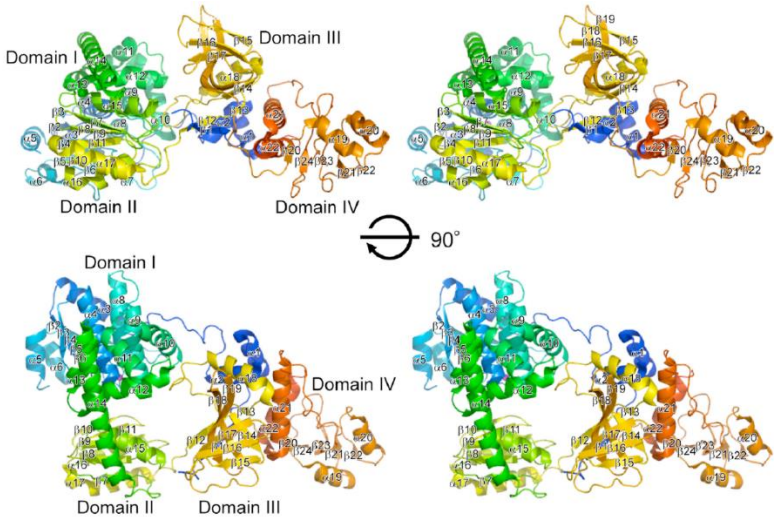

Figure 2.10. 3D structure of ttRecJ exonuclease, used over the course of the present study, which provides selectivity to the single-stranded DNA degradation in 5' to 3' direction.
Fig was taken from [95].

Next, PEN toolbox has 3 basic modules, which are encoded with DNA strands: activation, inhibition and autocatalysis. Thus, the last one can be considered as a particular case of the activation. Functioning of this framework is carried out with the three enzymes mentioned above. Reactions are kept far from equilibrium through continuous synthesis and degradation of DNA species by exonuclease thus consuming reaction "fuel" – a mixture of 4 deoxynucleotides (dNTPs).

Activation

Activation module (fig. 2.11 a) encodes by normal DNA template molecule. The first part of this module is complementary to the short DNA input, which is able, in case of hybridization, to activate production of output DNA, encoded by the second half of the template sequence. The activation module steps are the following. First of all, the input gets elongated by polymerase leading to new DNA molecules that are then cut by nickase enzyme thus regenerating the input and producing the output.

Inhibition

In this case, the DNA strand inhibitor is only partially complementary to the template. However, it is enough to prevent hybridization of new input molecule (fig. 2.11 b). In addition, since mismatches are present on the inhibitor 3' end. In that case, polymerase cannot perform elongation reaction and thus no output can be produced. The template remains temporarily blocked until inhibitor strand is eventually degraded by exonuclease, as there is an equilibrium between its single- and double-stranded states under the reaction conditions.

Autocatalysis

The principle of the autocatalysis module (fig. 2.11 c) is analogous to the activation one. The only difference is that the template strand consists of two repeatable sequences. Consequently, the output is the same DNA molecule as the input. The more input is produced, the faster reaction is, until reaching saturation. That is why this module is called autocatalysis.

Input, output and inhibitor strands are continuously degraded by exonuclease. It is not the case for the templates, because they are protected from exonuclease by introducing in their molecules 3 phosphorothioate (PTO) modified bases on the 5' end.

Reactions are performing under the temperatures, close to melting temperature of input-template and output-template double stranded DNA since reversible hybridization is crucial for functioning the framework. Elongated input is unlikely to melt and, since this process requires the highest temperature. Consequently, only nickase can release a new strand.

Output from one elementary reaction can serve as an activator or inhibitor for a downstream process, which provides modularity of the PEN toolbox and allows elaboration of complex circuits.

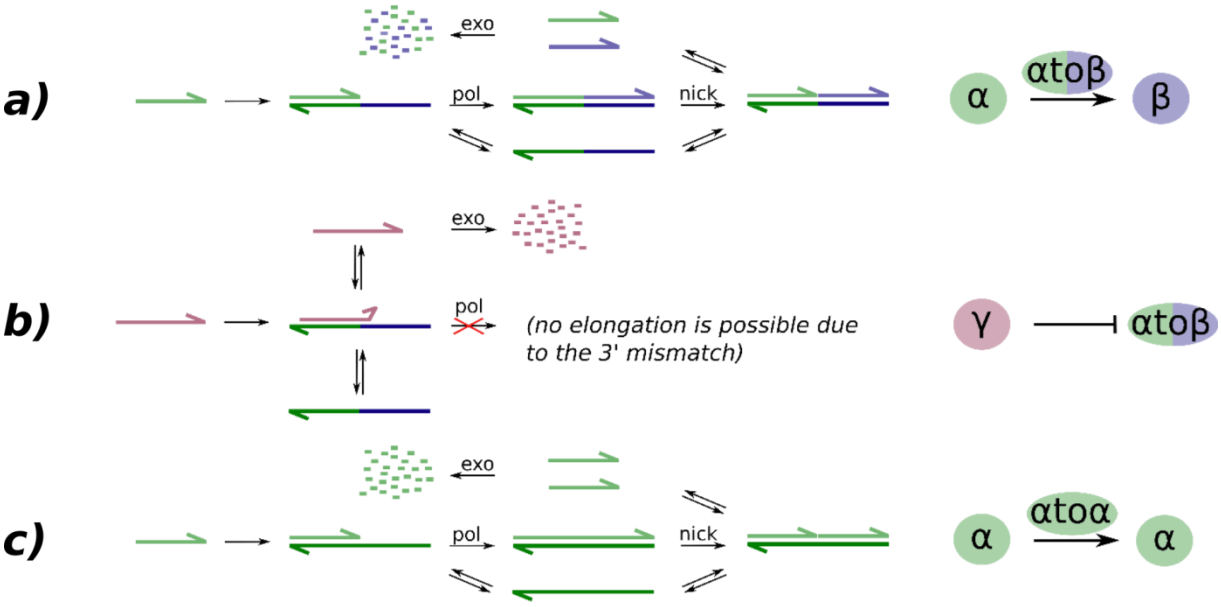

Figure 2.11. Basic modules in PEN toolbox reactions (left) and their schematic representation (right). (a) Activation. (b) Inhibition. (c) Autocatalysis.

In the next sections, we will discuss in details the process for developing the PEN toolbox in our laboratory, characterization of its elementary modules and, finally, we will demonstrate some successful attempts by building complex dynamical circuits.

2.4.1 Determination of the melting temperature

Temperature is a crucial parameter for the proper functioning of the PEN toolbox. For the simple autocatalytic reaction, which was chosen as a starting point for our experiments, it must be selected to be close to the melting temperature (temperature under which 50% of DNA duplex is dissociated) of input-template double-stranded complex. Then, it allows dissociation of this DNA duplex and then releasing input, now free to participate in the subsequent reaction. On the same time, it will provides a sufficiently long living time to make possible polymerase action. Additionally, such choice of the reaction temperature maintain elongated input in double-stranded form thus making possible its dissociation only after nickase cutting in two parts with lower melting temperatures. Otherwise, reaction mixture would be quickly contaminated with this intermediate, which will uncontrollably interfere on the system behavior.

In this way, we recorded a melting curve of autocatalytic template-input double-stranded DNA (fig. 2.12 up) in order to select the optimized working temperature for further experiments. The obtained data were then processed to build a graph/curve of negative first derivative of intensity in function of the temperature, -d(I)/dT, (fig. 2.12 down) which is the standard method to facilitate the determination of the melting temperature.

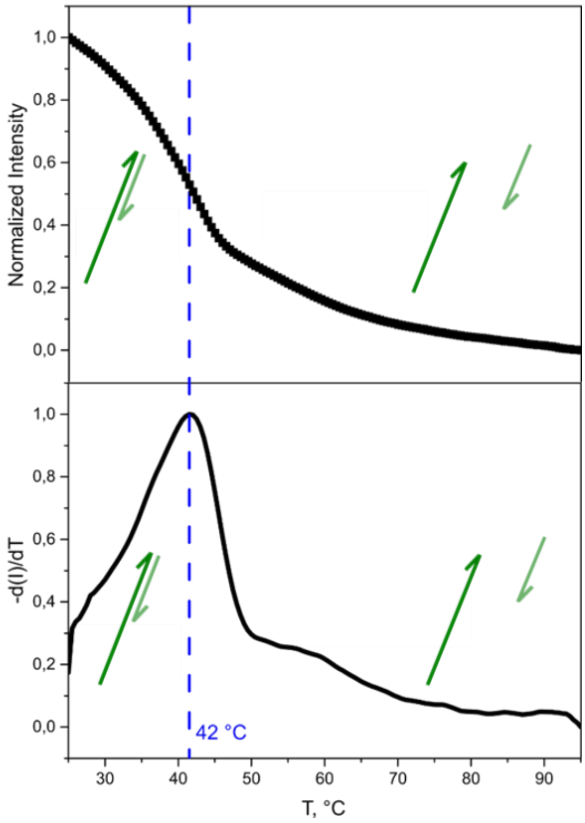

Figure 2.12. Determination the melting temperature. (Up) melting curve in coordinates I(T). (Down) in coordinates –d(I)/dT(T), received by processing these data. Solution contained 100 nM of input and 100 nM of template in TE buffer.

The obtained value of 42°C, was then chosen as a working temperature for experiments with simple autocatalysis. Although we used 2 different systems of this kind, they both comprised inputs with the same length (11 nucleotides) and with the same number of [G + C] bases, 5, which strongly influence the melting temperature. For this reason, we did not change the obtained temperature value, while launching simple autocatalytic reactions, based on different template sequences.

2.4.2 Effect of concentration of DNA input on kinetic of autocatalysis

After having defined the working temperature, we launched an autocatalytic reaction with a range of input concentrations ranging from 0 to 3 nM and a fixed concentration of template (fig. 2.13). The reaction buffer is composed of 50 mM NaCl, 10 mM $(NH_4)_2SO_4$, 10 mM KCl, 8.4 mM $MgSO_4$, 0.8 mM of each dNTP [New England Biolabs (NEB)], 0.1% Synperonic F108

(Sigma-Aldrich), 500 μg/mL BSA (NEB) and 2 μM of Netropsin (Sigma-Aldrich). Unless otherwise indicated, the same parameters were used for all other experiments described in the following sections.

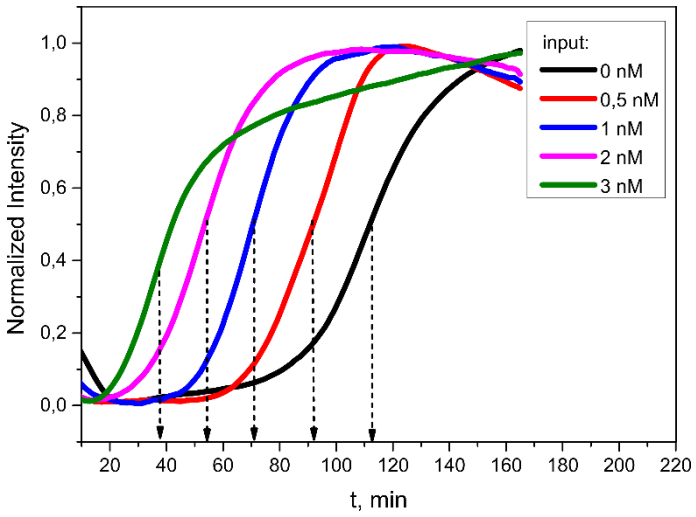

Figure 2.13. Influence of input concentration on kinetic of the autocatalysis. Each solution contained 50 nM template, 1% of polymerase, 2% of exonuclease and 3% of nicking enzyme. The temperature was 42 °C.

Data clearly indicate speed-up of the exponential amplification by increasing the input concentration. This finding allows us to make quantitative estimation of input concentration in the initial reaction mixture. Importantly, autocatalytic reaction occurs even when no input is added (fig. 2.13, black line). This phenomenon can be referred as a self-start, happening due to the system metastability, which is caused by spontaneous DNA synthesis from the template and polymerase. Since reaction is autocatalytic and input is producing in avalanche-like way, even traces of it input is enough to eventually trigger it. This particularity and practical issues will be discussed in details in chapters 3 and 4.

Although starting time of exponential intensity growth, ***t***, decreases with increasing concentration of input, ***C***, their relation, ***C(t)*** is not linear (fig. 2.14 a). In general case, this relation depends on reaction order. By knowing it we can better understand the mechanism of the system on which we are working with and make quantitative analyses of solutions with unknown input concentrations (fig 3.5). For the reaction A+B = C+D, its speed, ***V***(or ***dC/dt***), is equal $\boldsymbol{k}[C]^{x}[D]^{y} = \boldsymbol{k}([C][D])^{n}$, where ***k*** – constant of reaction speed, [C] and [D] – concentrations of products, ***x*** and ***y*** – partial reaction orders. In this case, reaction order, ***n***, is equal ***x*** + ***y***. Reaction order can be determined only experimentally and is defined by reaction mechanism. It shows the number of chemical species, concentration of which is changing over the course of the reaction. The easiest way to determine it, is to build graphs with variation of

C, ln(C) and (C^{-1}) in function of time. If one of them is linear, the order of the reaction will be 0, 1 or 2, respectively. This methods derives from the integration of the equation for the reaction speed, which was showed above, with different values of ***n*** (= ***x***+***y***)

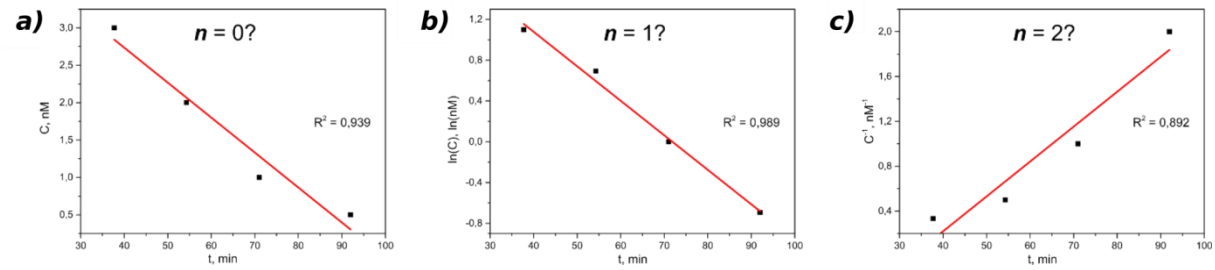

Figure 2.14. Graphical method of finding the reaction order for the autocatalytic reaction. Linear behavior of the curve b) shows that the reaction order is equal 1.

Using data from fig. 2.13, we built 3 graphs in coordinates ***C(t)***, ***ln(C)(t)*** and ***C^{-1}(t)*** in order to verify whether or not the reaction order value is equal 0, 1 or 2 respectively. ***ln(C)(t)*** (fig.2.14 b) is mostly straight line (R^2 = 0.989), which is not the case for two other graphs (***C(t)***: R^2 = 0.939; ***C^{-1}(t)***: R^2 = 0.892). Therefore, the order of the autocatalytic PEN toolbox reaction is one. Several important consequences derive from this.

Firstly, ***n*** = 1 means, that under our conditions, no side products, such as "parasite" species (see section 2.4.5) are formed. Secondly, the template concentration was stable: neither degradation by exonuclease nor other undesired processes were taking place. Thirdly, enzymes concentrations were stable as well. Finally, by knowing the way to obtain a linear relation between ***C*** and ***t*** allows us to apply external standard method for the analysis of the input solutions with unknown concentrations.

2.4.3 Effect of template concentration on kinetic of autocatalysis

Although it is kept constant over the course of the process, the starting template concentration has a strong impact on reaction kinetics. In fig. 2.15 are displayed results obtained from experiments for the triggering of autocatalysis with different starting concentrations of template.

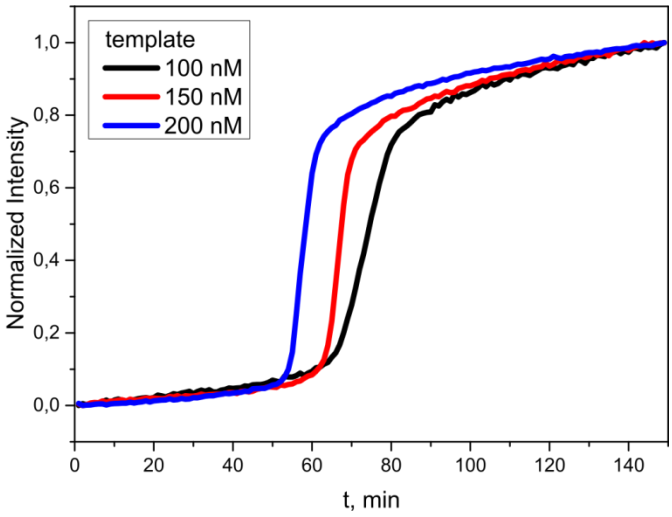

Figure 2.15. Influence of the starting template concentration on autocatalysis kinetic. Each solution contained 2 nM input, 1% of polymerase, 2% of exonuclease and 3% of nickase enzyme. The temperature was 42 °C.

There is a clear tendency of input production speed up, while increasing the template concentration. We believe, that such particularity can be explained as follows. More template strands under same input concentration, provide higher concentration of input-template double stranded DNA, and, consequently, higher production rate. One might however noticed that template concentration (fig. 2.15) has a slightly lower impact than input (fig. 2.13). The reason for it, according to our understanding, is that reactions were conducted under melting temperature of input-template complex and input was taken initially in much lower concentration than template. That is why, template concentration can have an impact only when concentration of input becomes on the same range as concentration of template. In other words, under the same initial concentration of input, 2 nM, for instance, increasing the template concentration from 100 to 150 nM, will not substantially change the number of single stranded input molecules in solution, which supposed to be around 1 nM under the melting temperature. When input concentration will increase to be comparative with the template one, the difference in template concentration starts to have an impact due to the autocatalytic amplification.

2.4.4 Effect of enzymes concentration on kinetic of autocatalysis

Based on predictable behavior of autocatalytic reaction (fig. 2.13 and 2.15), we concluded a proper functioning of polymerase and nickase. For the simple autocatalysis, running along, degradation of species is not necessary and cannot be stated, based on amplification profile under standard conditions, while production and decay are balanced over the course of experiment. Since optimized exonuclease activity is crucial for more complex PEN toolbox systems, we had to assess the optimal working conditions. To do so, we have launched several "turnover" experiments with a low (10% from usual) concentration of reaction fuel, dNTPs. Exhaustion of this component, coupled with continuous DNA degradation, within monitoring time caused the decay of fluorescence intensity. Indeed, under such conditions and at some point, the production of input became slower than decay and eventually vanished. Data in fig. 2.16 show the comparison of the reaction behavior under the standard (0.4 mM/each) and low (0.04 mM/each) concentrations of dNTPs for two solutions, containing different amount of template, 100 mM and 150 mM.

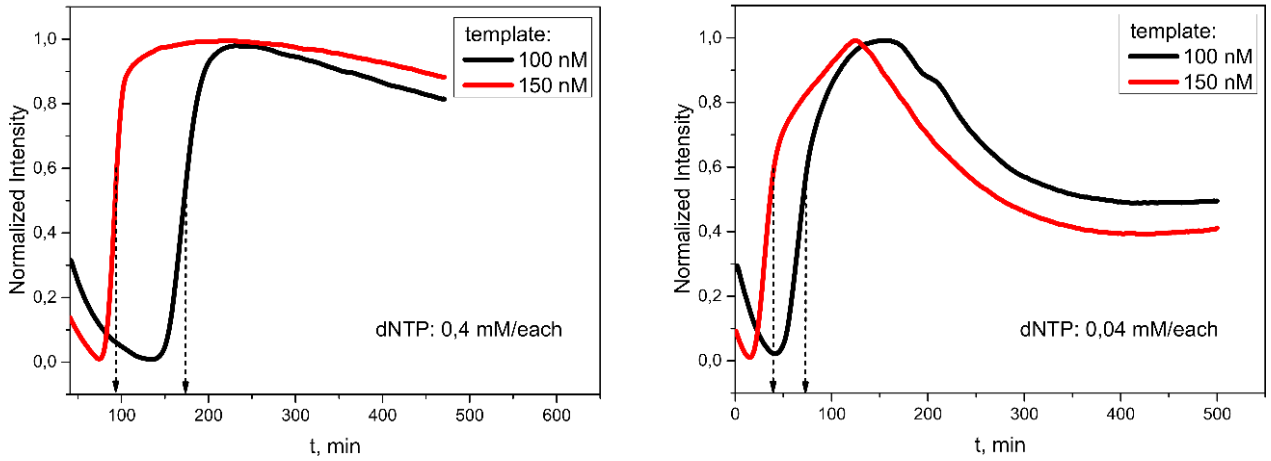

Figure 2.16. Autocatalytic reaction in presence of ttRecJ exonuclease under normal dNTPs concentration (left) and 10% from normal dNTPs concentration (right). Each solution contained 2 nM input, 1% of polymerase, 2% of exonuclease and 3% of nickase enzyme. The temperature was 42 °C.

First of all, the data proved that the degradation module (exonuclease enzyme) worked correctly since for the experiment done with low dNTPs concentration, intensity profiles start to decline, as expected. At these points, the input decay prevails over its production, which leads to the fluorescence decrease.

Secondly, from these data, we made an important observation. Indeed the current reaction proceeds substantially faster when the concentration of dNTPs is lower with the shift of the exponential increase starting from 50 to 100 minutes for template concentration of 100

and 150 nM, respectively. According to our understanding, such change in reaction kinetics is caused by the inhibiting role of dNTPs on the following mechanisms. Indeed, regarding the huge excess of dNTPs compared to the DNA concentration (more than 10^3 times), they can be associated with both, template and input and thus slowing down their hybridization. By removing 90% of the dNTPs from the reaction mixture, it made this impact substantially weaker, leading to reaction speed up occurring. This particularity must be taken into account, while tuning dNTPs concentration in the reaction medium.

The exonuclease concentration has also an impact on the reaction dynamics. Data, displayed in fig. 2.17 are corresponding to the autocatalytic reaction under the low (10% from usual) dNTPs concentration and ttRecJ gradient (0-5%). When no exonuclease is present in the reaction medium, the intensity profile does not decline after the growth increase region (black curve). Instead, a moderate increase, due to the slow input production (and no decay) at this reaction phase is observed. When exonuclease is present in solution at relatively low concentration (1%), the fluorescence profile at this phase remains stable during 100 minutes due to the balancing between the production and degradation rates. As dNTPs get consumed, the decay process dominates and fluorescence intensity decreases. When exonuclease concentration is higher (2.5% - 5%), such a plateau is not reached under these conditions because of higher degradation rate: dNTPs consumption is faster than reaching the end of exponential production. For the same reason, the higher ttRecJ concentration is, the shorter exponential intensity increase region is observed.

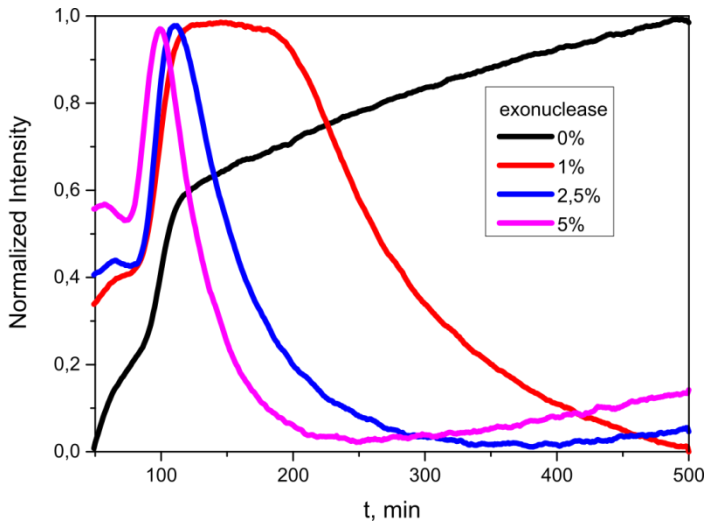

Figure 2.17. Influence of exonuclease concentration on kinetic of the autocatalysis under low dNTPs concentration (0.04 mM/each, which is 10% from usual). Each solution contained 3 nM input, 60 nM template, 1% of polymerase, 2% of nickase enzyme. The temperature was 38.5 °C.

Increasing the concentration of nickase enzyme, led to substantial slow-down of the autocatalytic reaction (fig. 2.18).

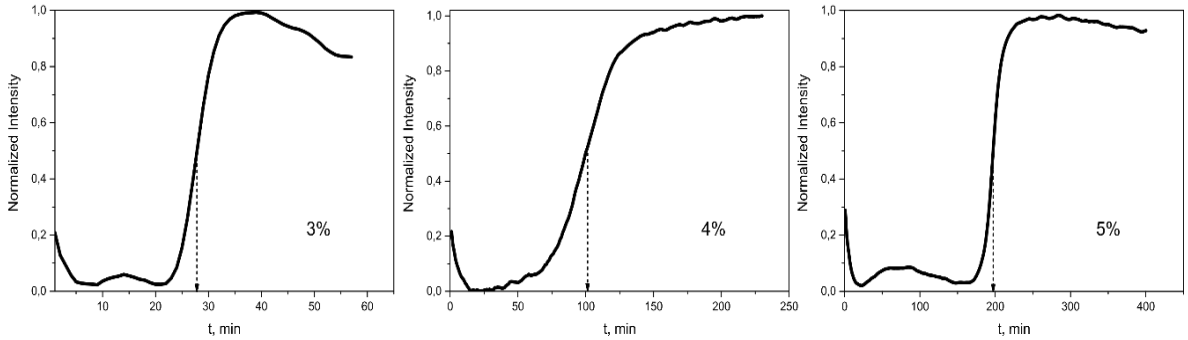

Figure 2.18. Influence of nickase enzyme concentration on dynamic of the autocatalysis module. Each solution contained 2 nM input, 40 nM template, 1% of polymerase. The temperature was 42 °C. One can see that increasing of the nickase concentration slows dawn the amplification reaction.

Such effect can be explained by the competitive interaction between this enzyme and polymerase in a following way. Nickase Nt.BstNBI, used in this part of our work, is a restriction enzyme cutting at specific DNA recognition sequence (fig. 2.19)

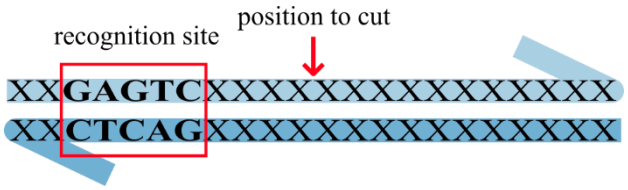

Figure 2.19. Schematic representation of Nt.BstNBI nickase working principle.

As its recognition site is present in the non-elongated input-template double-stranded DNA as well as in elongated, nickase can bind to it and prevent the action of the polymerase. For this reason, concentrations of nickase and polymerase must be well balanced in order to provide proper functioning of PEN toolbox, especially in more complex systems.

2.4.5 Parasite issue

On the beginning of July 2015, we faced a problem that our experiments with autocatalytic template were running in a non-predictable way: intensity increased 10 times higher than previous and on the same time, an exponential increase region was substantially delayed and

lasted for much longer time (~ 200 minutes) (fig. 2.20 a). Such undesignable grows of the DNA species number during launching the PEN toolbox experiments have already been described [96]. In fact, DNA produced *via* these unpredictable reactions were named “parasites” or “parasitic species”. In order to get rid of these issues, we proposed and performed the following actions. First, PCR tubes, which were suspected to contain the parasite (in case of anomaly fluorescence signal), must be thrown away without opening. Second, new reaction buffer and enzymes solutions must be prepared. Finally, the reaction buffer must contain 2µM of netropsin (fig. b), a polyamide with strong DNA binding properties. In addition to this optimisation steps, we paid a particular attention to prevent any cross-contamination of stock DNA material and reaction solutions and also made regularly a cleaning of the laboratory working place by Nuclease Decontamination Solution (IDT). All this steps help us to fix this problem without eliminating it definitely. Indeed, this parasite issue happened several times more over the course of the present study.

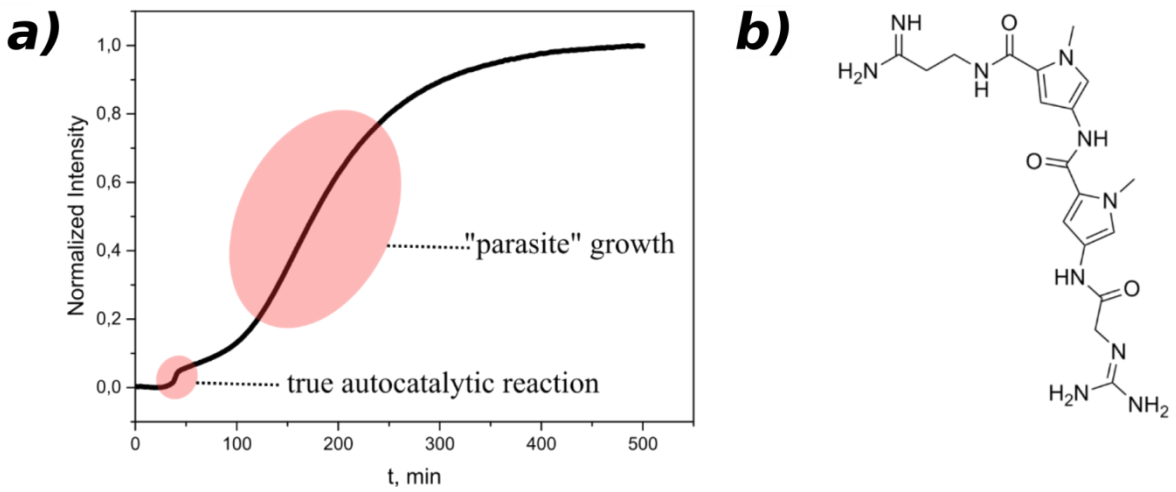

Figure 2.20. Typical fluorescence profile when side reaction, “parasite” grows, is taken place (a) and a component of reaction buffer, netropsin, aimed to prevent or delay such side reactions (b).

2.4.6 DNA-amplification reaction with non-autocatalytic template

Prior to use PEN toolbox systems with complex dynamics, one must ensure the proper functioning of their elementary modules. We have already discussed earlier the behavior of autocatalytic reaction and the influence of different components (concentrations of input, template, enzymes and dNTP) on it. In this subsection, we will see the particularities of a

similar PEN toolbox reaction, but with non-autocatalytic template, which is an essential part of more complex systems with, for example, oscillation or bistable behavior.

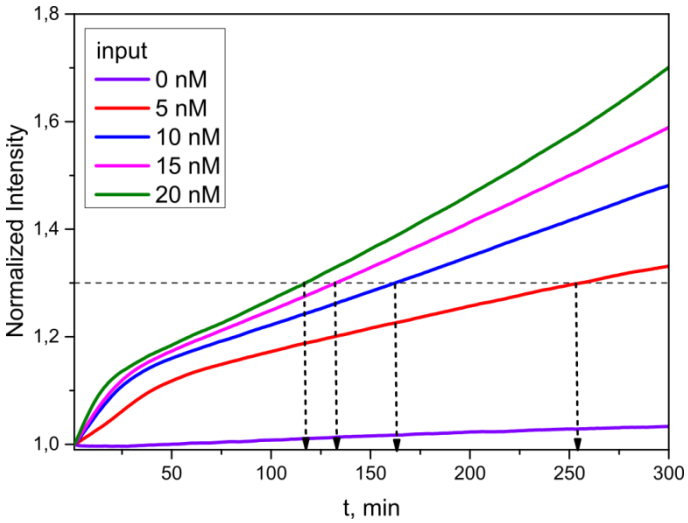

Figure 2.21. Influence of input concentration on kinetic of the activation reaction. Each solution contained 100 nM template, 2% of polymerase, 2% of nickase enzyme. The temperature was set to 42°C.

Data, showed in fig. 2.21, illustrate linear DNA amplification with non-autocatalytic template as a function of input concentration. The intensity profile corresponded to the sample with 0 nM input, is not completely flat due to the same reasons as for the self-start autocatalysis reaction. However, the changes, observed in this case, are negligible compared to the samples with the presence of input in the reaction mixture. The reason for it is the absence of avalanche-like DNA production. Consequently, spontaneously synthesized input or output DNA molecules do not have a substantial impact on reaction and in this approximation, one can say that this reaction is not metastable.

When input is added, clear intensity increase is observed. Thus, the higher concentration of input is, the faster signal growth is. Interestingly, this fluorescence profiles bends, which leads to slowing down the signal increase. It cannot be just a signal fluctuation, since this signal changes by following the same rule as the total profile: the higher input concentration is, the more curve bends. Additionally, this region is absent at all for the sample with 0 nM input. Consequently, it must be a rational explanation for such signal heterogeneity. According to our understanding, it is as follows.

At starting point of the reaction, there is no DNA but input and template in reaction mixture. Over the course of output production, template molecules became saturated. In this case, elongation cannot happen until dissociation of output. Therefore, the reaction is slowing down and fluorescence intensity profiles are bending.

To study the kinetic of this reaction in more details, data analysis was performed with the aim of finding a reaction order in a way, analogical to the previously described for autocatalytic reaction. Time, ***t***, at which signal increases on 30 % (normalized intensity is equal 1.3) for each input concentration, was arbitrarily chosen as a characteristic. Next, we built 3 graphs: $\boldsymbol{C}(\boldsymbol{t})$, $\boldsymbol{ln(C)}(\boldsymbol{t})$ and $\boldsymbol{C^{-1}}(\boldsymbol{t})$, where $\boldsymbol{C}$ – is initial input concentration, so as to verify if the reaction order is 0, 1 or 2 respectively (fig. 2.22).

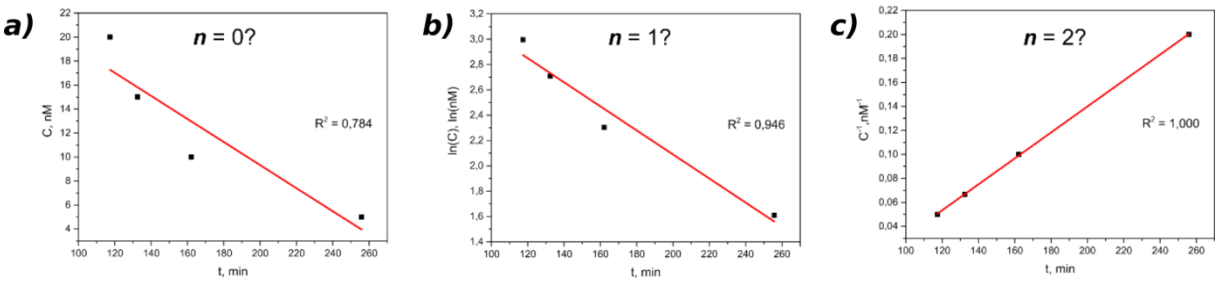

Figure 2.22. Graphical method of finding the reaction order for the activation reaction. Linear behavior of the curve c) shows that the reaction order is equal 2.

Data indicate, that non-autocatalytic DNA amplification reaction is second order reaction, since R^2 of function $\boldsymbol{C^{-1}}(\boldsymbol{t})$ is 1.000 (fig. 2.22 c). This fact can be explained by the existence of two kinetic events in this process. The first one corresponds to the binding of the input to the template in initial production of output. During this step, the production of new DNA species occurs faster, since templates are not yet saturated. The second phase of the reaction is taking place under conditions of templates saturation (new output to be produced requires displacement of old one *via* Bst polymerase). For this reason, amplification profiles, corresponded to this reaction (fig. 2.21) bend, after which amplification occurs slower.

2.4.7 Complex dynamics with PEN toolbox

Simple PEN toolbox reactions, which we have discussed above, can be connected in a way that the output from one module will be the input or inhibitor for another. Such cascadebility enable system to perform more complex dynamic behaviour. In order to illustrate this, we will next discuss two examples of such systems: the inversion module and the oscillator. They were implemented in present work and helped us to better understand this framework prior to the experiments in microfluidics.

Inversion module consist of two templates, non-autocatalytic and autocatalytic, connected in a way, that output of the first one can inhibit the second one (fig. 2.24 a). Initially, system does not contain any input for non-autocatalytic template, which permits the autocatalysis reach saturation. Introducing this input into the reaction mixture, provokes production of inhibitor and the suppression of the autocatalytic template. Because of the presence of exonuclease, the inhibitor can eventually be degraded and autocatalysis restarts. In terms of practical implementation, the input is injecting into the reaction mixture *via* micropipette after pausing the experiment and opening the PCR thermocycler. Such approach is very inconvenient and by itself motivates the development of novel methods of interaction with molecular system.

In order to monitor this system, one must apply a selective detection method, *i.e.* Eva Green is not suitable for this purpose, for the following reason. The degradation of inhibitor is followed by launching the autocatalysis. The total amount of double-stranded DNA is nearly constant in this case. Consequently, Eva Green detection method does not provide complete information about system behavior. To solve this issue, we applied a monitoring method, based on nucleobase-quenching of fluorophore (see section 2.3.1). It was attached to the 3' end of autocatalytic template. Hybridization with inhibitor does not provide substantial fluorescence changes, since it hybridizes on the middle of the autocatalytic template. Fluorescence shift, due to hybridization, strongly decreased as hybridization occurs further from fluorophore [97].

In fig. 2.23 are demonstrated results of experiment, aimed to testify this detection system. Since fluorescence declines when input is autocatalytically produced, the observed signal is changing in a following way. Initial region (until ~15 min) is fairly stable. After that, fluorescence signal strongly decreases due to the start of exponential producing of input. Finally, it stabilizes due to reaching the equilibrium between production and degradation rates. As the input concentration increase, the exponential production region is reaching faster and we can see proportional shifting of the intensity drop.

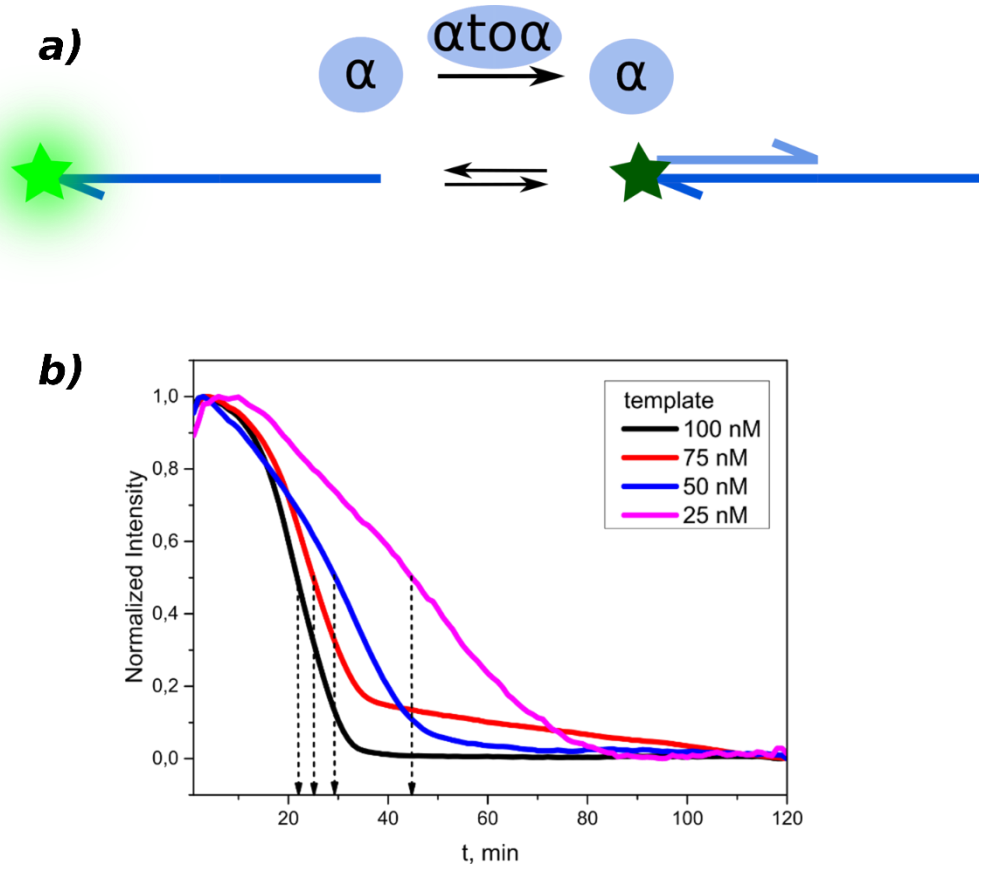

Figure 2.23. Monitoring of autocatalytic reaction using the DNA template with attached fluorophore DY 530. (a) Schematic representation of monitoring principle. (b) Experiment with gradient of template concentration. Each solution contained 2 nM input, 2% of polymerase, 2% of nickase enzyme. The temperature was 45 °C.

Results of one of the experiments with inversion module, obtained using selective reporting strategy are demonstrated on fig. 2.24 b. The first part of the fluorescence profile is analogical to simple autocatalysis, discussed previously (fig. 2.23 b). In this region, no inhibitor is produced and autocatalytic reaction is functioning in a standard way.

At t = 90 min, the input was injected for inhibitor production template. It provoked suppression of autocatalysis and for this reason intensity increased. Finally, we can see the moderate intensity decreased due to the decay of the inhibitor and progressive renewing of autocatalytic reaction. The injection of the input for non-autocatalytic template can be repeated several times, which led to some kind of controlled oscillations [74].

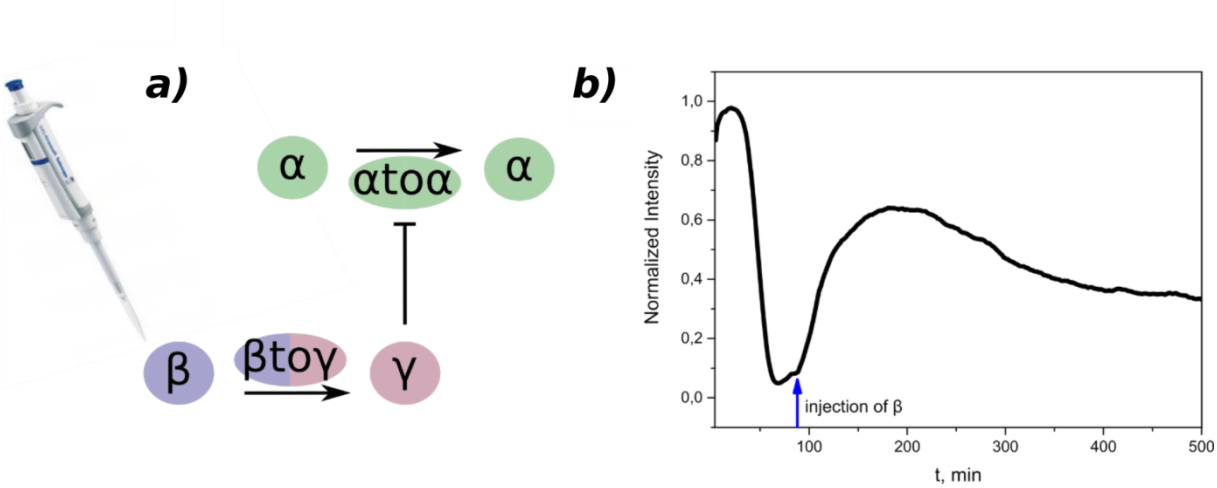

Figure 2.24. Inversion module system. (a) Schematic representation of network topology. (b) Experimental implementation. Solution contained 100 nM template αtoα, 50 nM template βtoγ, 2% of polymerase, 2% of exonuclease, 2% of nickase enzyme. At t = 95 min was injected 1 µl of input β solution to final concentration 100 nM. The temperature was set to 45 °C.

The next PEN toolbox system that we have considered has an oscillation behavior and is called "Oligator" [75]. It consists of three templates connected with a negative feedback loop (fig. 2.25 a). The first one, the template is autocatalytic. The second is non-autocatalytic. It serves as a "bridge" by taken an input from autocatalytic module and producing an output. The last one serves as a trigger for the third, non-autocatalytic template. This template produces an inhibitor for the autocatalysis, in a similar way as the inversion module.

In this way, the concentrations of species can oscillate between two successively repeated states: 1) autocatalysis is saturated, no inhibitor is produced; 2) autocatalysis is suppressed, the inhibitor concentration is maximal.

In fig. 2.25 are displayed results of experiment from the Oligator system. Unfortunately, we have observed only damped oscillations. It can be explained by using ttRecJ enzyme instead of RecJ, which was used in the original work, where was introduced the Oligator system [75 98].

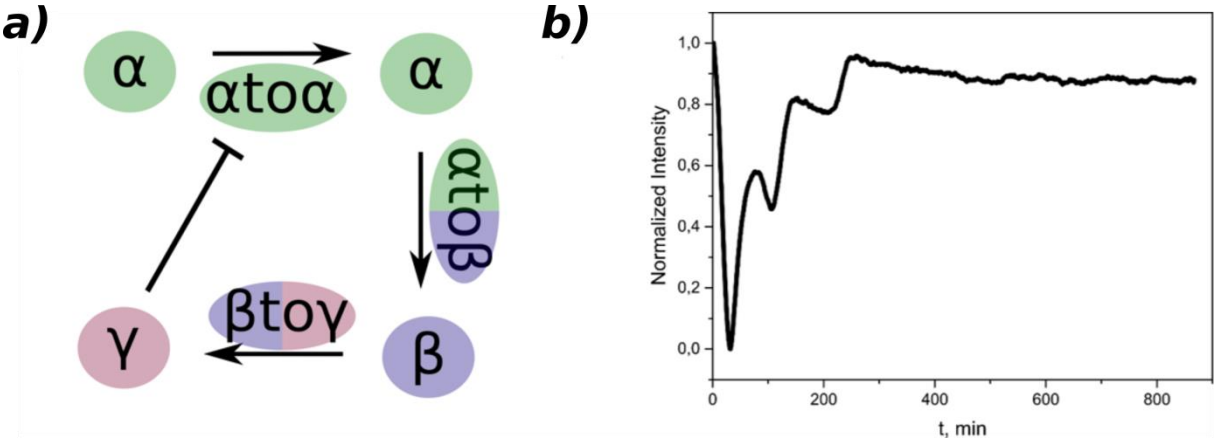

Figure 2.25. Oscillation PEN toolbox system. (a) Schematic representation of network topology. (b) Results of fluorescence intensity measurements during the experiment. Solution contained 30 nM template αtoα, 20 nM template αtoβ, 30 nM template βtoγ, 2% of polymerase, 5% of exonuclease, 2% of nickase enzyme. The temperature was 42.2 °C.

2.5 Conclusion

Such electrochemical methods as chronoamperometry, choronocoulometry and cyclic voltammetry are a simple and convenient tool for characterization of gold-DNA surfaces. Furthermore, they provide a reliable approach for irreversible cleavage of DNA-gold bond and perform release-on-demand of designed biomolecules.

PEN toolbox comprises 3 basic modules, activation, inhibition and autocatalysis, which can be connected with each other in order to form complex circuits with needed dynamical behavior. To monitor these reactions, by detecting hybridization events of different species, fluorescence quenching method seems to be the most attractive one among alternatives, since it provides more information about total and sequence specific amount of oligonucleotides. It offers a possibility to monitor reaction-diffusion events on surface *via* fluorescence microscopy and bulk reactions.

Various parameters (input, template, enzymes, dNTPs concentrations, temperature *etc*.) have a substantial influence on PEN toolbox reactions behavior and became crucial for the complex circuits, where very careful adjustment is essential.

Chapter 3

Assembly of the molecular system and the active surfaces in microfluidics

3.1 Introduction

DNA-based CRNs and, in particular, PEN toolbox appear to be promising biochemical tools for various applications such as design of novel biosensors [99], programming behaviour of microscopic particles [100], unconventional computation [101] *etc*. Handling such systems in microfluidics has an advantage of reducing costs of the experiments (because of operating with reduced volumes of reactants) and gives the possibility to explore spatial behaviour due to reaction-diffusion processes [102] [80].

However, several issues remain in our view to be solved to fully exploit these discoveries and turn them into real life technologies. Of particular interest is the ability to interact in real-time with these complex molecular systems is a key requirement for their complexification. As information is materialized through DNA strands in these systems, the on-demand injection of DNA input strands might be a useful way to provide a versatile and controllable method to do so. There are several ways to make biomolecules available in a reaction medium that are compatible with microfluidics. A first approach is to rely on microfluidics to inject in the main channel where information processing takes place a volume of solution which contains the input DNA strand. One can do so using microfluidic valves [81] which can be opened and closed at will to enable the solutions to come in contact and exchange DNA strands through diffusion. This approach, however, requires multilayers microfluidics chips to be produced and is rather complex to operate. Furthermore, information exchange can only be done at a limited number of locations and always at the edges of a reservoir or channel.

Rather than leaving the DNA strands in solution, we propose an applying surface immobilization and release strategies. There exist a number of approaches of release biomolecules form solid supports, among them photocleavage of photolabile linker molecules [103], using an alternating electromagnetic field and Fe_3O_4 as a substrate [104] or simple thermal desorption [105]. In this chapter we will discuss applying of the electrochemical properties of the Au-S bond to release DNA from gold electrodes [106]. This approach has several advantages such as potential easiness of combining with PEN toolbox system without changing the reaction conditions (temperature, ionic strength) and no need for expensive equipment. Furthermore, this method can be potentially used to provide complex spatiotemporal actuation in microfluidics as one can pattern microelectrodes of various shapes and sizes in reservoirs or channels, which can be addressed individually as required.

In this way, we have fixed an objective of developing a strategy of on-demand electrochemical release of DNA activators, capable to perform time- and space-controlled triggering the PEN toolbox system, and initiate the propagation of reaction-diffusion fronts.

The following requirements to these technologies were established: comparability with usual conditions of PEN toolbox, inactivity in absence of an external command (electrical pulse), including both molecular system and surface-attached DNA stability and, finally, low cost and maximal simplicity of manufacturing.

3.2 Designing active surfaces

We have chosen electrochemistry as a promising way to interact with the PEN toolbox in microfluidics. From this perspective, thiol-gold chemistry appears to be an attractive option as mono- or dithiol modifications of DNA are available from most companies such as Thermo Fisher or IDT for a relatively low price with respect to the total cost of oligo production. As a first step, the nature of such interaction was studied in details [107] [108] which permits to reliably immobilize thiol-functionalized molecules as self-assembled monolayers (SAM) on gold surface. As a second step, the Au-S bond can be electrochemically broken by applying a negative potential [109] [110].

In this way, we aimed to create a DNA-based active surface, which can interact with the PEN toolbox. For the simplest system within PEN toolbox, which contains only one template (either autocatalytic or not), one can imagine two possible alternative ways of designing the surface activator. The first one consists in the attachment of DNA input, followed by its release and resulting triggering of the reaction in solution. The second option is the attachment and subsequent release of a DNA template, followed by its interaction with the input strands, present in the reaction medium. We have chosen immobilization of input rather than template for the following reasons:

Firstly, the input DNA molecules are shorter than the template ones, and, consequently, carry lower negative charge, which leads to the lower repulsion between neighbouring strands. This fact permits better control of surface density and, consequently, a higher range of input concentration can be released in solution. Furthermore, for the same reason one can achieve higher surface densities with input DNA. This means that surface hybridization (and potentially unwanted triggering) will less likely take place in case of attached input rather than template.

Secondly, the typical PEN toolbox system solution normally contains exonuclease ttRecJ. This enzyme is responsible for the degradation of non-protected single-stranded DNA molecules and has 5’ to 3’ activity [111]. If one chooses a template attachment strategy, nothing

prevents the exonuclease to degrade the input strands in solution before the reaction start. This will substantially decrease possible working time range of potential technology and make more complicated prediction of reaction kinetics, which is essential for complex circuits. On the other hand, input can be attached only thru it 5' end in order to make possible elongation by polymerase, which works from its 3' end. Consequently, input, in case of attachment to the surface, is protected from degradation by exonuclease.

Another reason is that by releasing the input one can interact with bigger number of PEN toolbox reactions. While templates are involved only in output production and can react only on one given input sequence input can interact simultaneously with several templates. For example, in the Oligator system (see section 2.4.7), one input involved in both autocatalytic reaction and linear production of downstream output. Additionally, input species can be designed in a way to act as inhibitors for certain templates. All this gives higher level of control by input release.

A second aspect, which was taken into account for the designing of our DNA-activators, was the nature of thiol linker. Two major options, mono- and dithiol functionalization, are available in this context. We have decided to work with dithiol-modified DNA (fig. 3.1 a) for the reason of it higher stability versus chemical agents such as dithiothreitol (DTT) (fig. 3.1 b) [112] [113]. This factor is important, since the PEN toolbox buffer contains DTT in millimolar concentrations in order to maintain enzymes' function in long-term experiments (DTT reduces oxidized S-H bonds and, consequently, prevent loss of enzymatic activity). In the same way as DTT reduces bonds in oxidized proteins it can potentially break Au-S bond and cause undesigned release of DNA input in solution.

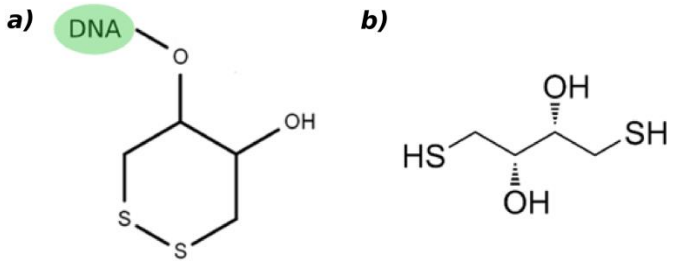

Figure 3.1. Chemical structures of dithiol linker (a) and reductive agent, DTT (b), used in the present study.

3.2.1 Practical implementation of DNA attachment and its controlled release

After having chosen the strategy for our active surfaces design, we first focused on DNA-thiol attachment. To do so, several DNA strands were used corresponding to DNA inputs in PEN toolbox and containing 5' dithiol modifications.

We applied the protocol of thiol-gold immobilization, described in [114]. According to it, several microliters of deprotected DNA-dithiol solution with 1 μM concentration were deposited onto a gold surface in a closed Petri Dish saturated with water vapour in order to prevent solution evaporation. For the initial deprotection step, we used one of the methods proposed on www.idtdna.com website, which relies on an extraction using ethyl acetate. We applied minor modifications to this protocol as we skipped the use of triethylamine. This compound is desirable during the separation of deprotected DNA from excess of dithiothreitol by extraction procedure with ethyl acetate. Its role consists in increasing the part of DNA in the water phase and, consequently, decreasing its losses. DNA losses are not crucial for our experiments since 1 μM concentration (large excess) led to a satisfactory surface coverage values. In this way, we decided to simplified our routine deprotection procedure and make it faster and more reproducible day-to-day.

We have tried several approaches over the course of the present study in order to verify the successful attachment of thiolated DNA to the gold surface and its subsequent release in solution.

First, we conducted contact angle measurements on gold surfaces before and after DNA immobilization and also after its electrochemical release (fig. 3.2). We observed a substantial decrease of the measured value (from 28±2° to 11±2°) after DNA attachment. These data are in agreement with those previously reported and can be explained by the increase of surface hydrophilicity after immobilization [86]. After application of a negative potential (-2V *vs* Au) to the interface with attached DNA, the contact angle returns back to the initial value (31±2°), which confirms cleavage of Au-S bond under our experimental conditions.

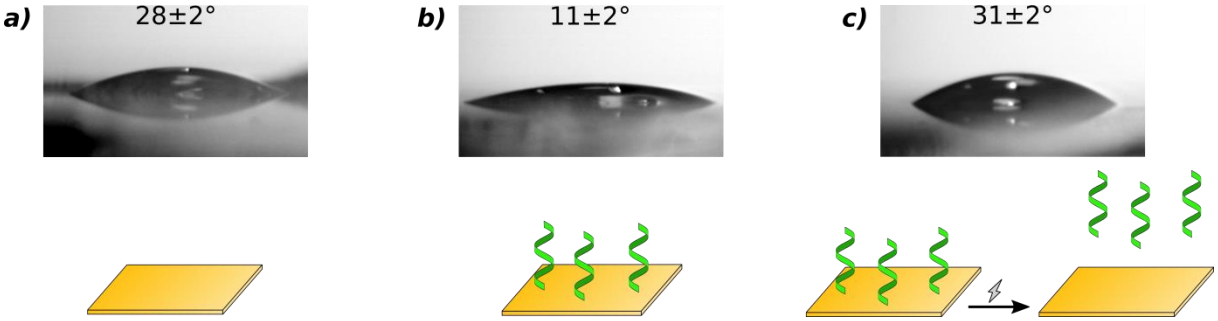

Figure 3.2. Verification of immobilization and release of DNA from gold surface by measuring the contact angles of bare gold (a), of DNA-functionalized gold surface before (b) and after electrochemical release of attached DNA(c).

The second proof of attachment and electrochemical release of DNA-thiol was obtained by cyclic voltammetry experiments (see section 2.2). We also used this method in order to define the potential value, necessary for the cleavage of gold-thiol bond and DNA release from the surface. The value of -0.9 V *vs* Ag/AgCl, that we found, was further optimized in our setup with gold reference electrode (fig. 3.3). To do so, the potential of the working electrode *vs* the counter/reference one was swept from -0.5 to -2 V by step of 0.1 V and pulse duration of 10 s for each voltage. Time intervals between the pulses were 90 s. Fluorescence images were taken every 30 s and their intensity measured. The resulting data are shown in fig. 3.3 a.

At U = 0 V, while fluorescently-labelled DNA is attached to the surface, nearly no fluorescence is measured due to quenching by the gold surface. No fluorescence increase was detected for voltage values lower than -0.9 V. At voltage value of -0.9 V, fluorescence begins to slowly rise up after each electrical pulse. A stronger increase starts to be seen around -1.2 V – -1.3 V. Afterwards, each pulse continues to release DNA from the surface until complete depletion. It has to be noticed that leaving the potential at -2 V for a longer period (40 s), confirms that no further release takes place.

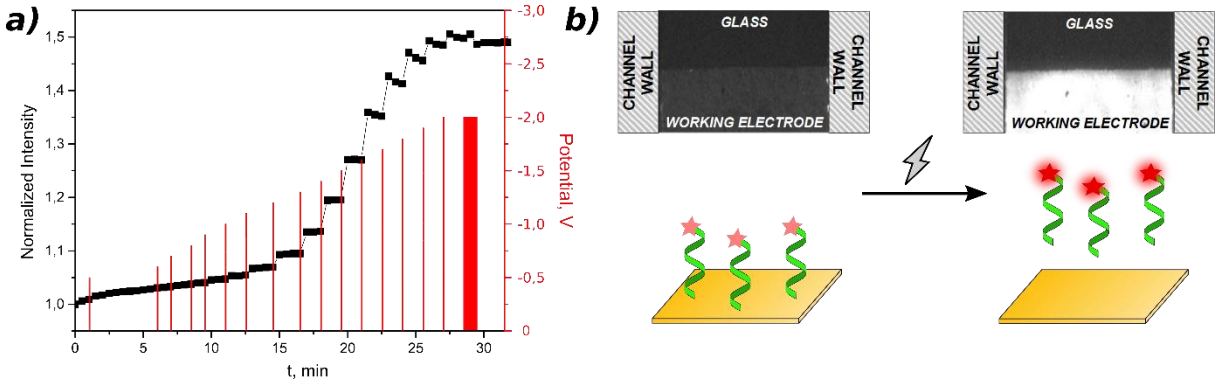

Figure 3.3. Electrochemical desorption of fluorescently-labelled DNA as a direct observation of the release procedure. (a) Sequential potential increase under continuous fluorescence recording to optimize the release potential. (b) Fluorescence image of sample before and after polarization at -2 V of the working electrode.

Since -2 V *vs* the gold counter electrode is within the solvent window, we choose to apply this potential for 30 s to efficiently cleave the thiol anchor of our DNA from the gold surface and enable them to diffuse away. Figure 3.3 b shows a region of the microfluidic channel where the working electrode occupies the bottom half of the field of view while the top half is glass. One can see the immediate and significant fluorescence increase, which was visible just after the potential was applied.

3.2.2 Autocatalysis triggering with an active surface

In this section, we have tested the possibility of launching PEN toolbox reactions using our DNA-functionalized surfaces. For this purpose, a simple autocatalysis system was chosen because it provides an exponential input production. Indeed, such experiments will allow both, a higher intensity of fluorescence signal increase (hence, making it easier to monitor the reaction) and, the possibility of triggering even at low input concentrations. That will permit to test our technology under bigger range of surface densities.

For this purpose, we designed the following experiment (fig. 3.4 a). We prepared 2 identical gold surfaces, covered by DNA-input and with on top of each of them, an assembled Parafilm chamber with 10 µl of the reaction buffer. The reaction buffer in this and further experiments is composed of 50 mM NaCl, 10 mM $(NH_4)_2SO_4$, 10 mM KCl, 8.4 mM $MgSO_4$, 0.8 mM of each dNTP [New England Biolabs (NEB)], 0.1% Synperonic F108 (Sigma-Aldrich),

500 µg/mL BSA (NEB), 2 µM Netropsin (Sigma-Aldrich). Unless otherwise indicated, the same parameters we used for all other experiments, described in this chapter.

To one of the samples, a negative potential of -1.3 V during 30 sec *vs* Ag/AgCl reference electrode was applied, while the second one served as a control with no potential applied. After that, solutions from each of the surfaces were recovered. Then 10 µl of reaction mixture containing enzymes and DNA template were added to each sample and then introduced in a PCR thermocycler at 42 °C. Results of this experiment are showed in fig. 3.4 b.

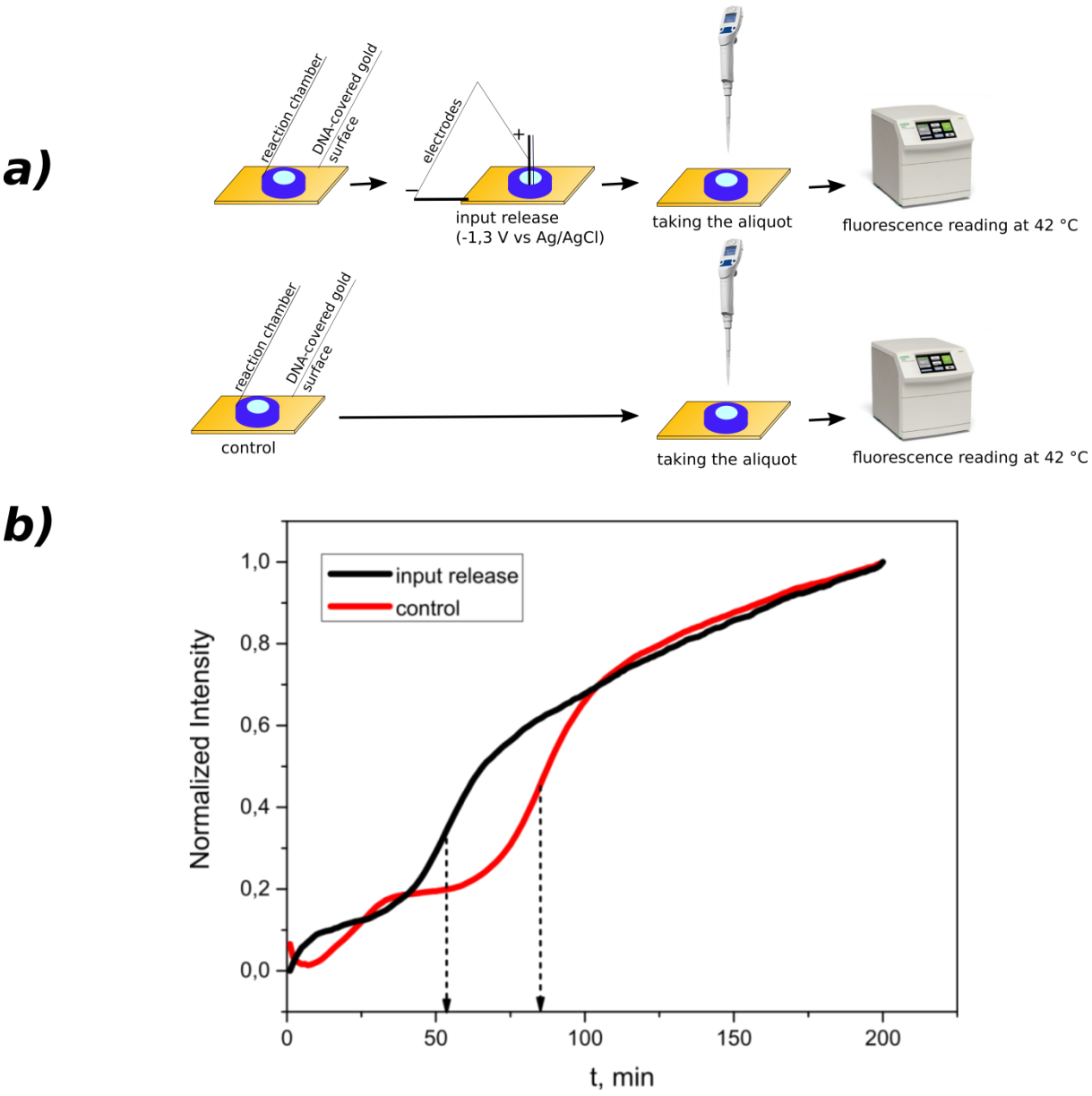

Figure 3.4. Experiment, aimed to verify principle possibility of triggering the PEN toolbox reaction by using input release from the DNA-functionalized gold surface. Each solution contained 30 nM template, 2% of polymerase, 2% of nicking enzyme. The temperature was 42 °C.

As an autocatalytic system is metastable, the reaction starts even in absence of input in the initial reaction mixture. Both fluorescence profiles therefore showed an exponential increase region. However, there is a clear difference in time delay (around 30 min) between them. Since solutions after contact with DNA-functionalized surfaces were mixed with the same reaction solution, we can conclude the successful triggering of autocatalytic reaction in bulk *via* electrical release of input from the surface. As it was mentioned above, the reaction can start even in case of absence of input release due to the self-start phenomena.

Another important conclusion that we made is that the fact of electrical release does not damage DNA input. Furthermore, the dithiol modification on the 5' end of the input sequence does not prevent it to activate the template and produce an output.

3.2.3 Determination of the input-DNA surface coverage

After the successful demonstration of the input release and the triggering of the autocatalysis, we attempted to estimate the exact amount of DNA, which we are able to introduce from the surface into the reaction medium. For this purpose, we have conducted a similar experiment as the one described above. The difference between this experiment and the previous one is the use of different bulk solution input concentrations. In addition, instead of using as a control the case with no electrical release as we did before, we performed one experiment with no input (0 mM) as a control.

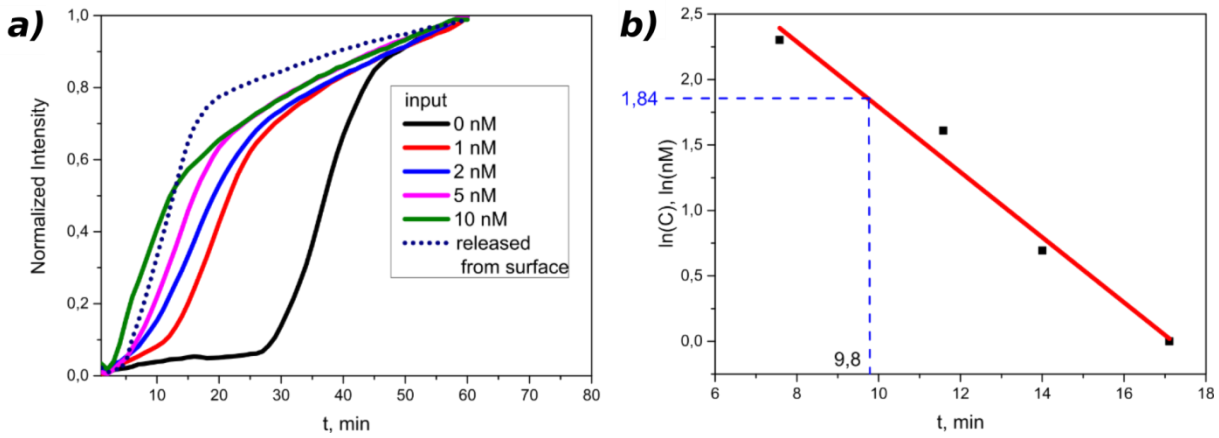

Figure 3.5. Determination of the surface coverage by using triggering of autocatalytic reaction in bulk solution with surface released input. (a) Raw data. (b) Processed data for determination of the released input concentration. See text for the details. Each solution contained 50 nM template, 2% of polymerase, 2% of nicking enzyme. The temperature was 42 °C.

From the fluorescence profiles obtained (fig. 3.5 a), we confirmed our ability to trigger an autocatalysis *via* surface release of input, since the amplification curve, corresponded to the input electrically released (dotted line) is in-between profiles for 5 and 10 nM input and far from the self-start profile (solid black line).

In order to perform a quantitative estimation of the surface coverage, a calibration curve ***ln(C)(t)*** was built (fig. 3.5 b). The value of ***t*** for the input release curve, 9.8 min, was determined from the fig. 3.5 a and used for the determination of ***ln(C)*** value, 1.84, from the fig. 3.5 b. Therefore, the concentration of input in the analysed sample is equal to $e^{1.84}$ = 6.3 nM. Taking into account the 2 times dilution of the solution after input release (due to the mixing with the equal volume of the reaction mixture), the concentration of DNA, ***C***, which was released in 20 µl of reaction medium volume, ***V***, from the functionalized surface with an area, ***S***, of 0.2 cm^2, is equal to 12.6 nM. We further calculated the surface coverage, Γ, from these data, using the following formula: $\Gamma = \frac{CVN_A}{S}$. Where N_A is Avogadro constant ($6.02 \cdot 10^{23}$ mol^{-1}). We obtained a surface coverage ~ 10^{12} molecules/cm^2 which is in good agreement with previous reported surface coverages of DNA-thiol SAM on gold, ranging from 10^{10} to 10^{14} molecules/cm^2 (see, for instance, [115]).

3.2.4 Stability of active surfaces in presence of DTT

We have also studied the stability of DNA attachment on the gold surface in presence of DTT by conducting a similar experiment as we did for the DNA surface coverage determination, which we have described above. As previously mentioned, the PEN toolbox reaction medium contains DTT in order to prevent loss of enzymatic activity for long-term experiments. However, DTT due to its disulphide bond reduction properties can potentially degrade the Au-S bond, which is why dithiol was chosen instead of monothiol for 5' end DNA modification.

The experiments we performed consisted in three parts. First, we exposed two DNA covered surfaces to 20 µl of 1 mM DTT in the usual reaction buffer. Then, in a second step, we applied a negative potential to one of the surfaces in order to release input DNA. In a third step, 10 µl of the solution from each surface were recovered and then mixed with 10 µl of solution containing both enzymes and DNA template and finally the DNA amplification done in PCR thermocycler was monitored. As controls, 2 experiments with 0 and 4 nM input with the same reaction mixture were conducted. We observed (fig. 3.6) that exponential amplification region

of fluorescence profile, which corresponds to the sample with input release after incubation with DTT is close to the one, which corresponds to the control (4 nM input). Consequently, at least some fraction of initial amount of the input molecules remains after incubation with DTT. On the other hand, this parameter in case of the sample without input release is shifted in a region of larger times from the control with 0 nM input. This fact means that no detectable traces of DNA input were present in it. We can conclude that under the investigated conditions the input-functionalized surface retains its activity and that surface-attached molecules are not being released in the liquid phase in absence of electrochemical pulse.

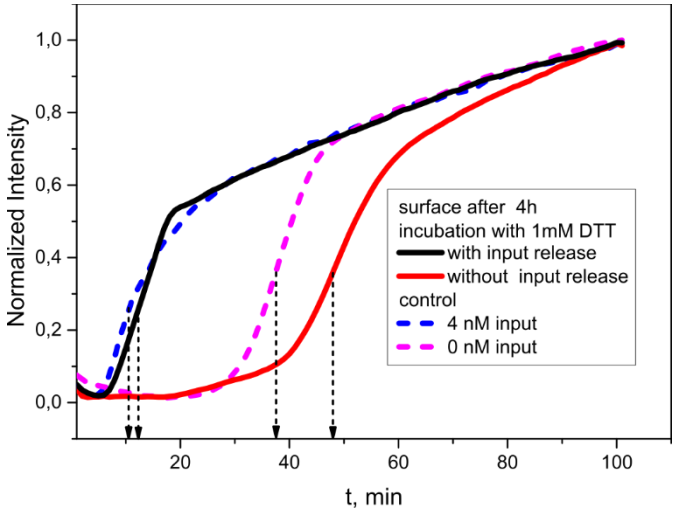

Figure 3.6. Investigation of the stability of DNA-functionalized gold surface after exposure of 1 mM DTT solution during 4 hours. Each solution contained 50 nM template, 2% of polymerase, 2% of nicking enzyme. The temperature was 42 °C.

It has to be noticed, however, that in this study, we nonetheless used DTT-free reaction buffers in order to simplify experimental processes. Such approach seems to be reasonable because of relatively short time of our experiments (several hours), during which enzymes retain their activity (such conclusion was done based on predictable behaviour in our experiment, which proves normal function of enzymes).

As a conclusion, we have demonstrated that under our experimental conditions, the DTT presence has no impact on DNA attachment to surface within four hours. Thus, it can be consequently reintroduced in the reaction mixture if this will be required.

3.3 Design of the microfluidic device

Conducting experiments in microfluidics allows decreasing the costs of the experiments by reducing reaction volumes. Another important benefit of microfluidics compared to the bulk experiments is the absence of thermo-convection processes, which allows monitoring precisely reaction-diffusion phenomena.

In order to perform experiments in microfluidics, a specific device was designed to maintain the reaction solution and to allow signal monitoring. In our particular case, the following requirements for the microfluidic device must be fulfilled.

Firstly, the reaction mixture must be hermetically closed to prevent leakage or evaporation.

Secondly, since the concept of our technology relies on an electrochemical activation, our microfluidic system must contain electrodes, accessible both from the outside of space and where the reaction is taking place.

Thirdly, it is desirable to minimize as much as possible the impact of reaction chamber materials on the PEN toolbox kinetics and on the monitoring of the signal.

In this section, we will go through all these issues and discuss the principle of design of the device eventually chosen to be used in the present study

The first task we had to solve was the integration of the electrodes in our device. Since the main goal was the cleavage of S-Au bond, there was not a need for accurate electrochemical measurements in our microfluidic system. As a result, we have considered a two electrodes setup as suitable and more appropriate for the present study.

The choice of the working electrode was dictated by our concept of DNA release. Metals like silver, copper, platinum, palladium, iridium *etc.* are known to react with thiol-based SAMs, which can be potentially broken electrochemically [116] [117] [118]. Although one can use alternative materials for working electrode, we have chosen a gold-based electrode because of numerous previously reported DNA-thiol SAM on it and their electrochemical cleavage and, consequently, the well-established nature and reproducibility of such interactions [119]. While we do not currently see additional benefits of using, for example, silver or platinum based working electrodes, we cannot exclude their use in the future if such benefits appear.

We examined several options for the second electrode. Several experiments were performed using indium tin oxide (ITO) covered glass slide electrode as a top surface of our device, or platinum wire, introduced in between top and bottom surfaces inside 4 layers of

Parafilm. We found such approaches extremely inconvenient because of the difficulty of assembling and connecting these electrodes to the potentiostat and the increasing risks of leakage. As alternative, we have made a device based on two gold electrodes made initially by photolithography and later on by simple thermal metal evaporation technique through a homemade nickel mask (fig. 3.7). This system configuration permits an easy and robust connection of electrodes with the potentiostat by soldering copper wires to them.

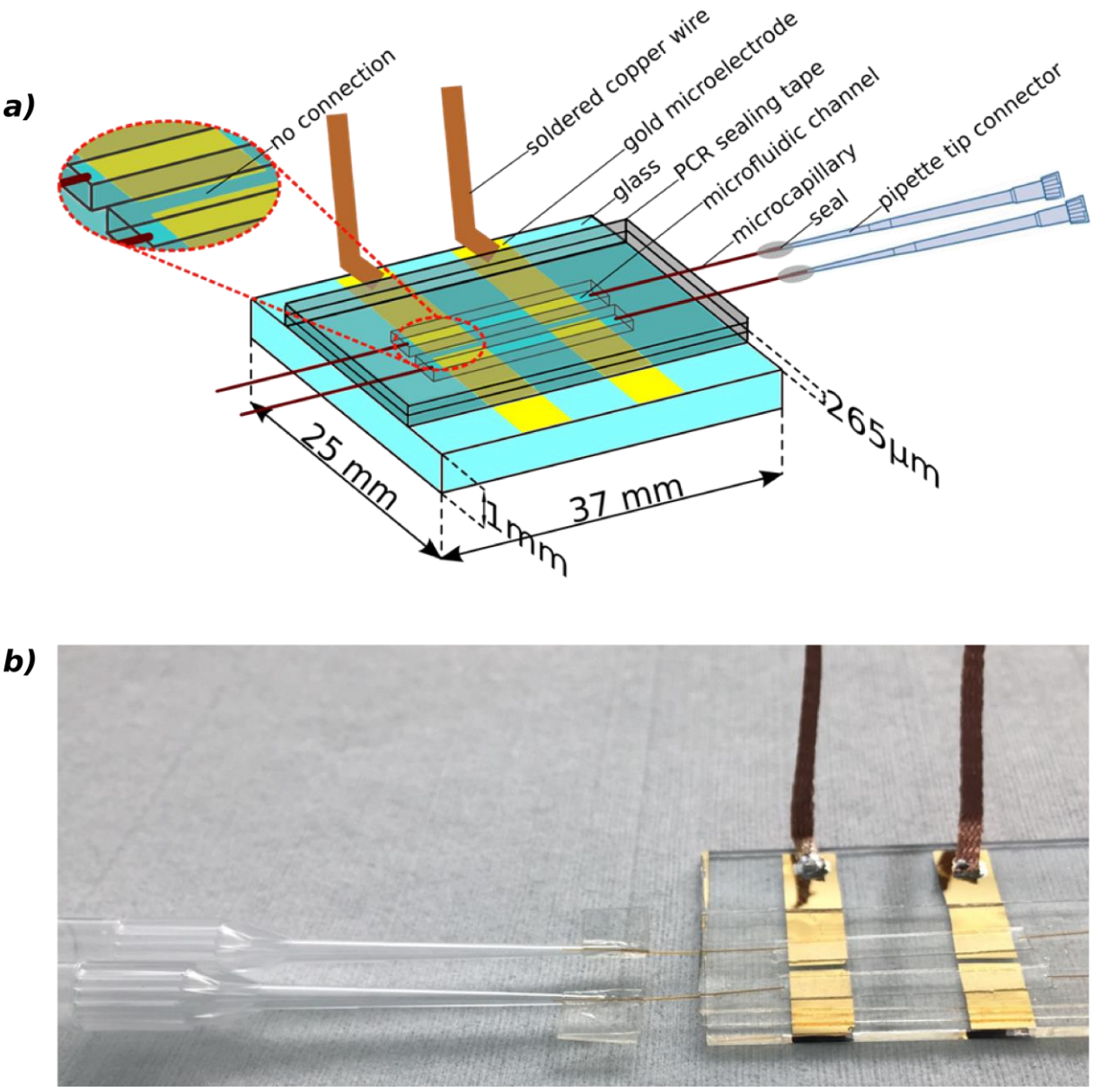

Figure 3.7. Schematic view (a) and a photograph (b) of the device, showing the two microfluidics channels in which a working electrode and a counter/reference electrode are located. The figure also represents the injection set-up used. Note that for better clarity, only one set of electrode is connected to copper wires.

We began by conducting the experiments in microfluidics using either round or oblong shape reaction chambers, made by PDMS or several (usually 4) layers of Parafilm, clamped by two glass slides with one with our two gold electrodes setup. In the case of Parafilm, we applied a pressure using flat ended tweezers under moderate heating (50-60 °C) in order to enhance adhesion between the different layers and between the Parafilm and the glass. The solution inside the chamber was initially introduced by simple opening then closing the top surface of the chamber. In this case, however, trapping an air bubble in the reaction chamber was nearly inevitable (fig. 3.8 a). Bubbles cause variations of the total volume of reaction solution and also can create turbulence and internal flow. In addition, they act as regions of inhomogeneity, make the system more sensitive in terms of the side reactions occurrence such as parasite growth, and thus can handicap the predictions of system behaviour.

In order to get rid of this issue, we used chambers with longer inlets. Then, we have introduced the solution inside by pipetting followed by closing the chamber by using epoxy glue. Besides, we tested the solution's injection using micro-capillaries, introduced in the reaction chamber in between layers of Parafilm. These approaches substantially improved the injection of solutions inside our devices. However, it was still difficult to prevent evaporation and leak issues (fig. 3.8 b). The latter occurs because of the higher affinity of water solution for the glass surface due to its hydrophilic nature rather than for the Parafilm (or PDMS), but also due to the tendency that it can penetrate between Parafilm (or PDMS) and glass either from the bottom or from the top side of our device. This problem occurred at least 50% of our experiments and was time and material consuming.

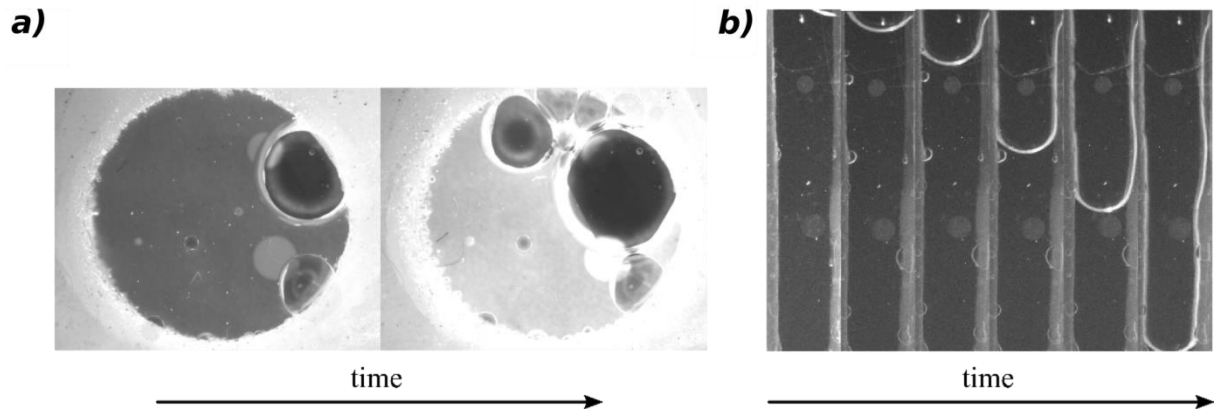

Figure 3.8. Typical issues while performing reactions in microfluidics. Evaporation from round shaped chamber within 2 hours (a) and fast solution leak from oblong shaped chamber within approximately 10 min (b). Both chambers consist of glass bottom with gold electrodes, 4 layers of Parafilm and glass top.

A partial resolution of the leakage issue was achieved by substituting the glass with polystyrene (obtained by cutting a Petri dish) or by using glass slides, covered by a hydrophobic agent, octadecyltrichlorosilane (OTS). In the first case, however, gold electrodes were very unstable on plastic surface and it was extremely hard (although feasible) to solder them. In the second case, the chemical modification increases the adhesion between glass surface and Parafilm and furthermore makes more difficult the introduction of the solution inside the chamber due to the decreased of the surface wettability.

To fix these difficulties, we found a possible solution that involved the elaboration of a reaction chamber made of two layers of adhesive PCR sealing tape (Biorad). It is the same material, which we were regularly used for our experiments in bulk solution and is designed to permit fluorescence detection through it and be highly adhesive even at high temperature. These features allow us to build a robust working device and to introduce the solution through microcapillaries that were previously inserted between the two layers of the sealing tape (fig. 3.7). Furthermore, the ease of fabrication makes it an easily transferable approach especially to biolabs with no microfabrication facilities.

3.4 Launching the PEN toolbox in microfluidics

It has to be noticed that our first experiments in microfluidics were performed, while fluorescence microscopy setup had not been yet optimized. In particular, the sample exposure by the illumination system was controlled in different experiments either manually (by opening and closing microscopy shutter by hand at fixed time intervals, usually 5 minutes) or by homemade shutter (motor with a piece of cardboard assembled to it, integrated through the Arduino hardware with Micromanager, the microscopy software). In the case of manual operation with microscopy shutter and because of obvious inconvenience of conducting experiments in such non-automatized procedure, the measurements were usually terminated as soon as a clear exponential grows of intensity was observed. At that time, we had not yet started monitoring travelling reaction fronts, so, such approach was considered as reasonable. Furthermore, it allowed us to perform more experiments within the same period of time. However, the main problem with our homemade shutter was that it was often disassembled from or simply not functioning because of software errors.

Later, this issue was successfully fixed and all important RD experiments were done using proper setup with an automated CoolLED illumination system, integrated with Micromanager. However, first few experimental results of launching the PEN toolbox in microfluidics are not optimized from the point of view of measurements duration. Nevertheless, we believe that this imperfection is not crucial because of simple behaviour of the observed signal: it is initially constant and after certain time interval (typically less than 1 hour) starts to increase exponentially until eventually reaching a plateau. Onset of exponential reaction was applied in most cases as a controlled parameter.

3.4.1 Verification of signal stability

While working under microscope observation, we noticed a systematically declining fluorescence signal. Such behaviour was not the case in bulk experiments and we therefore decided to study it in more details. For this purpose, it was designed the following experiment. A working device with one microfluidic channel containing solution of Eva Green and DNA template in a normal reaction buffer (with no enzymes) was monitored by measuring a fluorescence signal using usual microscopy settings every 10 seconds. First 96 measurements were conducted at room temperature and after that the heating plate was switched on (with programmed temperature value of 42 °C) while measurements were conducted (fig. 3.9 a). Identical experiment was further performed with another sample, which contained similar solution but with the addition of complementary input (fig. 3.9 b).

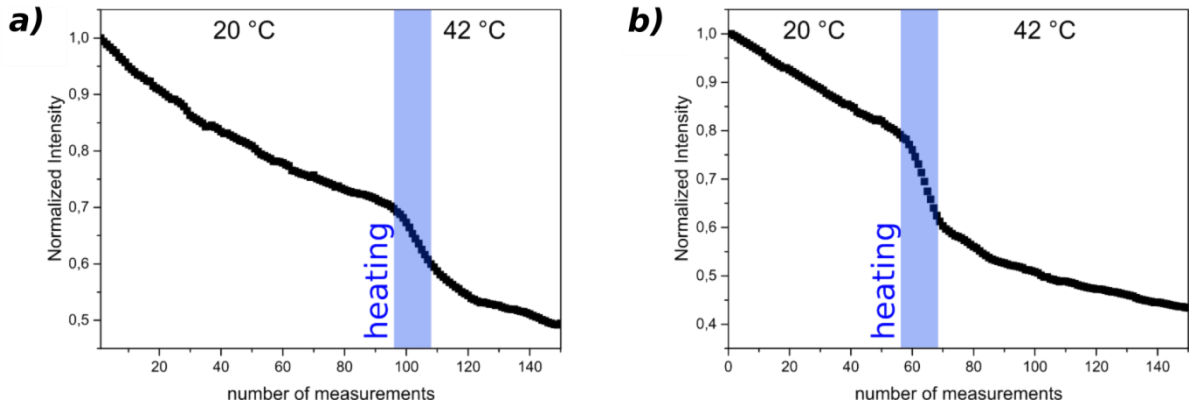

Figure 3.9. Intensity decreases as a function of number of fluorescence measurements and the heating temperature. Solution of DNA template (30 nM) and Eva Green (1x) in standard reaction buffer without (a) or with (b) addition of complementary input (10 nM).

The first conclusion we made by examining these data was that initial intensity decrease in microfluidics does not depend on DNA amplification reaction, since the analysed solutions were enzymes-free. Second, the substantial intensity losses are taking place due to the heating. In this test, we reproduced the standard heating procedure, which normally was taking place at the beginning of the experiments in the microfluidic channels. Thus, the detected intensity losses during heating were supposed to be the same as in our usual surface experiments. The data from fig. 3.9 a were modelling experiment with no DNA input in the reaction mixture and data from fig. 3.9 b were showing behaviour of the triggered system. In the first experiment, intensity losses during heating can be explained by partial dissociation of DNA-Eva Green complex. In the second one, besides this factor, it occurs DNA melting as well. That is why relative intensity changes, during heating in the second test, are bigger than in the first (20% and 11% respectively).

Finally, the strong intensity changes, observed in both experiments when the temperature was stable, were probably caused by interference of the chamber material. Indeed, according to our observation, the resulting fluorescence signal after excitation at 490 nm, when Eva Green is used on the reaction chamber edges (where no solutions was present, but were assembled two layers of PCR sealing tape) was substantially higher, than on bare glass, meaning that the material is weakly fluorescent at this wavelength. This issue does not prevent us to monitor PEN toolbox reactions, but make more difficult the comparison between surface and bulk experiments.

3.4.2 Alternative way to monitor the autocatalysis in microfluidics

In order to minimize the signal deviations caused by our microfluidics setup, we have investigated an alternative way to monitor our reaction (see section 2.4.7). This method relies on the use of DNA template conjugated to a fluorophore (dye-530-NHS ester) and is based on the fluorescence quenching in double-stranded DNA configuration. As a result, in this configuration, the presence of a complementary strand decreases the fluorescence intensity (instead of increasing it when we are monitoring with Eva Green).

For this purpose, we launched an autocatalytic reaction in microfluidic channels. The DNA input was not present in initial solution or immobilized on surface in order to minimise possible signal deviations prior to the beginning of autocatalysis.

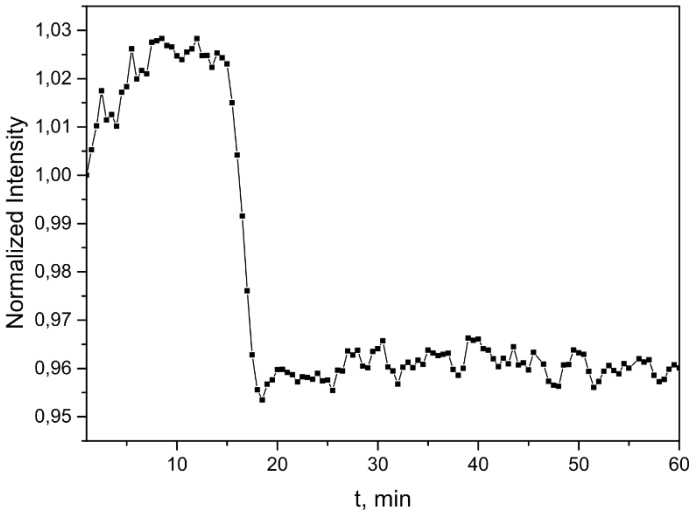

Figure 3.10. Alternative approach for the reaction monitoring by using a DNA template conjugated to a fluorophore, DY-530. Each solution contained 50 nM template, 2% of polymerase, 2% of nicking enzyme. The temperature was 42 °C. 20 x objective was used.

The data indicate an unwavering fluorescence signal on the beginning, followed by a rapid drop of intensity and a subsequent stabilization. Because of the stable signal (in a sense that no declining or increasing trend can be observed) at the end of the experiment, we made a conclusion, that under this experimental conditions, the impact of the material on the fluorescence intensity is minimal. The strong decline happened due to the start of the exponential input production.

In this way, we demonstrated the possibility to monitor the autocatalysis in microfluidic channels, by using the quenching based strategy of dye-530, attached to the DNA template, and in doing so got rid of the material issues. However, the data displayed in fig. 3.10 were obtained by using a 20 x objective (instead of 1.25 x, which was usually applied), which makes not possible to monitor the RD behaviour. Several attempts to reproduce this experiment, using lower magnification of fluorescence microscope, were not successful. For this reason, experiments, discussed further in this chapter were conducted using Eva Green monitoring.

3.4.3 Self-start issue in microfluidics

Back to the Eva Green detection technique, we made an experiment, designed to test the electrochemical triggering of DNA input in microfluidic channels. The course of it was as follows (fig. 3.11 a): We prepared two surface samples both containing gold electrodes but with and without immobilized thiolated-DNA input. After that, the channels were filled with reaction mixture, containing enzymes and DNA template, and were analysed subsequently by fluorescence microscopy. In the case of the channel with the DNA input attached to the gold electrode an electrical release was performed at t = 0 (-2V *vs* Au), whereas no electrical stimulus was applied to the second channel.

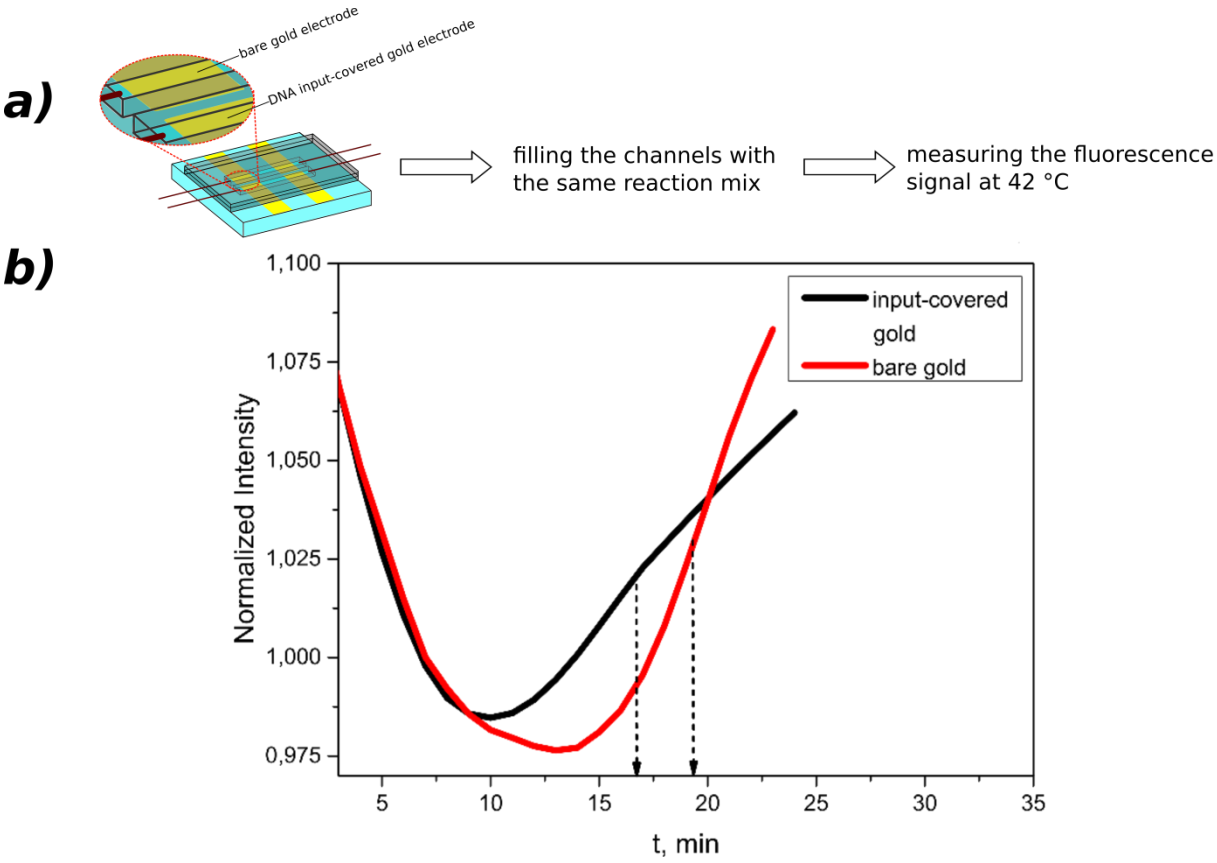

Figure 3.11. Triggering of autocatalysis in microfluidics and self-start issue in case of using non-functionalized electrode. (a) Principle scheme of the experiment. (b) Measured fluorescence profiles. Each solution contained 30 nM template, 2% of polymerase, 2% of nicking enzyme. The temperature was 42 °C.

The date obtained (fig. 3.11 b) serves as a confirmation of our ability to trigger autocatalysis in microfluidic channel and to monitor the reaction, since the amplification curve in the case of released input, presents an exponential increase region, shifted by 7 min from the one, corresponding to the sample with bare gold. However, this time delay (6 minutes) is

unsatisfactorily low. Although it might be improved to a certain extent within this molecular system by tuning concentrations of its components and the temperature, it causes substantial problems with time stability of our technology.

3.4.4 Launching the activation reaction in microfluidics

As we have already discussed (see section 2.4), the self-start is occurring only for the autocatalytic reactions within PEN toolbox. In this case, the input is produced in an avalanche-like way and even at very low amount of this DNA strands (which might be spontaneously produced by polymerase) it is enough to trigger the reaction. No self-start is happening when output and input DNA have different nucleotide sequences. Amplification in this reaction scenario is linear. Although some input or output DNA strands might undesignedly appear, they make no substantial impact on system behaviour and fluorescence profile stays fairly flat (see fig. 2.21). For this reason, such reactions appear as good alternatives to autocatalytic ones to test our electrochemical triggering approach in microfluidic channel and get rid of the self-start issue.

In this way, we aimed first to verify the possibility to monitor this kind of PEN toolbox reactions in microfluidic channels. To do this, we prepared two solutions with non-autocatalytic template and enzymes in usual reaction buffer. It has to be noticed, that exonuclease was excluded from these experiments in order to maximize the signal amplification and to increase the detection sensitivity. To the first solution, we added 5 nM of complementary input. After that, both solutions were analysed simultaneously in bulk and in microfluidic channels (fig.3.12).

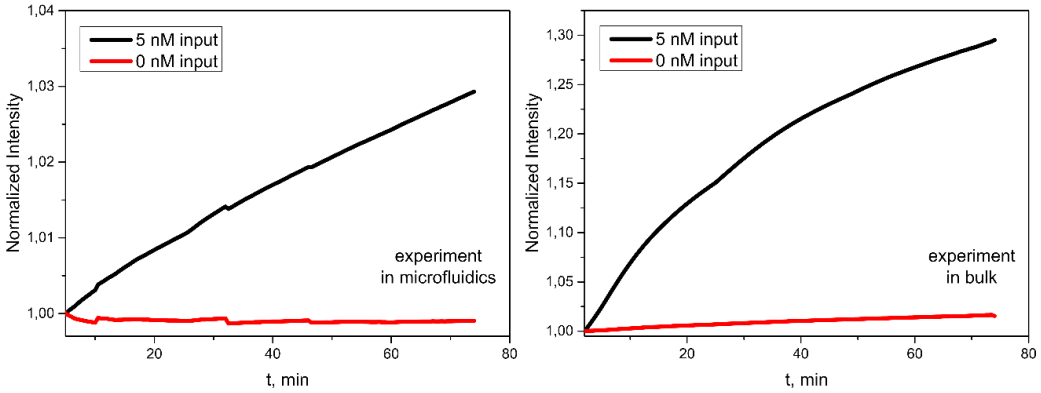

Figure 3.12. Testing of non-autocatalytic system in microfluidic channel and in bulk solutions (control). Input concentration was 5 nM. Each solution contained 100 nM template, 2% of polymerase, 2% of nicking enzyme. The temperature was 42 °C.

Data showed a clear reaction start in both bulk and microfluidic channel for the sample with 5 nM DNA input and a nearly flat fluorescence profile for the solution with 0 nM DNA input. Bulk test was performed in order to have an additional confirmation that the nature of the signal increase in microfluidic experiment is really due to DNA amplification reaction. However, the intensity increase in the second case (only 3%) is rather weak, which was expected due to the absence of exponential DNA production in this system.

As a next step, we launched an experiment in microfluidic channel with electrochemical triggering of non-autocatalytic template. The course of it was as follows: a surface sample was prepared presenting two identical microfluidic channels with working electrodes functionalized by thiolated input-DNA. Both channels were filled with reaction mixture, containing non-autocatalytic template, a complementary DNA sequence to the attached input, enzymes all mixed in standard reaction buffer. At 45 min (beginning of the time axis in fig. 3.13) from the experiment start, an electrochemical input release was performed (-2 V) in only one of the channels. It has to be noticed that the electrode was not polarized at t = 0 min, because we aimed to verify the system robustness in absence of triggering. Then, the fluorescence intensity was monitored using a 2x objective. Results of this experiment are shown in fig. 3.13.

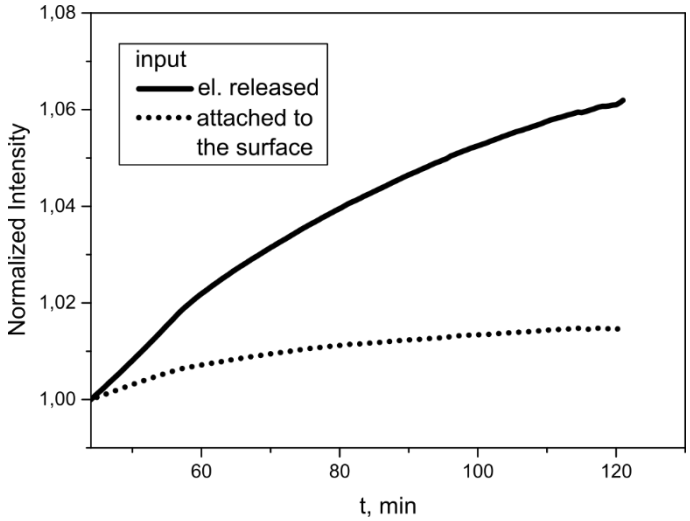

Figure 3.13. Triggering of non-autocatalytic system in microfluidics *via* input release. Demonstrated fluorescence profiles, recorded on working electrode surface and analogues part of the control channel after applying an electrical potential (-2V) at t = 45 min. Each solution contained 100 nM template, 2% of polymerase, 2% of nicking enzyme. The temperature was 42 °C.

Since the intensity profile, in the case of applying electrical potential, shows a clear increasing trend, whereas the second one is fairly flat, these data indicate that the triggering of the reaction on working electrode surface was achieved through the electrochemical release of the input. These results are coherent with the ones from the previously discussed experiment, where 2 solutions were analysed with and without input in the initial reaction mixture (fig. 3.12).

After having obtained these results of triggering the non-autocatalytic template on working electrode surface, we focused on launching the reaction fronts *via* input release. Additionally, we aimed to prove that the intensity increase (fig. 3.13, solid line) was initiated by PEN toolbox reaction, triggered by released input, and not by some system perturbations due to the polarization of the working electrode.

In this way, we have designed an experiment that pursued a double goal: 1) to trigger the reaction front *via* electrochemical input release and 2) to demonstrate that the observed signal is induced by DNA amplification and not by the impact of the electrical pulse on considered system. The course of this experiment was as follows. We have prepared two identical microfluidic channels with DNA input covering the working electrodes inside each of them exactly like in the previous test. After that, we performed 2 kinds of reaction in usual mixture but containing either a complementary sequence or a non-complementary sequence to the immobilized DNA input non-autocatalytic template. Other components (enzymes, buffer

were present in both solutions in equal concentrations). Each of these solutions was injected in one of the channels and the reaction was monitored by fluorescent microscopy at 42 °C. At time 25 min, the input was electrochemically released in both channels. Results of this experiment are shown in fig. 3.14.

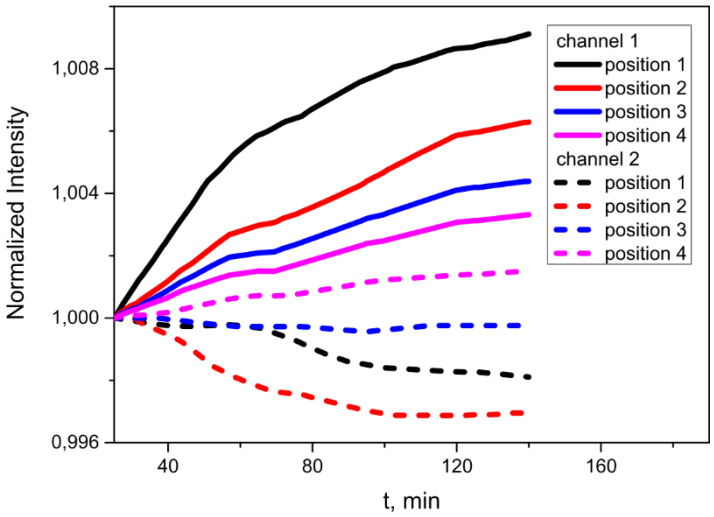

Figure 3.14. Triggering of non-autocatalytic system in microfluidic channels *via* input release and attempt to launch the reaction front (channel 1) and similar experiment with non-complementary template in solution, realized simultaneously (channel 2). Positions of the channels were chosen similarly to fig. 3.16 b. Demonstrated fluorescence profiles, recorded on glass surface of the channels after applying potential (-2V) at t = 25 min. Template concentration was 100 nM. Each solution contained 2% of polymerase, 2% of nicking enzyme. The temperature was 42 °C.

Data corresponding to the measurements in the channel, containing the complementary template and after the input release showed a linear increase of the fluorescence intensity, progressing in direction towards input release region: strongest signal growth was observed in position 1, the closest to the working electrode, and shows progressive damping while moving outwards to the working electrode. In the second channel fluorescence signal remains either stable or decline with no trend.

Such behaviour was expected to be seen in the case of launching the front of non-autocatalytic reaction *via* input release. In channel position where input was released, amplification reaction speed is maximal, since local concentration is the highest. As diffusion occurs, reaction is slowing down and, consequently, the fluorescence intensity farther from the working electrode increases weaker and weaker. All the profiles are not initially flat, although they expected to be so until the diffusing species reach the corresponding channel positions.

This is presumably due to the low intensity of measured signal and, consequently, high level of noise.

The maximal signal intensity gain was around 0.9 %, which is 1 order of magnitude lower than in case of monitoring on gold electrode surface. However, this fact can possibly be explained by the reflective nature of gold surface (which is, obviously, not the case for transparent glass) and, consequently, the accumulation of higher signal on it. Additionally, intensity deviations of fluorescence profiles, corresponding to the channel with non-complementary template are comparable with the signal increase in another channel (around one-half of it). This makes the system with non-autocatalytic template unsuitable to perform robust experiments in the configuration we used.

Therefore, we had to return to the autocatalysis in order to demonstrate a robust proof of the triggering of reaction fronts in microfluidic channel.

3.4.5 Chemical passivation of surfaces

As we conducted our experiments in microfluidic channels, where surface-area-to-volume ratio is much higher than in bulk tests, adsorption of components of reaction mixture, notably enzymes, played an important role on our system behaviour [120]. Enzymes with different affinity regions in their structures, are well-known to physically adsorbed on both hydrophilic and hydrophobic surfaces [121] , including glass [122]. This increasing adsorption phenomenon can potentially influence the behaviour of the molecular system we used by triggering the self-start of our autocatalytic system. The reaction buffer we usually applied over the course of the present study, designed elsewhere [77], already contains two surface passivation agents: Synperonic, a non-ionic surfactant, and Bovine serum albumin (BSA). The use of BSA in order to passivate surfaces is well-established [123] [124]. As enzymes and BSA are both proteins, we assumed that the last one could be particularly useful because of possible competitive adsorption on surface.

In this way, attempting to delay the self-start of autocatalytic reaction, we wanted to improve surface passivation by increasing concentration of BSA in the reaction mixture. For this purpose, an experiment was conducted with simultaneous analysis in bulk and in microfluidic channels of two reaction mixtures, containing both enzymes and template (but not an input). Reaction buffer in the first mixture contained usual BSA concentration (0.5 mg/ml in

the final solution), while in the second one, the BSA concentration was 4 times higher (2 mg/ml). Results of this experiment are demonstrated in fig. 3.15.

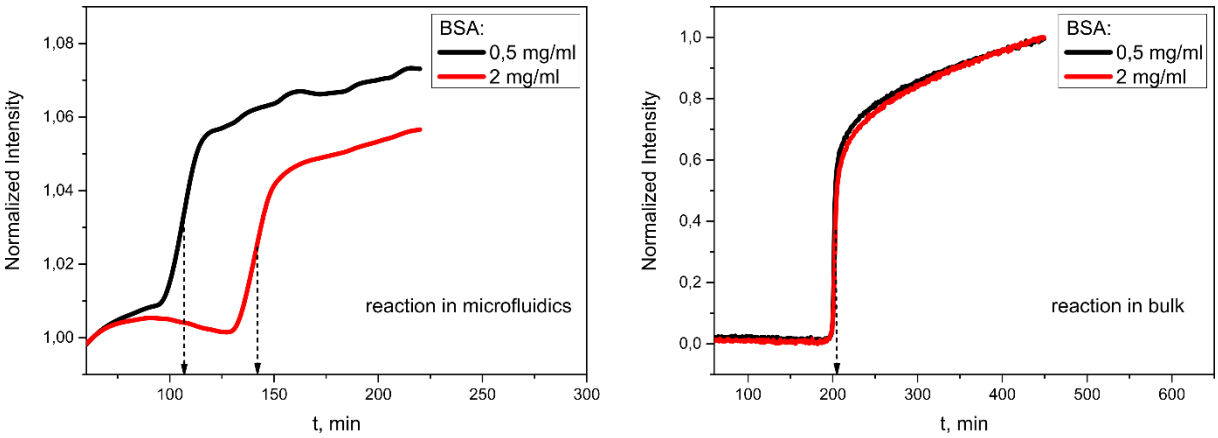

Figure 3.15. Passivation of the surfaces by increasing BSA concentration in order to delay the self-start. Two solutions with usual (0.5 mg/ml) and 4 times higher concentrations of BSA were analysed simultaneously in microfluidic channels and in bulk. Each solution contained 120 nM template, 2% of polymerase, 2% of nicking enzyme. The temperature was 42 °C.

Data indicate a substantial influence of BSA concentration on delaying the self-start in micrfluidics, while there is no impact in bulk solution. Thus, we can conclude that this impact is not given by BSA itself, but by materials of our microfluidic reaction chamber. Most likely, this effect occurs due to the slowing down of the enzymes (or DNA) adsorption by competitive adsorption of BSA. The concentration of this passivation agent plays a more important role in microfluidic channel rather than in bulk tests, which must be taken into account while launching experiments in microfluidics. These results can be explained by difference in surface-to-volume ratios (and, consequently, impact of protein adsorption processes on system kinetic) in these experiments.

Although, we have demonstrated a method of delaying self-start in microfluidics, it was desirable to completely get rid of this issue. Additionally, we aimed to modify original conditions of PEN toolbox as little as possible in order to enable the use of our technology in wider range of applications. Indeed, it is possible that, in case of systems with complex dynamics such as Oligator (see section 2.4.7), that is very sensitive to changes of experimental conditions, such modifications of reaction buffer can be detrimental and will lead to failing experiments. For these reasons, in the subsequent experiments were not adjusted BSA concentration and we were looking for alternative, more sophisticated methods of increasing the robustness of molecular system.

3.5 Launching the RD fronts with autocatalytic system in microfluidics

Finally, we wanted to establish our ability to observe reaction diffusion type of phenomena in our microfluidic set-up. We therefore performed an experiment for triggering the autocatalytic reaction *via* an active surface and subsequent launching RD front. First, we prepared two microfluidic channels both containing gold electrodes. However, only one working electrode in one of the channels was modified by thiolated input DNA. Next, a solution of complementary autocatalytic template and enzymes in reaction buffer was prepared and injected inside channels. The working electrode with attached input was polarized (-2 V) in order to release it and sample intensity inside the channels was monitored at 42 °C by fluorescence microscopy. As a control, we analysed an identical sample with the only one difference: the gold electrode inside microfluidic channel was not functionalised. The input was released at t = 0 min, since we expected a self-start in this system (which can be observed in the second channel which is our control). Propagation of the reaction front was detected by measuring intensity profiles in different connected parts of the channel with equal area (fig. 3.16 b). Results of this experiment are shown in fig. 3.16 a.

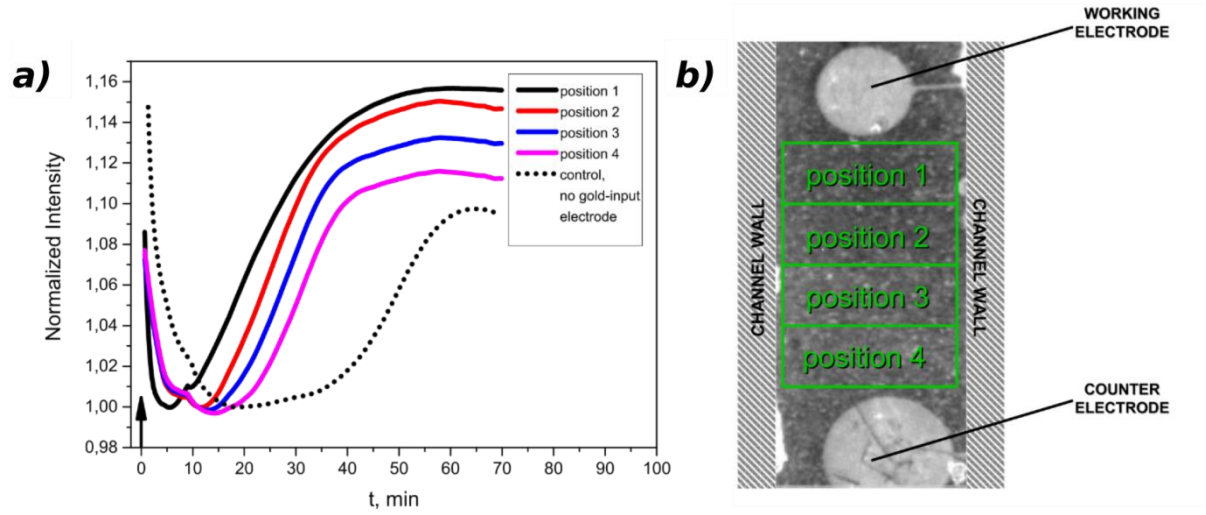

Figure 3.16. (a) Triggering of autocatalytic system in microfluidic channels *via* input release and launching the reaction front (solid lines) and simultaneous control experiment with a sample, containing non-functionalized and not polarized gold electrodes in the same reaction solution. (b) Different locations within the microfluidic channel. Solid arrow indicates the polarization of the input-functionalized working electrode at t = 0. Each solution contained 30 nM template, 2 % of polymerase, 2 % of nicking enzyme. The temperature was 42 °C.

Data show an exponential increase of the fluorescence intensity, which progresses alongside the channel, from where input was released, beginning at position 1, the closest to the working electrode. Similar intensity profile can be observed for the control, being however homogeneous alongside the channel and having the exponential increase start significantly delayed. These results proved successful triggering of autocatalysis and subsequent propagation of the reaction front, because of directionality of signal evolution and equal time intervals (~5 min) between intensity profiles, corresponded for equivalent channel positions, separated by equal distances.

On the other hand, these results showed system self-start in absence of triggering and any input DNA on surface or in reaction mixture, since average intensity profile in control channel has the characteristic shape for autocatalytic reaction. Such behaviour is highly undesirable since it aggravates the time control of the molecular system with active surface and is not satisfactory in terms of initially established requirements for our technological solution.

Therefore, further improvements were required in order to deal with such metastability.

3.6 Conclusion

We have discussed in this chapter the various manufacturing approaches of active surfaces tested in this thesis and the strategy of DNA release using them as well. We have confirmed successful attachment of DNA with 5' dithiol modification onto gold surface, followed by electrochemical cleavage of Au-S bond and its release in solution followed by fluorescence, electrochemical and contact angle measurements. We further demonstrated that input, released from the gold surface could successfully trigger autocatalytic reaction.

Moreover, we launched a PEN toolbox reaction using these active surfaces. For this purpose, we designed a suitable microfluidic reactors and surveyed several reporting strategies in our fluorescence microscopy setup. We compared the system's behaviour in microfluidic channels and in bulk solution and verified different factors influencing it in microfluidic channels (signal deviation due to material and temperature changes, enzymes adsorption on surface).

We performed successful triggering of autocatalysis and observed propagation of reaction fronts on surface. However, due to the self-start issue, our system possesses unsatisfactory stability and requires further improvements. For this reason, we applied our

triggering strategy on non-autocatalytic system. While amplification curve on working electrode surface after input release was clearly observed, we did not succeed to clearly demonstrate RD fronts with this system due to very weak signal increase. We believe, that such monitoring difficulties in case of the use of non-autocatalytic template are caused by moderate, non-avalanche-like amplification, which is harder to detect rather than autocatalysis.

Finally, for this reason we returned back to an autocatalytic system to verify our technology and were looking for further improvement in order to avoid the problem of the self-start and increase system stability. We demonstrated the ability of high BSA concentrations to delay it due to the surface passivation. However, substantial changes of reaction buffer were not desirable due to potential impact on complex systems within PEN toolbox.

In next chapter, we will demonstrate an approach for complete elimination of autocatalysis self-start and also optimized reporting and surface fictionalization strategy, which will allow us to better control spatiotemporal behaviour of the system in microfluidics and provides robust proofs of functioning of our technology.

Chapter 4

Spatiotemporal control of DNA-based chemical reaction network *via* electrochemical activation in microfluidics

4.1 Introduction

We have previously demonstrated the successful triggering of activation and autocatalytic reactions of the PEN toolbox using active surfaces (see chapter 3). Although we confirmed our triggering approach was sound (see, for instance, section 3.5), several issues remain to be solved. In particular, the molecular system must be optimized to ensure its stability in absence of external stimuli (input release) in order to enable the study whether the active surface can provoke unintended triggering. Additionally, a strong enough signal amplification is required to permit us the monitoring of the reaction-diffusion fronts.

In the present Chapter, we will demonstrate how we solved these issues using an autocatalytic CRN, based on autocatalytic module combined with "drain" reaction. The latter is added to deal with the metastability of the molecular system. Furthermore, we apply a selective fluorescence reporting strategy in microfluidics, which permits us to specifically monitor input strands and provides higher signal-to-noise ratio and, consequently, facilitate the observation of reaction diffusion fronts.

We will first provide a detailed description of the assembly and optimisation of autocatalytic CRN using bulk reactions. Next, we will transfer this system in our microfluidic setup and perform various control experiments (simulation of input release, influence of the electrodes polarisation on system behaviour, impact of reporter concentration *etc.*). We will further conduct the experiments with spatiotemporal control of the CRN *via* electrochemical activation and will perform step-by-step final optimisations of active surfaces and molecular system.

4.2 Autocatalytic CRN and its mechanism

In order to get rid of metastability issue, we introduced an autocatalytic CRN, which is composed as follows. The reaction shown in fig. 4.1 a, is based on 22 nt DNA template which produces an autocatalytic amplification of the input. When an input strand hybridizes on the 3' end, it gets elongated by the polymerase and cut by the nickase to produce 2 copies of the initial input. This in turn can be used to produce more copies of themselves. Such template thus induces an autocatalytic amplification reaction, which is a metastable in the sense that, even in the absence of initial trigger, it will always initiate spontaneously after some time [100]. A strategy is therefore required to prevent this self-start. To this end, the first input-binding part of the template is truncated by 2 nt to decrease its affinity to the input, and a second template is introduced.

This second template codes for the reaction shown in fig. 4.1 b. In order to suppress untriggered start of the autocatalysis an additional, non-linear degradation pathway is added through this pseudo-template. It is 17 nt long, with the same PTO modification as the other templates. It is fully complementary to the input on its 3' end and thus presents a higher affinity to it than the autocatalytic template. After hybridization on the pseudo-template, the input strand is elongated by the polymerase. The last 5 nt are not complementary to the autocatalytic template and the elongated input strand is therefore no longer able to participate in autocatalytic reaction. Furthermore, the absence of the nickase recognition site does not allow for recycling of the initial input through cleavage. As a result, the elongated sequence can only be degraded by the exonuclease. This degradation pathway has a limited throughput, controlled by the concentration of the pseudo-template and its turnover rate. When this throughput is exceeded, it is not able to process the additional inputs, and the amplification process encoded by the autocatalytic template can proceed. By tuning the template and pseudo-template concentrations ratio it is therefore possible to make autocatalytic reaction resistant for input concentrations lower than a chosen "threshold concentration" (fig. 4.2). The stabilisation of the OFF state, induced by the presence of the pseudo-template, is a key requirement to achieve a robust autocatalytic CRN, which only starts when purposely triggered.

The last DNA sequence added to the mixture enables monitoring in real time the input strand concentration. It was used only in experiments in microfluidic channels, since we faced an issue of fluorescence intensity deviations and a low signal-to-noise ratio (see fig. 3.9). As shown in fig 4.1 c, a sequence-specific DNA molecular beacon was used with a Cy-5 dye on

its 5' end and a BHQ2 quencher on its 3' end. When the beacon is in its closed, self-hybridised, configuration, the proximity of the quencher to the dye prevents any fluorescence from being emitted. In presence of an input strand, the beacon is stabilized in its open configuration through the polymerase-mediated elongation of the input and fluorescence can be observed. This reporting strategy is reversible, because the nickase cuts the extended input strand part of the duplex – as it contains its recognition site – and recycles the molecular beacon and the input. Additionally, it releases an another, later on inactive, short strand which gets subsequently degraded. Consequently, the monitoring process, unlike the two reactions, which compose autocatalytic CRN, has little influence on the input concentration.

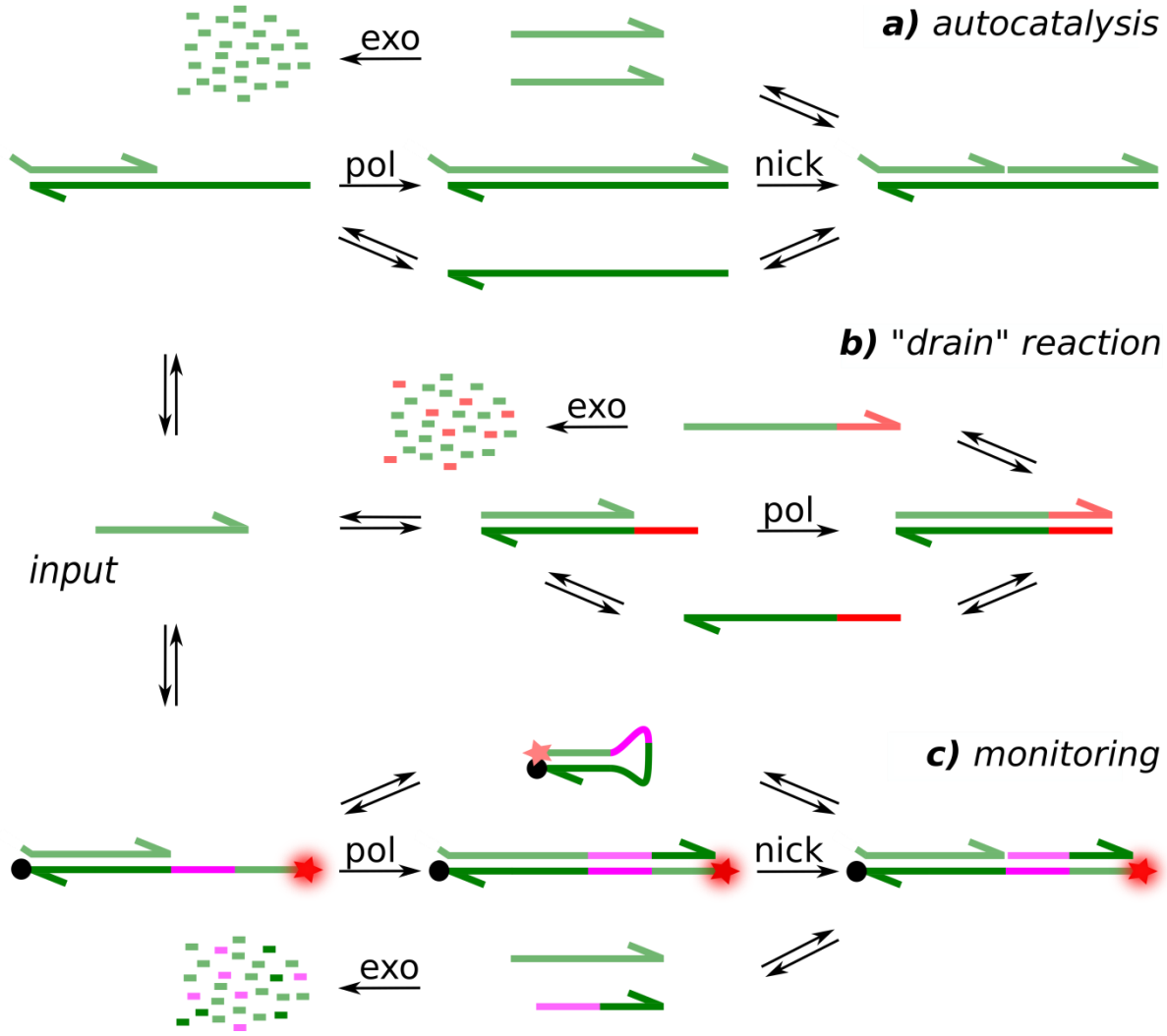

Figure 4.1. Schematic of the three reactions, which constitute the Chemical Reaction Network and its monitoring strategy. Subnetwork (a) is the autocatalysis core, (b) is the non-linear degradation pathway used to induce bi-stability and (c) the molecular beacon reporter whose intensity is proportional to the concentration of input strand, which was applied only in microfluidic experiments.

4.3 Assembly and optimization of the CRN

4.3.1 Verification of “drain” reaction

Prior to launching experiments in microfluidics, we had to assemble the CRN and optimize its working conditions. To do this, we studied the impact of drain reaction on its kinetic. Were analysed two series of solutions with (5 nM) and without (0 nM) the input DNA in the initial reaction mix. In both series was created the gradient of pseudo-template concentration. Concentrations of all other components (template, enzymes *etc.*) were equal in all analysed samples. The reaction buffer is composed of 50 mM NaCl, 10 mM $(NH_4)_2SO_4$, 10 mM KCl, 8.4 mM $MgSO_4$, 0.4 mM of each dNTP, 0.1% Synperonic F108, 500 µg/mL BSA (NEB), 2 µM Netropsin (Sigma-Aldrich). Unless otherwise indicated, the same parameters we used for all other experiments, described in this chapter. Results of these experiments are demonstrated in fig. 4.2.

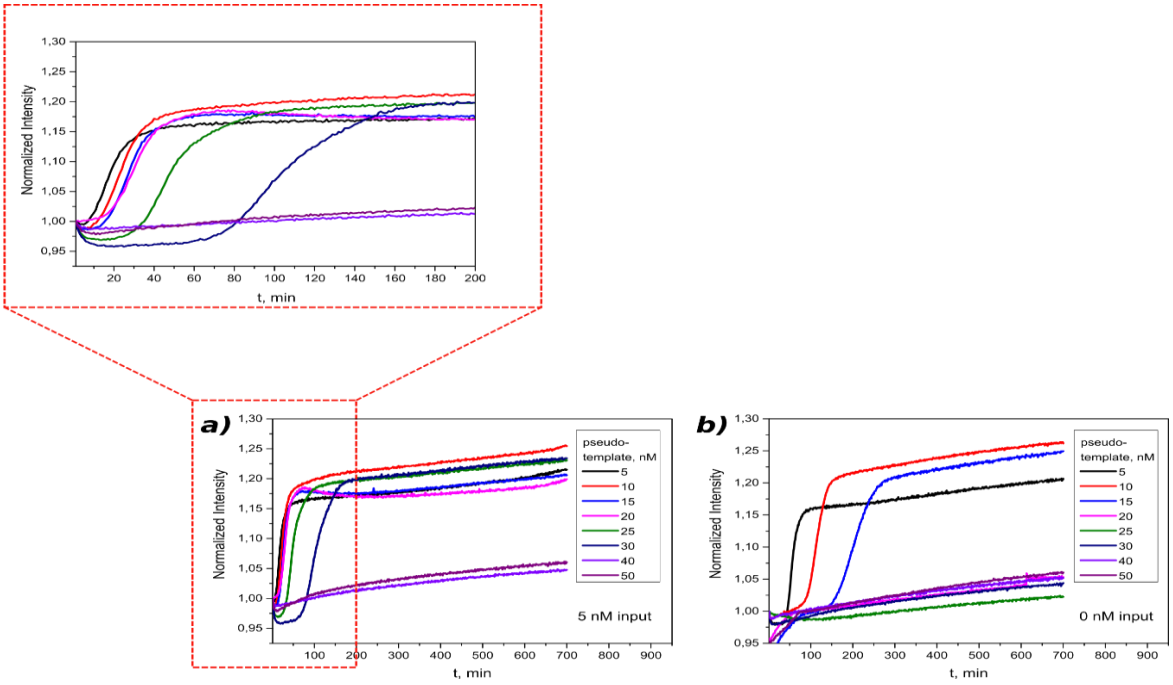

Figure 4.2. Fluorescent monitoring of an autocatalytic CRN with various concentration of pseudo-template at 42°C. (a) With 5 nM initial input DNA to check in which condition the autocatalysis can be triggered. Additionally, scale from 1 to 200 min is shown. (b) Without input to check the pseudo template perform its function to prevent self-start. Each solution contained 50 nM template, 1% of polymerase, 1% of exonuclease and 2% of nickase. The temperature was 42 °C.

The data indicate, that increasing the concentration of pseudo-template leads to delaying the exponential intensity growth region with eventual complete suppression of the autocatalysis in both experiment's scenarios – with input in initial reaction mixture (fig. 4.2 a) and without it (fig. 4.2 b). However, in the first case this factor makes substantial impact only from relatively elevated pseudo-template concentrations (higher than 20 nM under these particular experimental conditions). Contrary, in case of absence of input in reaction mixture this effect is stronger: for the concentration of pseudo-template, higher than 15 nM, no autocatalysis is taking place. In other words, at some concentrations range (15-25 nM in this experiment) drain reaction makes autocatalytic CRN resistant to the self-start, and, on the same time, impacts negligibly on its kinetic as can be seen from fig. 4.2. It has to be taken not account, however, that these pseudo-template settings must be carefully adjusted depending on experimental conditions (mostly due to tuning the enzymes concentrations and using new batches).

4.3.2 Optimization of the reaction temperature and pseudo-template concentration

In order to prevent the reaction self-start, we aimed to reduce as much as possible the impact of undesigned input thermodesorption (see section 4.5.5). For this purpose, CRN parameters (enzymes, pseudo-template concentrations and working temperature) were tuned in a way to make system resistant (or at least less sensitive) for a low input concentrations. Figure 4.2 shows that upon some critical concentration of the drain module, kinetics of autocatalytic reaction is not substantially changing. Moreover, at some point, it is changing strongly by responding on small addition of pseudo-template. This critical concentration for given experimental conditions provides the optimal suppression of side processes. To define it, we analysed the CRN with initial triggering and a range of pseudo-template concentrations under 3 different temperatures (38 °C, 42.4 °C and 45 °C). Just before the experiment's start, enzymatic mixture was added, 10 x solution of which contained: Bst 2.0 WarmStart DNA Polymerase (NEB): 8% of (/20) solution in diluent A (NEB); Nb.BsmI nicking enzyme (NEB): 40%; ttRecJ exonuclease (provided by collaborators): 15% of (/140) solution in diluent A; BSA, 20 mg/ml: 25%; diluent A: 12%. Unless otherwise indicated the same parameters of enzymatic mixture were applied in

all other experiments, described in this chapter. Results of this experiment are demonstrated in fig. 4.3.

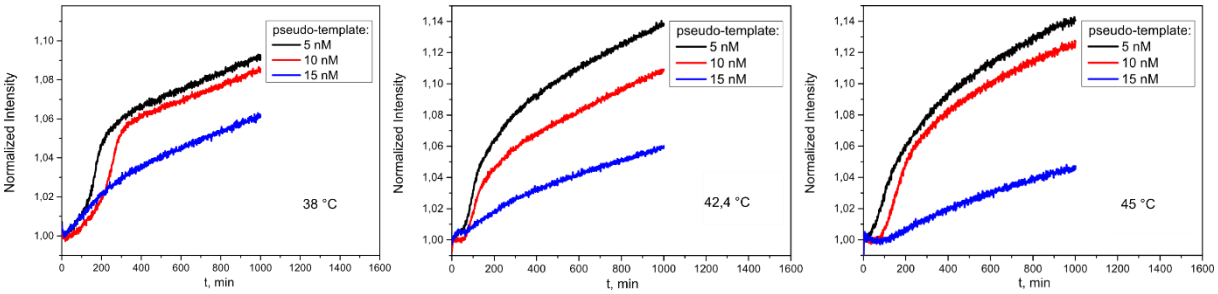

Figure 4.3. Finding optimal temperature and pseudo-template concentration for efficient suppression of autocatalysis ignition due to parasitic processes (self-start, thermal-desorption). Each solution contained 50 nM template and 5 nM input.

Based on these data, we chose 38 °C and 10 nM pseudo-template concentration as optimal conditions as under them triggered autocatalysis is strongly delayed (with comparison to lower drain module concentration), but can still take place. Further increase of pseudo-template concentration under 38 °C leads to complete blocking of the autocatalysis. It is also the case for experiments under 42.4 °C and 45 °C. Consequently, under investigated conditions the template and pseudo-template concentrations ratio equal 10:3 (=50:15) makes autocatalytic reaction resistant for input concentrations lower than “threshold” level of 5 nM.

4.3.3 Imitation of the CRN electrochemical triggering in bulk

After having successfully assembled the CRN and optimized its parameters, we first imitated in bulk the experiment with electrochemical input release, designed for microfluidics. To do so, we launched an experiment with non-triggered CRN under 38 °C and with 2 pseudo-template concentrations (5 nM and 10 nM) for 194 min and after that injected 1 µl of 100 nM input solution (~5 nM final concentration in the reaction mixture). Obtained results (fig. 4.4) show system inactivity before the input injection. After it, CRN behaves in a similar way as in case of initial activation (fig. 4.2 a): it takes ~50 min (5 nM pseudo-template) and ~200 min (10 nM pseudo-template) for the system to reach the exponential intensity growth region. These data indicate the CRN stability for at least 3h in absence of triggering and, from the other hand, proof the concept of the system activation at designed time *via* releasing the input DNA.

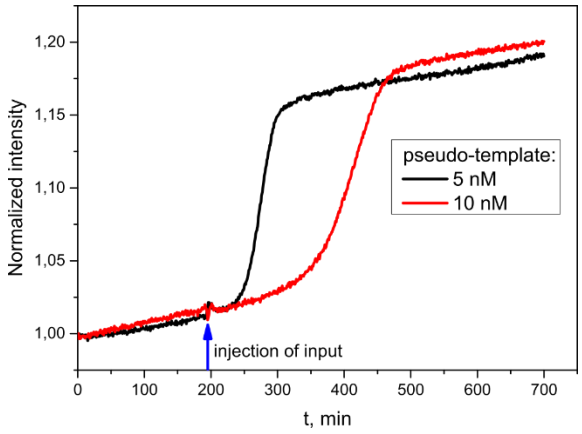

Figure 4.4. Activation of CRN at a chosen time in bulk for two pseudo-template concentrations. The system remains stable in its non-catalytic state before injection of input DNA. Each solution contained 50 nM template. At t = 194 min was injected 1 µl of 100 nM input solution (~5 nM final concentration) to each of the samples. The temperature was 38 °C.

4.4 Experiments with the CRN in microfluidics

4.4.1 Introducing the reporting reaction

As a next step prior to electrochemical activation experiments, we tested on surface the selective monitoring strategy in microfluidics (see fig. 4.1 c). We performed an experiment with two concentrations of reporter strand, 50 and 100 nM (each one in a separate microfluidic channel). Additionally, we designed a spatially controlled CRN activation by locally drying (at channels parts prior to position 1) a 0.5 µl droplet of 100 nM input solution. Results of this experiment are demonstrated in fig. 4.5.

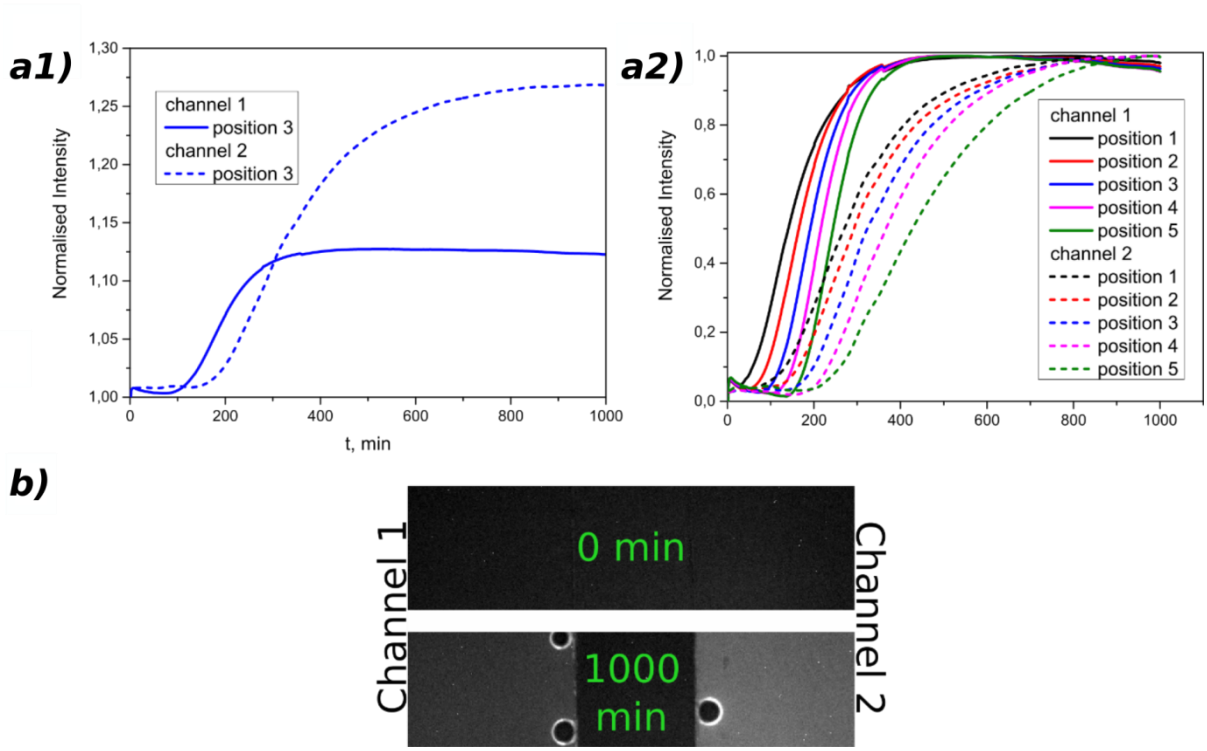

Figure 4.5. Verification of impact of reporting reaction on the CRN kinetic. Concentrations of the reporter DNA were following: 50 nM (channel 1) and 100 nM (channel 2). Data were normalized from 0 to 1 (a2) for clarity, since original signal increase in channel 2 (a1 and b) is ~2 times higher. Each solution contained 50 nM template. 0.5 µl of 100 nM input solution was dried near position 1 in each of the channels. The temperature was 38 °C.

Data show clearly an exponential intensity growth and propagation of reaction fronts starting from position 1 (the closest to the dried input region) in both channels (50 nM and 100 nM reporter). Increasing the reporter concentration, expectedly, leads to intensification of fluorescence signal (fig. 4.5 a1). On the same time higher reporter concentration slows down the reaction kinetic (fig. 4.5 a2). This phenomenon can be explained in a following way. Since input hybridizes in parallel to the template and to the reporter strand (fig. 4.1), increasing of concentration of the last one can partially block bigger fraction of input and slow down the autocatalysis. This parameter should be consequently adjusted in a manner, which makes feasible sensitive enough reaction monitoring, and, at the same time, not changing a lot reaction's kinetic. We will next demonstrate that the reporter concentration 50 nM under these experimental conditions is satisfactory in terms of CRN behaviour and detection sensitivity.

4.4.2 Verification of reporting reaction on fluorescence signal

Reporter DNA strand participates in an activation PEN toolbox reaction (fig. 4.1), which was designed to stabilize its duplex with input and enhance the sensitivity. For this reason, one can imagine that such process can induce the intensity increase over a time and, consequently, interfere with autocatalytic reaction. If so, the data in microfluidic experiments, obtained using this monitoring strategy would be not representative. In order to verify whether reporting reaction by itself can influence time evolution of detected signal, was done the following experiment. In each of two separate microfluidic channels was locally deposited a 0.5 µl droplet of 100 nM input solution. After it dried, first channels was filled with the reaction mixture, containing all the components of CRN, and the second one with the same solution, but without the template (*i.e.* solution in the second channel contained only reporter and enzymes in a standard reaction buffer). Time evolution of intensity along the channels was recorded.

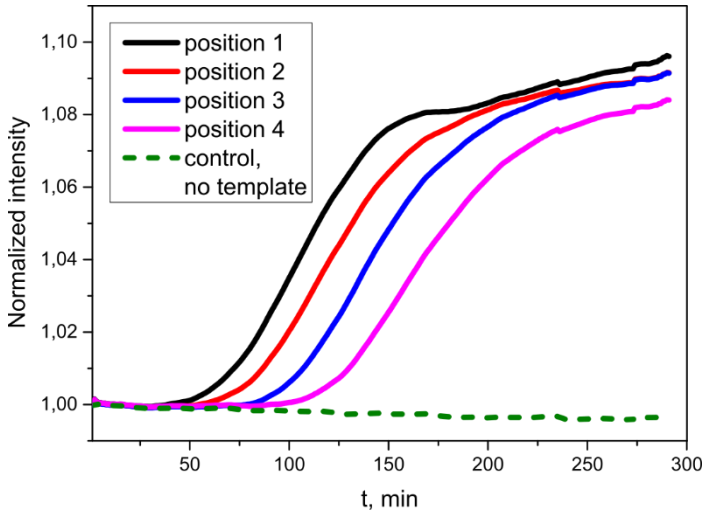

Figure 4.6. Control for initial input DNA release impact on reporter strand fluorescence. Profiles in two channels respectively with 50 nM (position 1-4) and without (control) the autocatalytic template. Each solution contained 50 nM reporter and 5 nM pseudo-template. 0.5 µl of 100 nM input solution was dried on the edge in each of the channels. The temperature was 45 °C.

Obtained data show no signal changes for the channel with no template in reaction solution (fig. 4.6, dashed line). Expected intensity growth and reaction front propagation from the input deposited region of the channel was observed in case of fully assembled CRN (fig. 4.6, solid lines). These results mean that the input DNA, when released is not concentrated enough to change the reporter strand intensity and only autocatalytic amplification with the template can result the evolution of the fluorescence signal in our experiments. In this way,

lower reporter concentration (50 nM) not only perturbs less the reaction kinetic, but also makes no additional impact on detecting signal until the start of autocatalysis.

4.4.3 Verification of impact of the surface on kinetic of the CRN

Since our electrochemical activation requires the presence of gold electrodes in microfluidic channels, we investigated whether or not this factor makes an impact on reaction kinetic. For this purpose, we launched an initially triggered autocatalysis on glass surface, half of which was which was covered by gold. Experiment was performed for two concentrations of reporter in order to verify impact of gold on the monitoring of the reaction (one can imagine such undesigned effects as, for instance, partial deactivation of reporter DNA due to its Cy-5 fluorophore quenching near the gold surface).

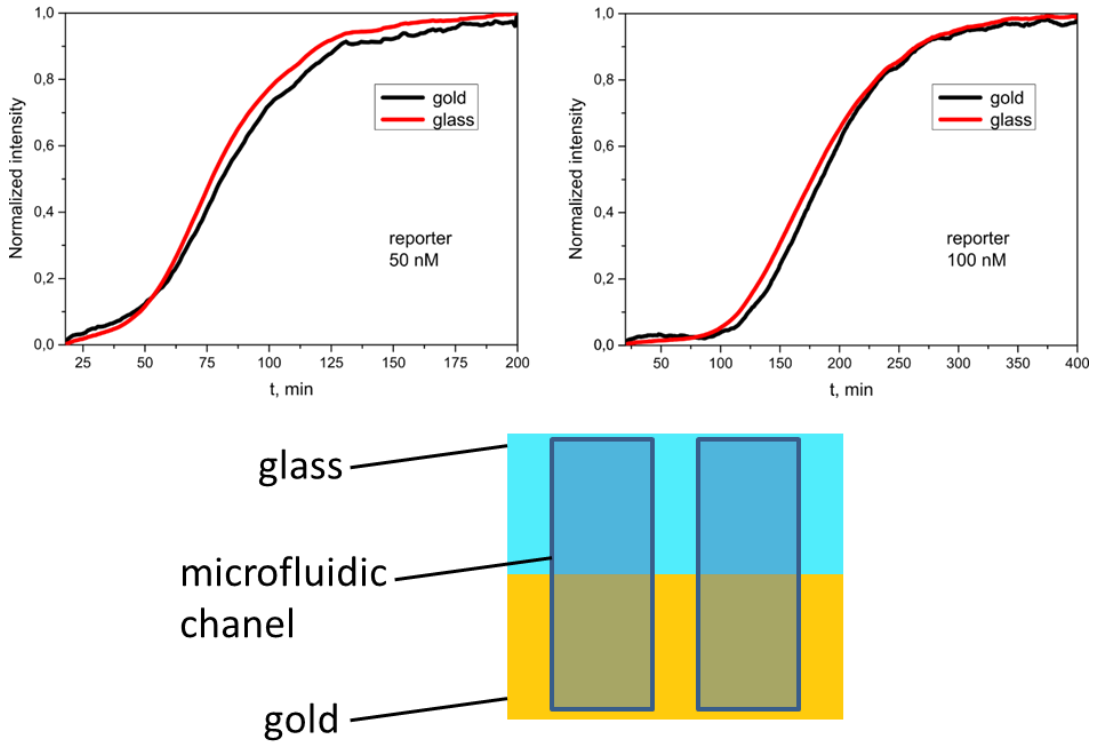

Figure 4.7. Impact of a gold surface on autocatalytic and reporting reactions. Note that for these particular data was applied 0-1 normalization, since due to the reflective properties of the gold surface original signal on it is substantially higher rather than on transparent glass. Schematic representation of analysed sample is shown for clarity. Each solution contained 50 nM template and 5 nM input. The temperature was 42 °C.

Data indicate identical reaction kinetic on gold and on glass surface for both reporter concentrations: the time of onset of exponential growth is 3 and 5 minutes for 50 nM and 100 nM of reporter concentration respectively (fig. 4.7). Thus, in the first case this reaction on gold delayed and in the second case on glass. Therefore, these onsets are most likely caused by signal deviations in different location on the channel, and not by properties of the surface. We can consequently conclude that integration of gold electrode in our microfluidic setup does not additionally perturb neither autocatalysis kinetic nor reporting reaction.

4.4.4 Verification of impact of the electrical pulse on fluorescence signal

Electrochemical cleavage of Au-S bond occurs nearly instantaneously (within 5 seconds) followed by DNA release in solution (see section 2.2.2). Electrode polarization time was chosen as 20 sec in order to ensure complete release of thiolated DNA into the reaction medium. Long time periods of applying voltage can however potentially make an impact on the CRN or the fluorophore in one way or another. Aimed to study these effects we conducted the following experiment. Microfluidic channel was assembled on glass surface with gold electrodes on top of it, which were close enough to each other to be visible simultaneously by our fluorescence microscopy setup (fig. 4.8 b). Channel was filled with our normal reaction buffer, contained 100 nM solution of DNA (11 nt long) with attached Cy-5 fluorophore on its 5' end. We have not use the reporter DNA in this experiment, since in absence of autocatalytic amplification of input it remains quenched and no signal can be detected (fig. 4.1 c). We used a model-DNA instead, with the same fluorophore (Cy-5), but no quencher. Sample was imaged during 15 minutes under fluorescence microscopy in order to verify time evolution of fluorescence signal in absence of polarization. Next, at t = 15 min -2 V (*vs* Au) pulse was applied to the working electrode during 200 sec with simultaneous recording of fluorescence signal (every 1 min). Imaging was continued after electrode polarization was finished.

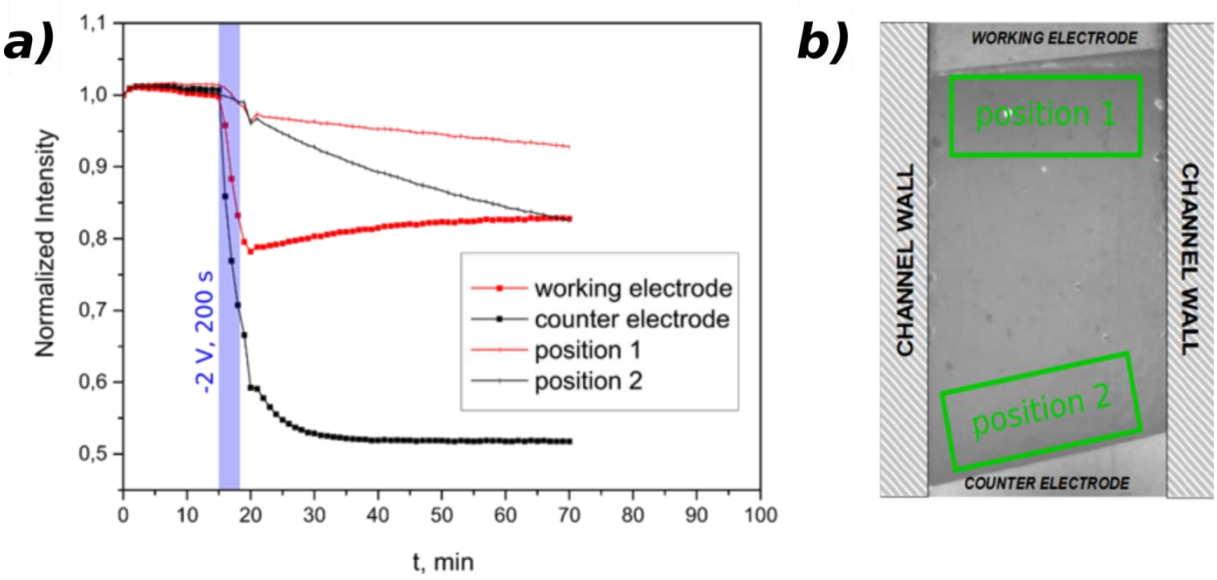

Figure 4.8. Impact of electrode polarization on Cy-5 fluorescence signal (a), detecting on different parts of microfluidic channel (b).

Obtained data (fig. 4.8 a) show stable fluorescence signal before applying the voltage. Consequently, in contrast with Eva Green (fig. 3.9), Cy-5 fluorophore permits more reliable monitoring in our experiments. After polarization, an interesting behaviour can be observed. Fluorescence intensity decreases in all locations of the sample. However, this effect is quantitatively very different on working and counter electrodes and on glass parts of the channel, close to them. Additionally, over the electrodes surfaces signal behaviour substantially differs during and after the pulse: it decreases strongly (up to 20 % during 200 s for the working and up to 30 % for the counter electrode) and then, when polarization is finished, it continue slowly decreasing until stabilization at t = 30 min in case of the counter electrode and moderate increase is observed for the working one. Contrary, on glass surface (fig. 4.8 a, positions 1 and 2) moderate intensity decline can be observed for all experiment time after the pulse. However, in case of position 2 (glass region close to the counter electrode) this tendency is substantially stronger.

We suggest that during polarization of the electrodes the following effects can take place, affecting the detecting fluorescence signal. Firstly, is adsorption of negatively charged DNA on counter electrode surface, which carry positive charge during the pulse time, followed by quenching of Cy-5. Secondly, partial degradation of the fluorophore under pulsing conditions. Finally, at high anodic potentials (>1,45 V *vs* RHE) is forming auric oxide, Au_2O_3 [125]. This compound can decrease reflective properties of gold surface and in this way result the decrease of the signal, which is not linked to the molecular system or the fluorophore. We

believe that all these effects can take place in our experiments. Consequently, the duration of the electrical pulse should not be too long in order to minimize these effects. As at the first minute after the pulse start signal perturbation is relatively low, one third of this time, 20 sec, seems to be a reasonable duration of applying the voltage.

4.4.5 Electrochemical triggering of autocatalytic CRN in microfluidics

After assembly of the CRN, performing model experiments and all other tests, described above, we finally started electrochemical activation of this molecular system in microfluidics. Although preliminary goal, activation the reaction front propagation at needed location *via* input release from the electrode, was rapidly achieved, we faced with a problem of undesigned activation in absence of pulse. This unwanted process was always taken place from the working electrode surface, functionalized with input DNA. Even though, certain time delay (around 1 hour on average) between triggered and non-triggered reaction diffusion front was present, these results were not satisfactory in terms of stability of our technology. Typical data, obtained from the experiment of this kind are demonstrated in fig. 4.9.

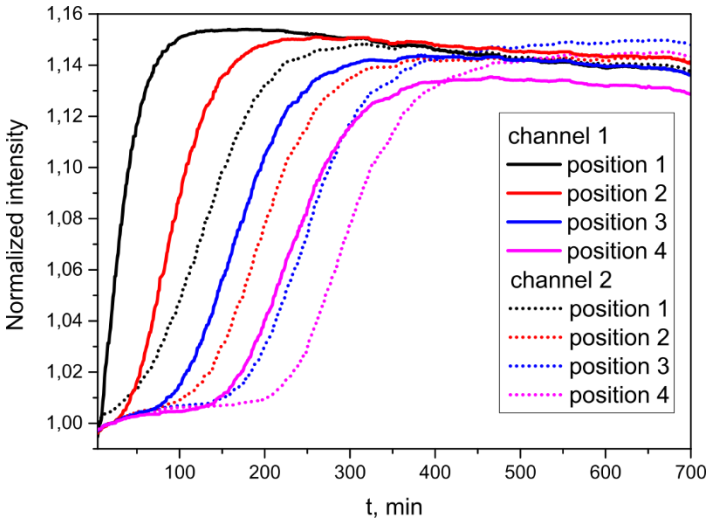

Figure 4.9. Triggering of autocatalytic CRN in microfluidics at t = 0 min (channel 1) and control experiment with no potential applying (channel 2). Each solution contained 50 nM template and 50 nM reporter. The temperature was 38 °C.

One can clearly see immediate start of propagation of the reaction front from the working electrode area after applying -2 V (*vs* Au) potential (fig. 4.9, channel 1). Nevertheless,

the similar behaviour can be observed in a control experiment with no pulse (fig. 4.9, channel 2). In this case, a delay of ~100 min is present between two reaction fronts propagation. However, fluorescence intensity starts to increase from the beginning of the experiment in case of no potential applying at position 1, indicating the undesigned system self-initiation, induced by the DNA-functionalized surface.

We proposed three possible mechanisms, which can be behind system instability. First, surface grafted DNA input can be attached to the gold surface in a weak, unspecific manner, for instance, through the nitrogen atoms in DNA bases. We introduced additional procedures in our rinsing protocol after DNA deposition: with a surfactants tween-20 and Decon-90, in order to minimize this factor. Second, surface hybridization of the template can potentially take place and induce reaction start from the surface. This mechanism appears unlikely, because hybridization on surface at elevated temperature happens less likely than in solution [126] due to the steric hindrances and, additionally, polymerase functioning on surface should be limited as a result of its high molecule size (few tens of kilodaltons). Finally, unwanted surface activity can be caused by thermodesorption of grafted DNA-thiol [105].

It is therefore necessary to optimize the surface design in order to make triggering time user-defined and increase the system stability.

4.5 Optimization of active surfaces and molecular system

4.5.1 MCH backfilling

Aiming to minimize the number of non-specifically adsorbed DNA on surface, we applied a backfilling strategy, which based on additional surface functionalization after attachment of input. 6-mercapto-1-hexanol (MCH, $\boldsymbol{HS(CH_2)_6OH}$) was chosen as a backfilling agent, as it is well known to "dilute" DNA-thiol layers on gold surface and optimize their characteristics, such as robustness and uniformity [127].

Sample with a gold electrode after usual DNA-thiol attachment procedure was backfilled during 30 min in 1 mM solution of MCH in ethanol. After that on top of the sample was assembled our usual microfluidic setup with 1 channel, which was filled with optimized reaction mix (no input) and placed under fluorescence microscopy observation at 38 °C. No

electrical pulse was applied in order to study system self-activation after MCH backfilling. Results of this experiment are demonstrated in fig. 4.10.

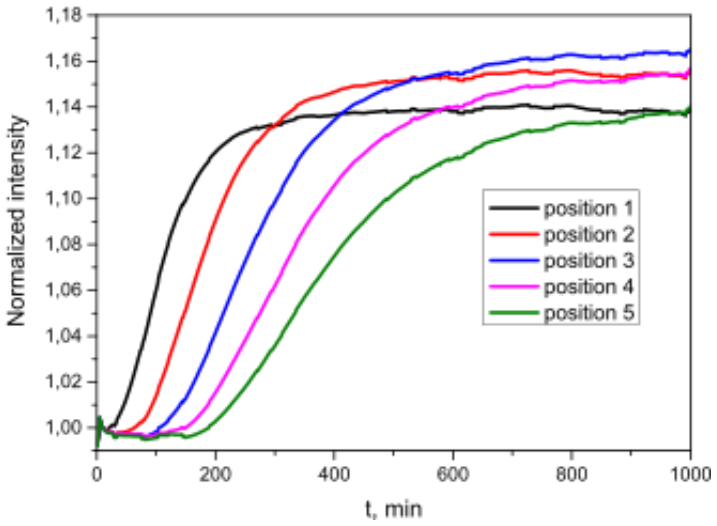

Figure 4.10. MCH backfilling in order to prevent the undesigned activation of the CRN. Solution contained 50 nM template, 50 nM reporter and 10 nM pseudo-template. The temperature was 38 °C.

Data show no substantial improvement of system stability after applying MCH surface functionalization. Although during first ~ 20 minutes of the experiment intensity remains stable on position 1, close-in to the working electrode (fig. 4.10, black line), this cannot be considered as a substantial upgrading of our technology and further optimizations were needed. In this way, detachment of non-specifically adsorbed DNA does not play the major role in undesigned activation of the CRN.

4.5.2 Shielding the surface DNA by graphene oxide

As a next step of surface optimization, we were attempting to prevent triggering of the CRN due to amplification start from the surface. To do so, we extended the surface coverage procedure by an additional step - deposition of graphene oxide (GO) on top of the attached DNA. It can be non-covalently attached to the DNA layer thanks to π-π stacking and, therefore, protect it from further hybridization with a complementary strand (the template) in solution. Finally, GO is water-soluble and should not prevent the CRN activation, as input will be electrochemically released.

In order to verify this optimization strategy, it was performed an experiment, similar to the previously described one, but with an additional step of deposition of 5 µl of 0.5 mg/ml GO solution instead of MCH backfilling. It was additionally used a higher pseudo-template concentration (15 nM) with the aim of improving resistance of the CRN to undesignedly produced input strands. Results of this experiment are demonstrated in fig. 4.1.

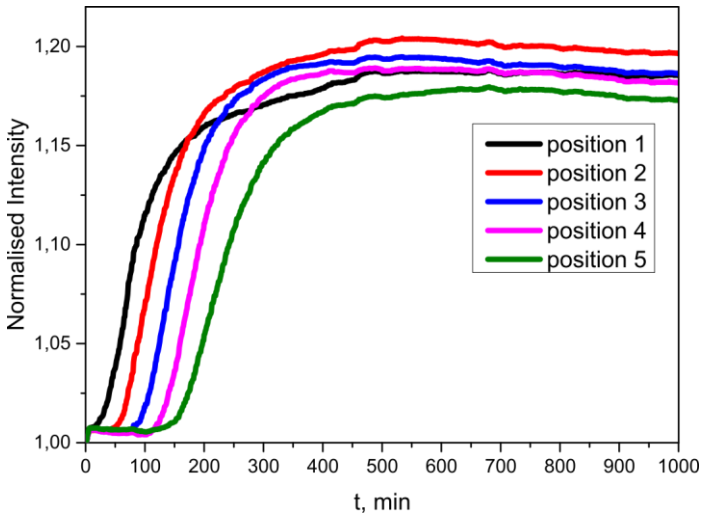

Figure 4.11. Backfilling with GO (0.5 mg/ml) in order to prevent the undesigned activation of the CRN. Solution contained 50 nM template, 50 nM reporter and 15 nM pseudo-template. The temperature was 38 °C.

Obtained data indicate no benefits from using the GO shielding strategy. Undesigned initiation of the reaction start still taken place on the beginning of the experiment. It is not delayed with compere to the usual surface functionalisation protocol or MCH backfilling. This can be explained by thermodesorption of attached DNA, which thereafter triggers the autocatalysis. GO in this scenario plays less important role. As DNA became in solution and since its affinity to the complementary strand (template) is higher than to GO, it thereafter triggers the autocatalysis.

4.5.3 Application of positive potential to prevent DNA desorption

In this way, the most likely mechanism of undesigned system activation is the thermodesorption of DNA input. To verify this assumption we designed a strategy, based on the polarization of the working electrode by applying a positive potential (+1V *vs* Au). As DNA at neutral pH

carries a negative charge due to deprotonated phosphate backbone, positively charged surface can attract it and prevent or at least diminish its release in solution.

To do so, it was conducted an experiment in microfluidic channels with assembled CRN in solution and surface-attached input DNA. No potential was initially applied in order to detect any system self-initiation. It was reasonable to investigate on the same time not only the delaying of self-initiation, but also the possibility to control the inhibition of autocatalysis. Then, at t = 100 min, the working electrode was polarized during 90 min by +1 V *vs* Au by applying consecutive pulses with 15 min duration (limitation from the potentiostat software). During polarization, the time fluorescence intensity was successively declining in exponential manner until reaching a plateau at the end of the positive pulse (fig. 4.12). After it, we applied a short (20 sec) reverse potential of -2 V *vs* Au with the intention to release DNA input and restart the autocatalysis.

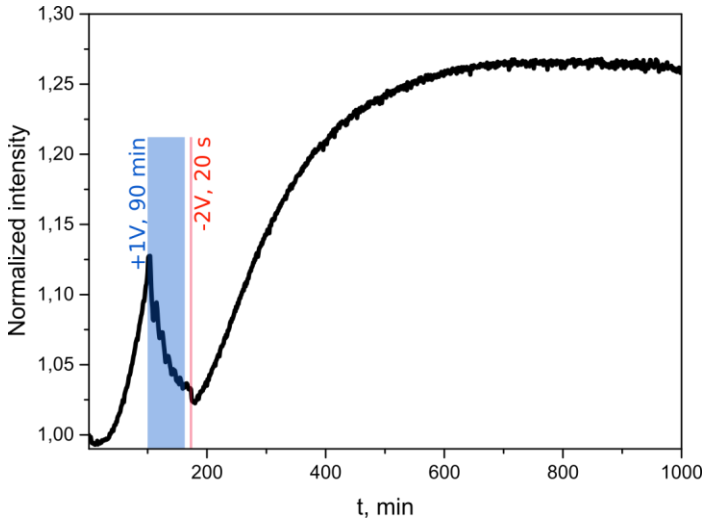

Figure 4.12. Positive polarization of the working electrode in order to prevent the undesigned activation of the CRN. Solution contained 50 nM template, 50 nM reporter and 20 nM pseudo-template. The temperature was 38 °C.

Data show that self-activation takes place fast (as in previously discussed experiments) and signal intensity rapidly increases. Since +1 V *vs* Au electrical pulse caused the reverse tendency (signal decreased), we believe that thermodesorption indeed has taken place and after that input DNA molecules were readsorbed on positively polarized gold surface. Importantly, after subsequent -2 V *vs* Au pulse, it was observed regeneration of intensity growth, which proves, to our opinion, the relaunching of autocatalysis.

In this way, it was obtained an additional confirmation of thermodesorption mechanism of undesigned system triggering and successfully testified a method of delaying it. However, it is inconvenient and, more importantly, long polarization times can perturb a system in non-designable way (see fig. 4.8). Therefore, another method was required to reduce the impact from thermodesorption. It is known, that, this process has a radical nature [105], *i.e.* temperature increase induces cleavage of the Au-S- covalent bond and formation of thiol radical, ·S-, which can thereafter interact with another Au-S- bond and form a new thiol radical. The likelihood of this process is highly depend on distance between thiol bonds. Thus, decreasing the surface coverage should suppress an impact of the thermodesorption.

4.5.4 Changing the surface density

Using this logic, we decreased the concentration of thiolated input DNA during the deposition procedure form 1 μM to 50 nM. The following procedure (based on Demers *et al.* [128]) was used to estimate the resulting surface density of grafted DNA on the gold electrodes.

A surface with working gold electrode, grafted with Cy5-labelled DNA dithiol (5′-dithiol ATGAGTCAGTAA-Cy5-3′), with microfluidic channel was assembled. The channel was filled with the standard reaction buffer in order to reproduce the usual electrical release conditions (ionicity, pH). An electrical pulse of -2 V (*vs* Au) the counter electrode was applied during 30 sec to the surface. Then, the fluorescence intensity, $\boldsymbol{I}$, as close as possible to working electrode was measured as equal to 7540 a.u.

Four identical channels on glass surface were prepared and filled with solutions of the same Cy5-tagged DNA as used for attachment. All solutions were prepared in reaction buffer with DNA at the following concentrations (nM): 1; 5; 10; 15. Fluorescence intensities were measured inside the channels, using the same microscopy settings as for the previous experiment. A calibration curve with equation $\boldsymbol{I} = (6937 \pm 126) + (328 \pm 13)\boldsymbol{C}$ was obtained (fig. 4.13). By using this calibration curve, the intensity measured above the gold electrode after release was estimated to correspond to a concentration equal to 1.80±0.04 nM. Using the ImageJ software, we measured geometrical parameters working electrode surface area, S, and channel height, h, obtaining 0.11 cm^2 and 265 μm respectively. The channel volume on top of the working electrode, $\boldsymbol{V}$, was calculated as $\boldsymbol{V} = \boldsymbol{Sh} = 2.9 \cdot 10^{-6}$ (l). Finally, using the formula $\boldsymbol{\Gamma}$

= $\boldsymbol{CVN_A/S}$, where $\boldsymbol{N_A}$ is Avogadro's number, we calculated the surface coverage, $\boldsymbol{\Gamma}$, as $2.8 \cdot 10^{10}$ molecules/cm^2.

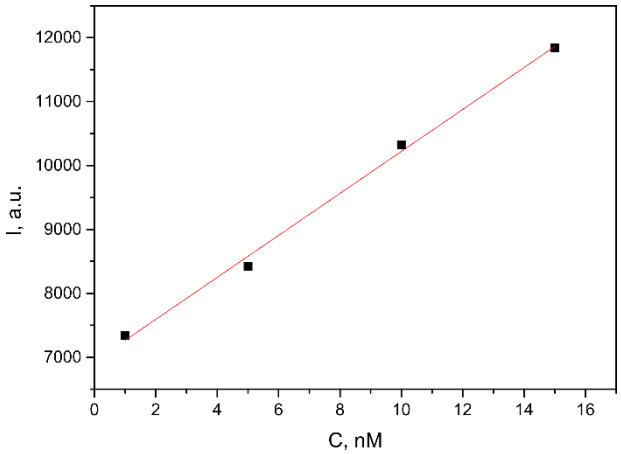

Figure 4.13. Calibration curve, used to determine the grafted DNA surface density.
R^2= 0. 995. $\boldsymbol{I}$ = (6937±126) + (328±13)$\boldsymbol{C}$.

4.5.5 Verification of thermostability of active surfaces with optimized density

In order to verify the thermostability of our low-density active surfaces, a monitoring experiment was conducted. As previously, the gold electrode was functionalized with Cy5-tagged ssDNA. The microfluidic channel was filled with the reaction buffer and was placed on the heating plate at 38 °C to reproduce the actual experimental conditions. Fluorescence intensity on top of the electrode was measured during 1000 min at 1 min intervals. Results of this experiment are shown in fig. 4.14 and demonstrate the layer stability for at least 240 min. It has to be noticed, that our CRN is designed in a way to be resistant for subcritical amounts of input and start of thermal cleavage of Au-S bond does not necessary means the activation of the CRN. The point here is balance the surface coverage sufficiently high to provide a critical amount of input to activate the autocatalysis, and sufficiently low to make system tolerant for undesignedly desorbed input. Precise balancing, however, seems to be complicated, since radical mechanism of thermodesorption means avalanche-like intensification of this process and, therefore, even very low amounts of desorbed species eventually caused the exponential growth of the total process.

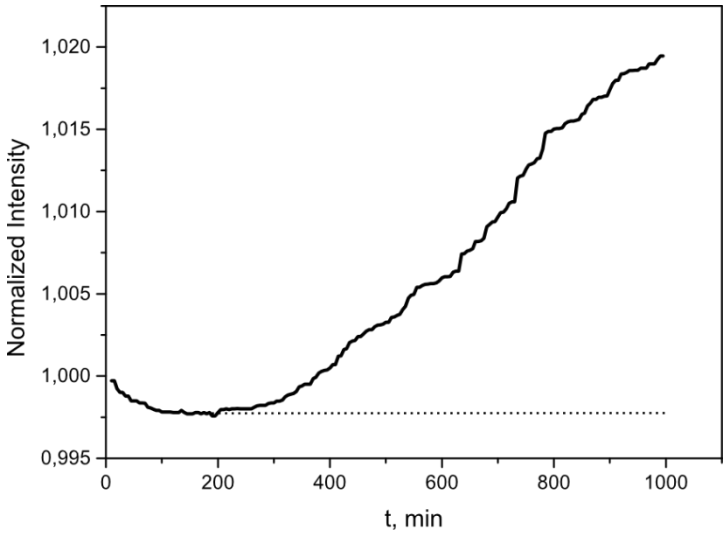

Figure 4.14. Fluorescence monitoring of the thiol grafted DNA at 38 °C. After 240 min without increase, the fluorescence starts to rise.

4.5.6 Electrochemical activation of the CRN with optimized active surface parameters

After optimization of the surface density, an electrochemical activation of the CRN was performed. A usual microfluidic setup with 2 channels was assembled and then filled with an optimized reaction mixture solution. -2 V *vs* Au was applied to the working electrode in the first channel at t = 0 min in order to verify whether the surface conserved its activation properties after reducing the grafted amount of DNA. Fluorescence signal in the second channel was remaining stable during 2 h. Then, was applied a pulse within the second channel in order to check that the surface is still active even after being under reaction conditions during this time. Results of this experiment are shown in fig. 4.15.

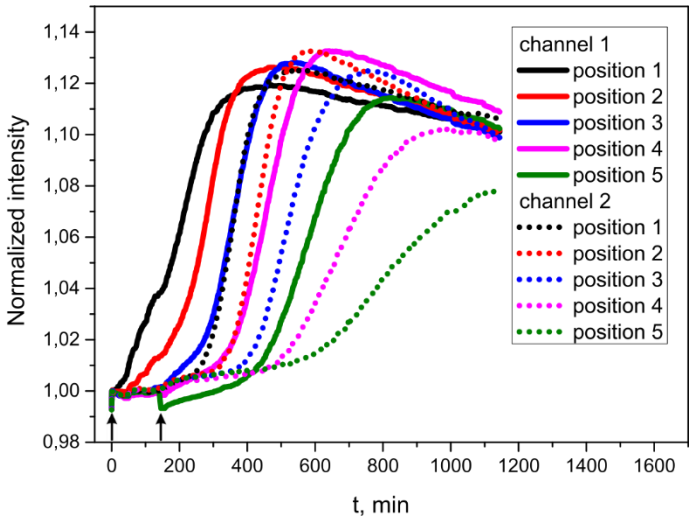

Figure 4.15. Triggering the CRN in two separated channels at t = 0 min (channel 1) and t = 130 min (channel 2). Solution contained 50 nM template, 50 nM reporter and 10 nM pseudo-template. The temperature was 38 °C.

Data show increased stability of the system without losing the activation properties of the active surface: reaction fronts propagate from the working electrode areas after the electrochemical input releases at t = 0 and t = 120 min. However, amplification profiles start to damp in both channels after t = 400 min. We have assumed that in origin of amplification profiles damping was consumption of dNTPs. For this reason, we tried higher concentration of dNTPs (0.8 instead of 0.4 mM/each) for further experiments. In this way, we tuned dNTPs concentration and reproduced an experiment with activation of the CRN at t = 0 min. We performed as well two controls with identical reaction mixtures, but on different surfaces. One was covered with non-complimentary input, while the second one was non-covered.

4.5.7 Electrochemical activation of the CRN with optimized molecular system parameters

Figure 4.16 presents the triggering of the molecular system *via* input release at t = 0 min. The electrochemical cleavage of the grafted DNA produces an instantaneous local increase of the trigger strand concentration above the working electrode, which is enough to overcome the pseudo-template inhibition effect. As a result, the autocatalytic core starts its exponential production of strands. As expected in such systems, a reaction-diffusion front starts to propagate

from the working electrode area and progressively invades the whole channel length. Propagation takes place with uniform velocity, a finding coherent with Zadorin *et al.* [102], which can be measured at 23±3 µm/min (from Z-profiles, knowing the distance between the positions). Furthermore, the amplification kinetic is identical for all curves.

When an identical experiment is reproduced, but the working electrode is not functionalized with DNA, the fluorescence intensity remains on a base-line level during the complete experiment duration – 1000 min (fig. 4.16, dashed blue curve). Similar results are obtained with release of a non-complementary DNA (fig. 4.16, dashed purple curve). We can thus confirm that the electrical pulse of bare gold by itself does not provoke triggering of the reaction (for example, by local heating) and only the correct input strand initiates the autocatalysis.

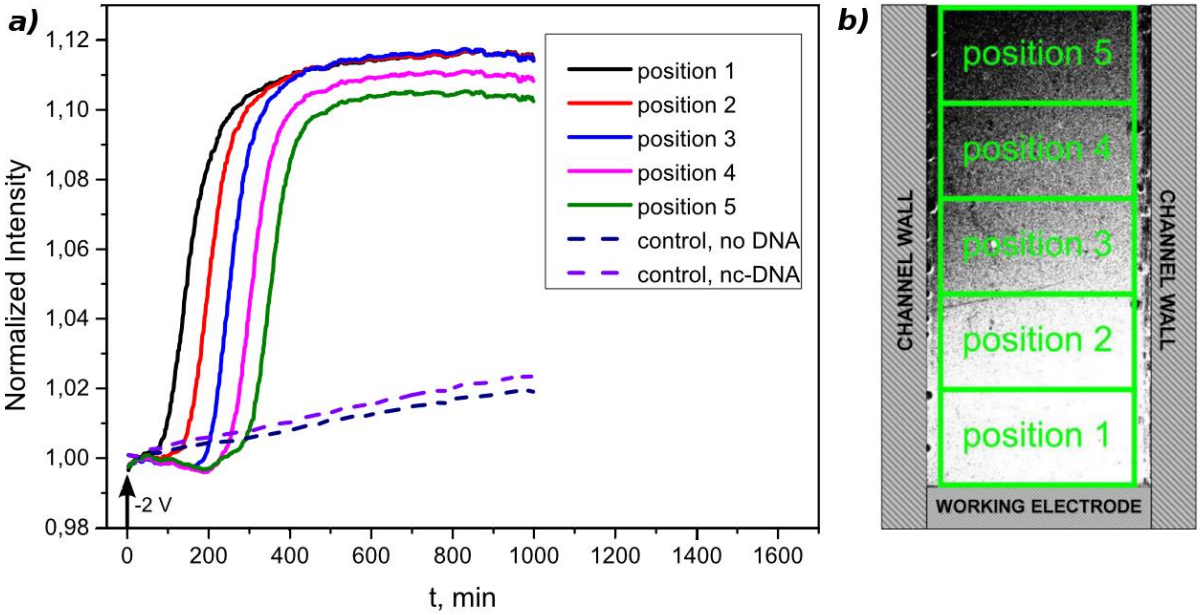

Figure 4.16. Electrochemical triggering of a reaction-diffusion front at t = 0 min. (a) The Z-profile taken along the channel length showing propagation of the autocatalytic front as well as two controls with no DNA or non-complementary DNA on the gold electrode. (b) Fluorescent micrograph shows the propagating front within the microfluidic channel with integrated positions. The temperature was 38 °C.

4.5.8 Spatiotemporal control of the CRN

We wished to illustrate how this principle can be extended to trigger at multiple times or positions within a microfluidic set-up. This ability is of particular importance if one wants to rely on such a strategy to interact with the molecular system in a versatile way. Figure 4b shows

kymographs of the reaction-diffusion front propagation from the two channels. The first channel is triggered at t = 0 min whereas the second one at t = 145 min. The fronts propagate at constant velocity in both channels 26±3 μm/min and 28±4 μm/min. Time intervals between amplification curves are consistent with triggering delay, which confirms our ability to perform time controlled triggering.

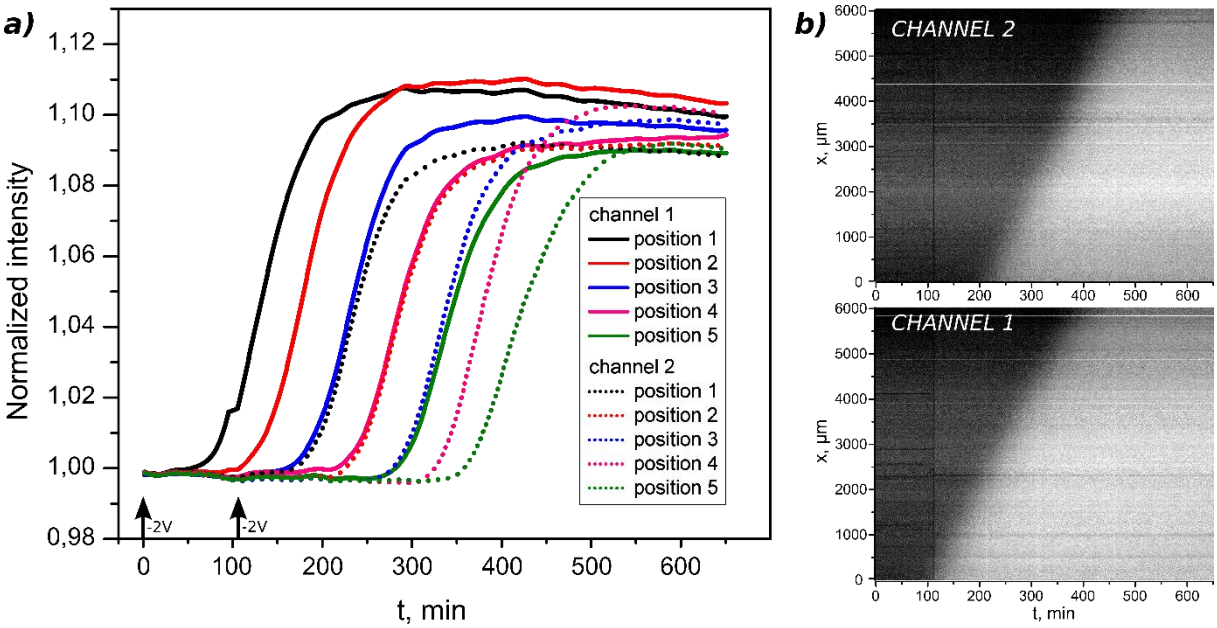

Figure 4.17. Time-controlled triggering of the molecular system. (a) Z-profiles of propagating fronts in the two channels. System in channel 1 was triggered at t = 0 min and in channel 2 at t = 108 min, as shown by the arrows. (b) The kymographs showing independent time controlled triggering in channels and the constant speed propagation of the fronts. Solution contained 50 nM template, 50 nM reporter and 10 nM pseudo-template. The temperature was 38 °C.

4.5.9 Verification of the maximal system stability in absence of electrochemical triggering

The previously described experiment was also reproduced for two identical channels, one of which was electrically triggered at t = 0 min, and the second one left under the same conditions, but without electrical triggering. Results of this experiment are demonstrated in fig. 4.18.

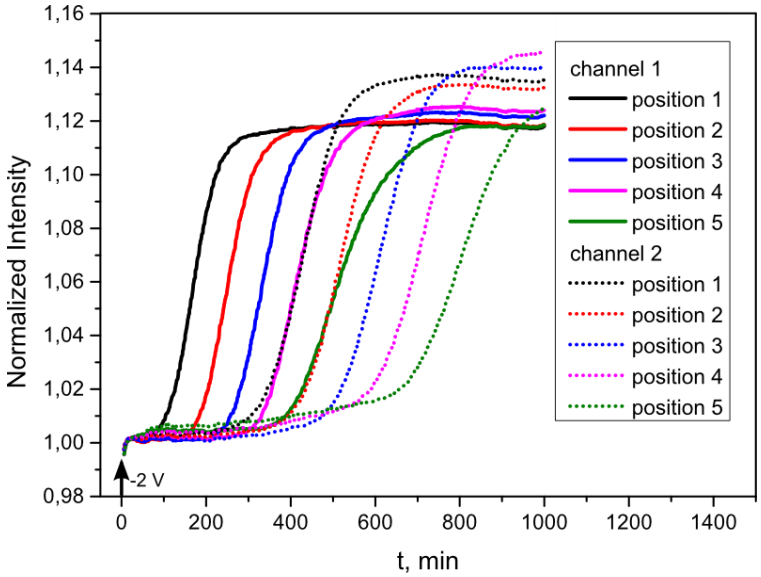

Figure 4.18. An example of the involuntary self-triggering of the autocatalytic system (channel 2). System in channel 1 was triggered at t = 0 min. Solution contained 50 nM template, 50 nM reporter and 10 nM pseudo-template. The temperature was 38 °C.

For the first channel, a behaviour already seen in fig. 4.17 was observed, while the fluorescence profile in second channel remains stable during ~300 min. Then, the fluorescence signal starts to increase from the working electrode area, which is probably due to a triggering of the system due to thermal desorption of the attached input.

In this way, even if the system is left without being electrochemically triggered, it eventually self-triggers. The typical delay, observed in these cases is well correlated to the thermal stability experiments (fig. 4.14). Indeed, as the input DNA strands are released in solution, they reach the minimal triggering concentration established by the drain strand and initiate the autocatalysis. We therefore believe that the only current limitation in the triggering delay comes from the limited stability of the dithiol grafted DNA at 38 °C.

4.5.10 Potential optimisation of DNA immobilization chemistry

Edwarson *et al.* described recently an approach of grafting DNA to the gold nanoparticles, based on bisdisulfide linker (fig. 4.19 b), which provides more robust attachment of DNA rather than dithiol, we used [129].

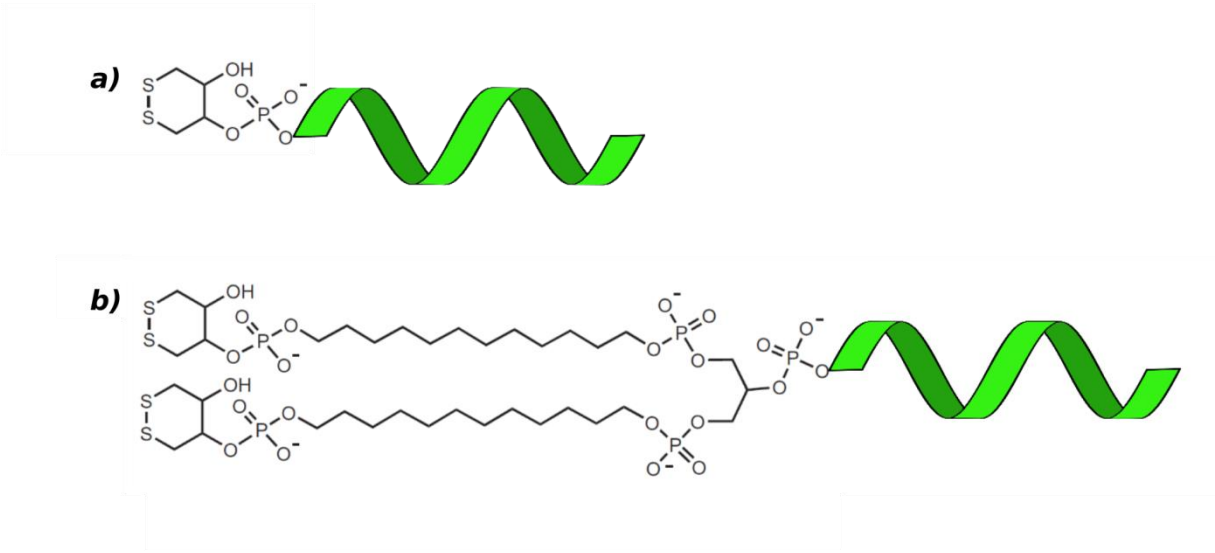

Figure 4.19. (a) Chemical structure of dithiol-linker, applied in this study. (b) Bisdisulfide modification, proposed in [129], which provides more robust attachment to the gold surface.

4.6 Conclusion

In this way, the extension of molecular system by addition of the "drain" reaction and using a new reporting strategy allowed us to verify and improve the robustness and stability of our technology. We have realized a reliable spatiotemporal control of the autocatalytic CRN by user-defined initiation of reaction-diffusion fronts in microfluidics. Detail analysis of factors, decreasing the active surfaces stability, shows that it is caused mainly by temperature driven desorption of thiolated DNA from the gold electrode. Decreasing of surface coverage allowed us to optimize this parameter and increase system stability to 300 minutes. It can be potentially further improved, if needed, by using an alternative thiol-based linkers. The versatility with which one can produce gold microelectrode in microfluidic channels or reservoir makes it possible to use this approach to manage complex spatiotemporal interaction with the molecular system.

Chapter 5

Reusable DNA-functionalised active surfaces with controlled geometry

5.1 Introduction

We have previously demonstrated development of surface activators in microfluidic system, capable for both, spatial and temporal control of DNA-based CRNs. This approach allowed achieving a controllable triggering of reaction-diffusion fronts in precise location with the advantage to be easily implemented in any biochemistry lab. However, such systems have some limitations, in particular, the difficulty to tune the concentration of the surface-attached DNA. Indeed, there is an inverse proportional relation between it and the stability of the interface. Also, with this approach, it is hard to create a concentration gradient along the channel or launch PEN toolbox reactions from surface, which is important for such applications as DNA-based artificial morphogenesis [82]. For these reasons, active surfaces, with covalently attached DNA template appear a very attractive alternative. Indeed, it is much easier to localize PEN toolbox reactions if DNA template will be present exclusively on surface. This approach will ensure the output production only in defined locations (covered by DNA template molecules). It cannot be achieved with immobilization of input, since in this case some fraction of template will inevitably be in solution and, consequently, reaction will take place in all locations of the reservoir.

From the other hand, attachment of DNA template to the surface followed by applying potential can serve for triggering or suppression of hybridization and, consequently, PEN toolbox reaction on surface. This strategy is attractive from the perspective of creation of reusable DNA activators and operation with multiple reactions (programed by different DNA sequences) within one surface.

In this chapter, we will discuss such strategies for irreversible attachment of DNA templates for launching PEN toolbox reactions. We will first introduce several approaches for patterning of these surface DNA molecules. Next, we will discuss the creation of reusable DNA controllers, capable for both activation and inhibition of amplification reactions.

5.2 Attachment of DNA template *via* biotin-streptavidin strategy

Patterning of surfaces can not only control the geometrical shape of region, covered with DNA template molecules but also create concentration gradients. In nature, such concentration gradients are involved in many crucial processes in living cells. For instance, motion of glucose and proteins across the cell membrane is driven by the potential energy differences of it [130].

For the surface patterning, we have chosen DNA attachment to the surface *via* biotin-streptavidin linkage. It is simple, well established and rebuts approach. Another important advantage of this strategy is due to the very high affinity between biotin and streptavidin. Thus, one can easily tune the density of attached DNA molecules conjugated to a biotin moiety on streptavidin-terminated surface.

The details of the surface attachment strategy are represented in fig. 5.1 a. Briefly, the microscopy glass slides were firstly cleaned and activated (*via* creation of surface OH groups) with piranha solution and then exposed to PEG-biotin silane (3400 Da) solution in toluene for 2 hours to create biotin-terminated surface. The resulting interfaces can react with a solution of fluorescence-labelled streptavidin. The successful attachment after this step was confirmed by fluorescence measurements. In fig. 5.3 a one can see a fluorescence image of the interface after reaction with a spot of streptavidin solution. Strong fluorescence is observed inside a droplet and outside it image remains black, which confirm the presence of streptavidin on surface. Sharp border (S/N = 7.1) of the fluorescence image proofs attachment only in the region of droplet and no contamination during the rinsing step. Due to the high affinity, this process occurs rather fast (several minutes). Each streptavidin molecule contains 4 biotin binding sites and, consequently, can serve for attachment of another molecules conjugated to biotin moiety. This strategy was applied for achieving our final molecular construct leading to attachment of biotin-labelled DNA to the interface.

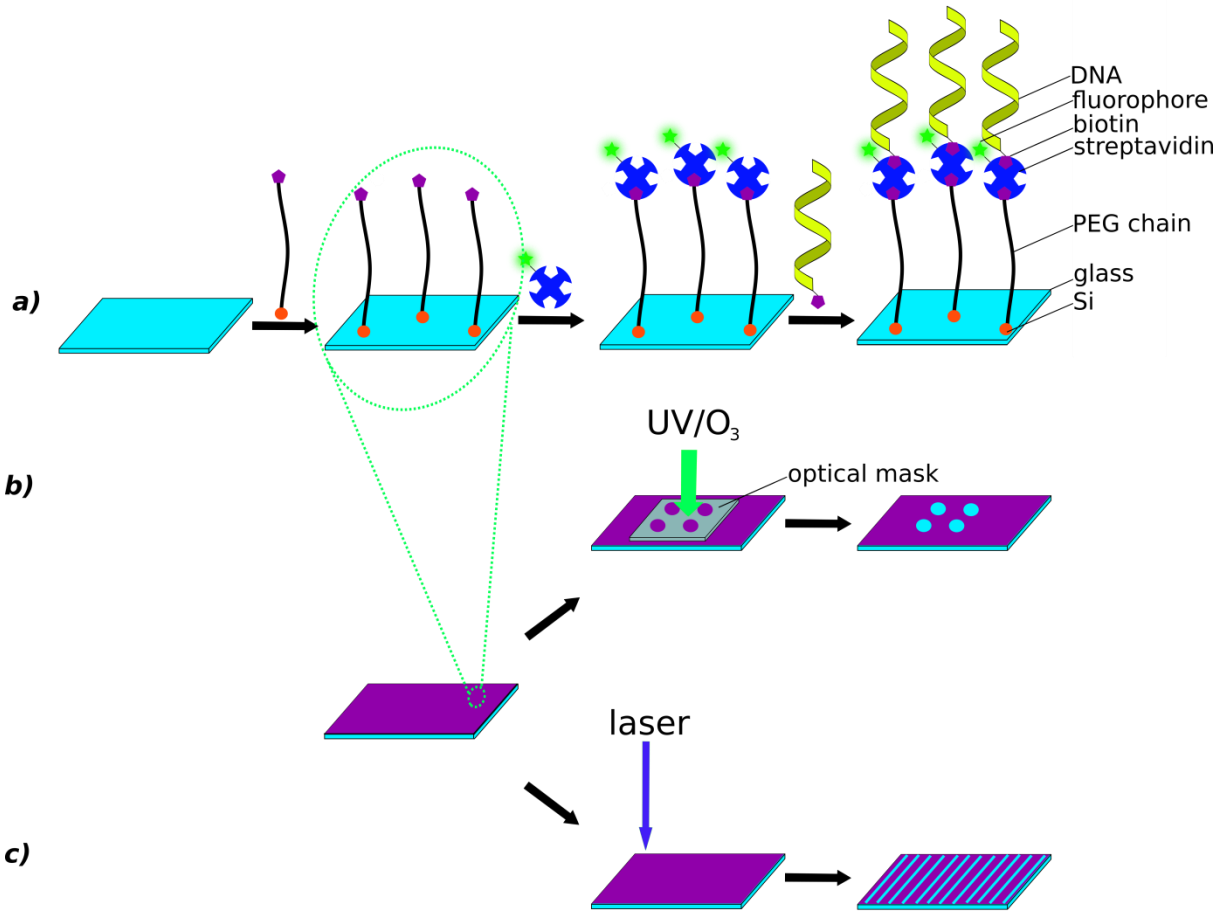

Figure 5.1. (a) Chemical modification of glass surface with biotinylated DNA. (b) Patterning of such surface *via* UV/O_3 treatment with optical mask. (c) Surface patterning *via* laser treatment.

5.2.1 Autocatalytic reaction with surface-attached DNA template

As a next step, we aimed to confirm the presence of DNA on surface and, from the other hand, verify its activity as a template in PEN toolbox reactions. For this purpose, it was designed the following experiment. On top of the surface, presumably covered by DNA template, was assembled a microfluidic channel (see fig. 3.7). Then a standard reaction mixture for autocatalytic reaction (50 mM NaCl, 10 mM $(NH_4)_2SO_4$, 10 mM KCl, 8.4 mM $MgSO_4$, 0.4 mM of each dNTP, 0.1% Synperonic F108, 500 µg/mL BSA, 2µM Netropsin) with Eva Green as a reporter, 1x enzymes mixture and 5 nM input, was introduced inside the channel. The sample was placed on heating plate at 42 °C under fluorescence microscope observation. Obtained data are showed in fig. 5.2.

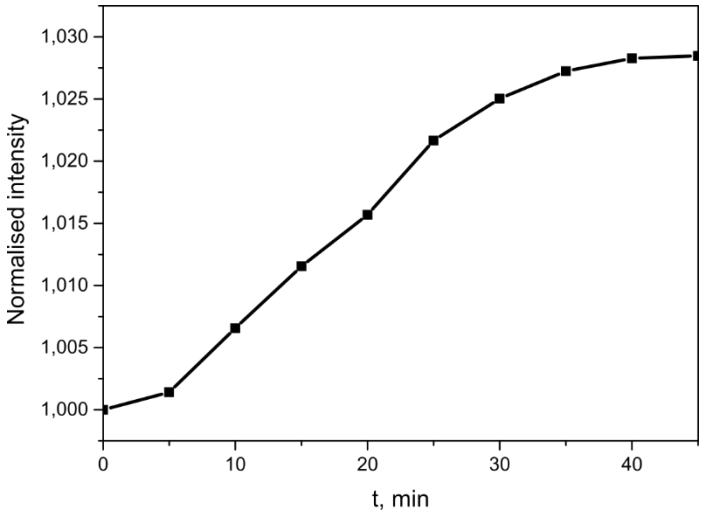

Figure 5.2. Autocatalytic PEN toolbox reaction with DNA temple, covalently attached to the surface. Solution contained 5 nM input, 1x enzymes mixture and 1 x Eva Green. Temperature was 42 °C. Fluorescence intensity was measured every 5 minutes. The following settings of the fluorescence microscope were applied. Exposure time: 400 ms. Binning: 4.

Data indicate a growth of fluorescence signal after t = 5 min, followed by a saturation after t = 30 min. Relative intensity is lower compared to experiments with the template in solution phase (see, for instance, fig. 3.16). This can be explained by less efficient binding of Eva Green to the double-stranded DNA on surface due to the steric effect [131]. Another explanation can be lower equivalent concentration of surface-attached template. These data confirm presence of DNA template on surface. Consequently, surface functionalization approach we applied is suitable for launching PEN toolbox reactions on surface.

5.2.2 Patterning of the surfaces

In order to precisely control the geometrical shape and surface density on designed locations of the immobilized DNA we aimed to testify different patterning strategies (fig. 5.1 b and c). The first one relies on UV/O_3 treatment of a sample through a quartz mask (fig. 5.1 b). Such masks are normally using for photolithography. The one we used can be seen in fig. 5.3. b. UV irradiation passes through the optical mask and creates locally ozone molecules:

$$O_2 + hv = 2O\cdot$$

$$O_2 + O\cdot = O_3$$

Ozone is a strong oxidative agent, capable for denaturation of organic layer on surface. Thanks to the optical mask, only the molecules, located on zones that have been irradiated, are degraded. In these locations, the initial surface groups (Si-OH) are regenerated. CO_2 and H_20 are released as products of ozonolysis.

It is more reasonable to perform this operation after PEG biotin immobilization, rather than after streptavidin attachment or DNA-biotin grafting. Firstly, the less surface functionalized is, the easier is to destroy the organic layer. Secondly, one can easily imagine a situation, when fluorophore, assembled to streptavidin, is deactivated (for instance, by photobleaching) but streptavidin and DNA remain on surface. From the other hand, DNA molecule can be decomposed, but fluorophore not. In such cases, fluorescence imaging after UV/O_3 treatment will provide a false information about the surface coverage.

We applied a mask with different size “negative” patterns with round and cross shapes (fig. 5.3 b). Fluorescence images of the resulting surfaces are displayed in fig. 5.3 c and 5.3 d.

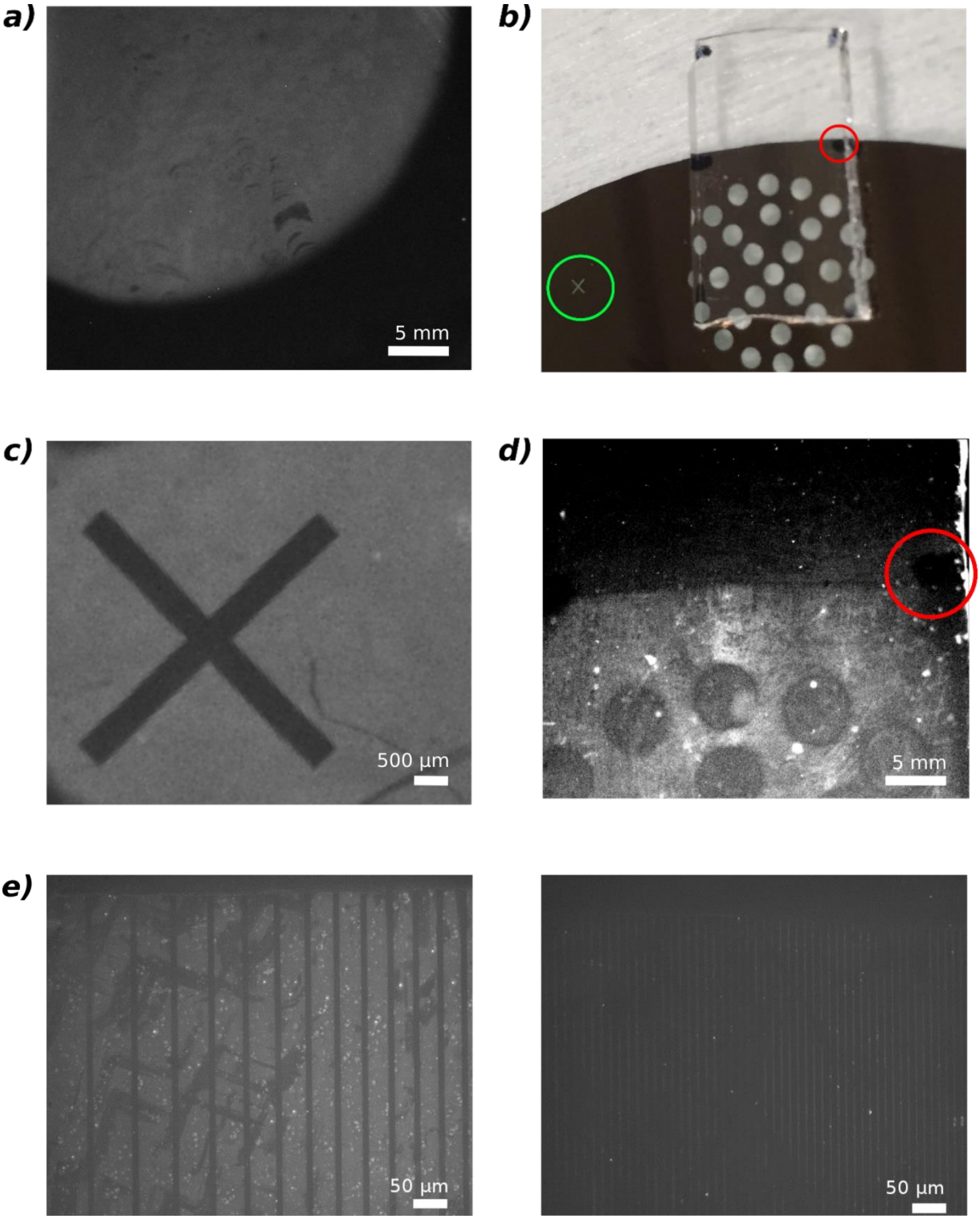

Figure 5.3. Fabrication of patterns on PEG-biotin functionalized surface. (a) Fluorescence image of PEG-biotin covered surface after deposition a droplet of fluorescence-labeled streptavidin solution and subsequent rinsing; surface regions inside and outside this droplet can be seen. S/N = 7.1. (b) Optical mask, used for patterning and glass interface on top of it prior to UV/O_3 treatment. (c) Fluorescence image of PEG-biotin covered surface after UV/O_3 treatment, using the cross pattern, marked by green circle on (b). S/N = 6.4. (d) Fluorescence image of PEG-biotin covered interface, showed on (b) after

UV/O_3 treatment, using the circle patterns from mask, showed on (b); sample was treated in the same position with respect to the mask as showed on (b); by red circle showed the same black mark on the interface in order to distinguish different parts of the interface. S/N = 2.2. (e) Surface patterning with a laser treatment, which was auctioning along 5 μm lines and decreasing (left) and constant (right) intervals. The following settings of the fluorescence microscope were applied. Exposure time: 400 ms (a and c); 1200 ms (d). Binning: 4.

Fluorescence image in fig. 5.3 c shows successful formation of surface pattern with a cross shape and the side size 5 mm. Sharp borders and high contrast (S/N = 6.4) proof the denaturation of the organic layer with a high selectivity. Unfortunately, it is not the case for patterns with a bigger surface area. Fig. 5.3 d shows results of patterning of surface, demonstrated in fig. 5.3 b. The sample was positioning on the border of Chromium-covered region of the mask in order to investigate the efficiency of UV/O_3 treatment. In this case, high level of organic layer decomposition on sample locations, protected by chromium-covered mask, is observed. Complete layer decomposition with a sharp linear border was observed for a part of the sample, which was outside Chromium-covered region of the mask. It has to be taken into account that this image was obtained with microscopy setting for high sensitivity (exposure time = 1200 ms). For this reason, some fluorescence signal can be observed on the sample locations, which were directly exposed by UV/O_3. S/N ratio was equal 2.2. The residual signal is most likely correspond to non-specific attachment of fluorescence-labelled streptavidin (see for instance fig. 5.6 a). Lower efficiency for larger patterns can be explained by higher probability of damaging neighbourhood sample locations due to the bigger amount of O_3, formed in this case.

In this way, such patterning strategy is suitable for creation of programmable shapes with a relatively low dimensions size (mm scale) and is less efficient as the size of designed patterns increases.

The second patterning strategy, which was testified, included treatment of the sample with a laser (fig. 5.1 c). The laser was programed in a way to be functioning only in specific (user defined) locations of the sample with linear shapes and few micrometres width. This approach was designed in order to create a programmable gradient of density of attached DNA molecules. We assumed, that functionalized surface with locally decomposed layer with sufficiently narrow linear shapes is equivalent to continuous surface with a lower coverage: total amount of surface-attached molecules in case of low coverage and partially covered surface with low density is equal. If uncovered regions are narrow enough, attached strands are

presumably equivalently accessible as in case of low coverage. In this way, high-resolution concentration gradient with designed shape can be potentially created.

The results of such patterning are demonstrated in fig. 5.3 e. These data were obtained with a help of Alexis Vlandas. In the first case (fig. 5.3 e, left) laser was irradiated the surface with 10 μm width lines and progressively decreased intervals between these lines. In the second experiment (fig. 5.3 e, right) laser worked with the constant intervals of 5 μm. One can clearly see complete denaturation of organic layer in needed locations in both experiments with a high resolution. However, we faced the problem of non-designed denaturation outside regions, where the laser was applied. The possible explanation of such unwanted effect is that the laser irradiation creates ozone molecules in a similar way as UV/O_3 machine, which, in their turn, react with organic layer on surface. This effect can be potentially suppressed by covering the surface with protective layer of polymer, such as polystyrene. Laser will decompose the polymer first and the organic layer under it after that. Ozone molecules, formed during the irradiation, will affect only the polymer, but not the surface-grafted molecules (or at least this effect will be substantially suppressed). At the end of the process the polymer will be dissolved in an appropriate solvent, liberating the surface attached molecules [132].

In this way, such patterning strategy appears to be promising, since it allows creation of surface motives with high resolution. However, it needs to be improved in terms of protection of regions, where the laser was not applied. This can be achieved, for instance, by decreasing the laser power or by using the approach, described above.

5.3 Reusable DNA activators, based on covalently grafted DNA template

In order to enlarge functionalities of active surfaces (see section 3.2) was designed a strategy, aiming to fabricate a reusable activators. They were based on covalently attached DNA templates in a non-reversible manner and capable for user-defined activation or inhibition the PEN toolbox reactions.

Under neutral pH conditions, DNA carries a negative charge due to dissociated phosphate. For this reason, it exists an electrostatic repulsion force between two DNA molecules. It is normally inferior to the attraction force of hydrogen bonds of complementary nitrogen bases, which makes possible hybridisation. Increasing or decreasing the electrostatic

repulsion force leads to the decrease or increase of hybridization rate, respectively. This can be achieved by applying either negative or positive potential to the surface-attached DNA [106]. It was demonstrated that under -0.3 V *vs* Ag/AgCl, DNA hybridization on surface is substantially lower that when no potential is applied. The opposite results were obtained with a reverse potential (fig. 5.4). For this strategy, surface material must satisfy the following requirements. Firstly, it has to be easy to functionalize in order to allow attachment of DNA. Secondly, electrical conductivity is needed to allow polarization of attached molecules. Indium-Tin oxide covered glass appears to be suitable for these purposes. This material is transparent and has no fluorescence background (same as a normal glass), which facilitates fluorescence monitoring on surface.

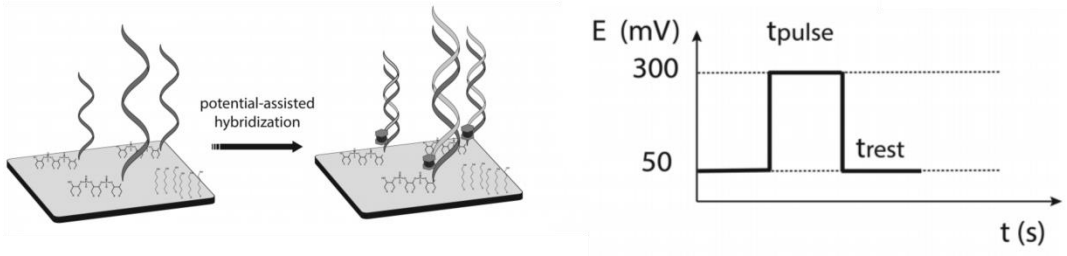

Figure 5.4. Application a positive potential (0.3 V *vs* Ag/AgCl) to DNA-functionalized surface enchase the hybridisation rate. Figure was taken from [132].

We have chosen DNA immobilization approach, based on epoxy-amino coupling (fig. 5.5). This strategy is simple (there are only 2 steps and only one of them requires an organic solvent) and provides a short enough spacer between attached DNA and surface to enable the charge transfer. At the first step, samples were cleaned with piranha solution, which also serves for creation of –OH groups on surface. Next, they were exposed to (3-glycidyloxypropyl) trimethoxysilane (GPTMS) solution in toluene (100 µl of GPTMS in 10 ml of toluene) for 2 hours. Finally, samples interacted with amino-DNA in PBS buffer (pH 8). It is important to resuspend DNA (after receiving it form provider). For this purpose, water was preferred to TE buffer, since the last one contains 100 mM tris. It is a compound with prime amino function. This amino group can competitively interact with epoxy groups on surface, leading to substantially decreasing yields. We applied amino-DNA with biotin linker in order to possess a method for monitoring surface attachment, since we has already fluorescence streptavidin in our lab and biotin functionalization of DNA is relatively inexpensive.

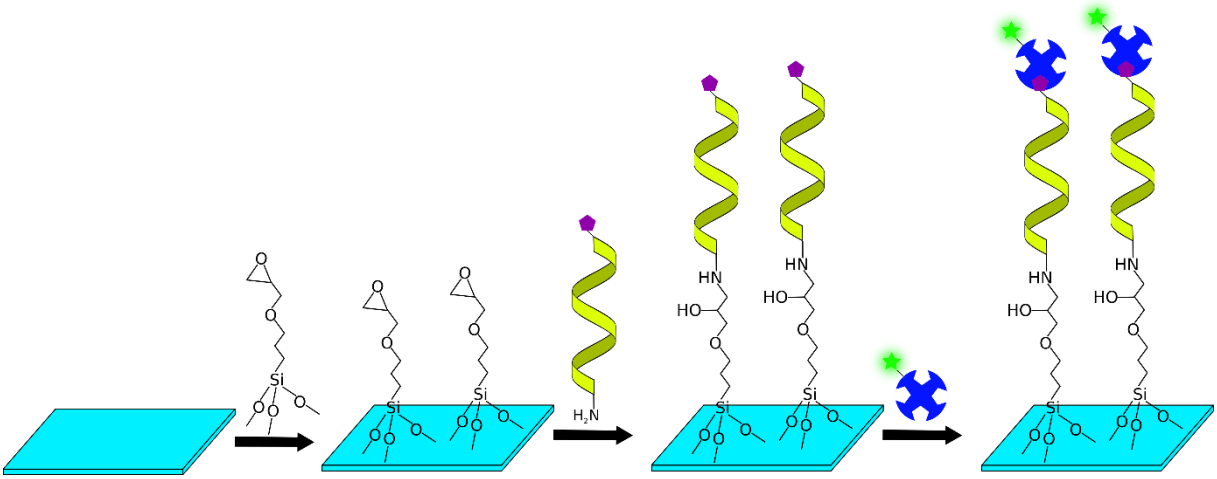

Figure 5.5. Schematic representation of surface functionalization strategy for covalent attachment of DNA through epoxy-amino linkage and subsequent approach for confirmation of surface chemistry with fluorescence-labelled streptavidin.

Resulting interfaces after surface functionalization were characterized in a following ways. Firstly, fluorescence images of amino-DNA-biotin covered surface after reaction with labelled streptavidin was recorded. We used, as a control, an epoxy covered surface incubated with the same reagent under identical conditions. Obtained data (fig. 5.6 a) show fluorescence increase on DNA-covered interface with respect to the control. The contrast, however, was not as strong as while PEG-biotin silane functionalization was used. This is probably due to the additional functionalization step, required for epoxy-amino chemistry, and, consequently, lower final yield. Secondly, were measured water contact angles of epoxy- and DNA-covered interfaces (fig. 5.6 c and d). Obtained values were 46±2° and 34±2° respectively, according to our expectations: attachment of DNA makes surface more hydrophilic and contact angle decreases. Alternatively, surface hydrophilicity after DNA grafting was demonstrated in a following way (fig. 5.6 e). On top of the epoxy-terminated surface was placed a droplet of amino-DNA-biotin solution in PBS buffer, insuring only local attachment of DNA. After that surface was rinsed and placed in a Petri dish and filled with DI water. After accurate declining of Petri dish water moved from one side to another and the interface became uncovered. Only in location, functionalized with DNA, residual water droplet remained (fig. 5.6 e, right). It confirms increased hydrophility, and, consequently, successful functionalization in this region of the surface.

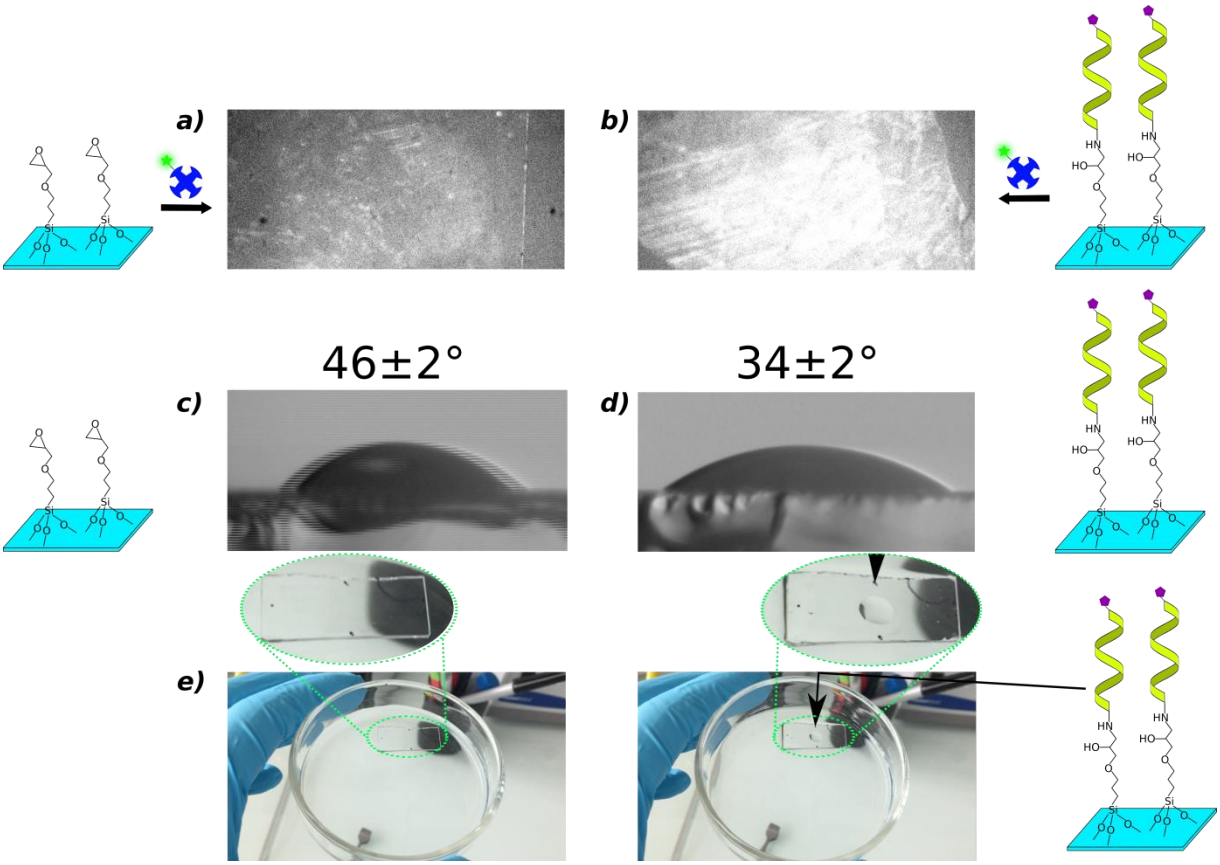

Figure 5.6. Characterization of interfaces with covalently attached DNA *via* epoxy-amino linkage. (a) Fluorescence image of surface after functionalization with GPTMS followed by interaction with fluorescence-labelled streptavidin. S/N = 1.1. (b) Fluorescence image of surface after attachment of amino-DNA-biotin followed by interaction with fluorescence-labelled streptavidin. S/N = 2.4. The following settings of the fluorescence microscope were applied. Exposure time: 800 ms. Binning: 4. (c) Water contact angle measurements of surface after functionalization with GPTMS. (d) Water contact angle measurements of surface after functionalization with amino-DNA-biotin. (e) Photographs of an interface, fully covered with GPTMS and functionalized in the middle with amino-DNA-biotin, immersed in a Petri dish with DI water before (left) and after (right) declining the Petri dish. A residual droplet of water on surface region, covered by DNA can be seen.

Several attempts were done in order to launch an autocatalytic reaction with surface attached template. Neither of them was successful. Several explanations are possible. Firstly, since the enzymes, we used, are large biomolecules (few tens of kilodaltons) some steric hindrance are fairly likely in case of reaction on surface, especially if DNA is linked with a short carbon chain. This cannot be easily overcome, since the number of enzymes, suitable for PEN toolbox is rather limited. From the other hand, spacer between DNA and surface cannot be substantially elongated since it will aggravate charge transfer from the surface to DNA. Another possible reason of experiments failure is low density of attached DNA template

molecules. We have already seen (fig. 5.2) that with PEG silane chemistry, while fluorescence signal from streptavidin-labelled is much more intense, autocatalytic reaction is less efficient than in case of template in solution. It makes this assumption rather realistic. If it is indeed the case, alternative surface functionalization strategies (preferentially contained only 1 step) are needed.

5.4 Conclusion

In this chapter, we have demonstrated two promising approaches for patterning surfaces, suitable for precise control of geometrical shape of attached DNA and its surface density. First was UV/O_3 treatment with optical mask and second – application of a laser. Designed shapes with sharp borders were obtained in the first case and denaturation of organic layer on surface with high resolution in second. Several limitations must be noted however: UV/O_3 treatment shows good results only for narrow mm scale patterns and was much less efficient as pattern area increased. Laser application has a drawback of non-controllable denaturation of surface attached molecules, outside designed locations. We proposed a potential solution of these issues, which relies on protecting of surface molecules, which supposed to be conserved after the treatment, by a layer of polymer (such as polystyrene). The polymer can be dissolved after the denaturation of organic layer in needed locations.

Importantly, applied surface chemistry (PEG-biotin silane, followed by streptavidin and biotinylated DNA attachment) was proven to be compatible with PEN toolbox reactions.

We also discussed a strategy of creation a reusable surface DNA activators, suitable for both activation and inhibition of PEN toolbox reactions. We testify for this purpose covalent attachment strategy, based on amino-epoxy chemistry and performed fluorescence and wettability characterizations of resulting surfaces. Our attempts to launch PEN autocatalysis with these interfaces were not successful, probably due to not sufficient surface density of immobilized DNA template. We proposed an approach, aimed to optimize attachment chemistry and overcome this issue.

Conclusions

The use of molecular framework to perform information-processing tasks is increasingly gaining traction in the community. However, controlling and interacting in real time with these molecular systems in microfluidics is a barrier to study ever more complex scenario and to produce technologies, which can be deployed outside the laboratory. In an attempt to solve this problem, we have investigated the interaction with PEN-DNA toolbox system electrochemically using DNA-grafted surfaces.

Firstly, we have studied the step-by-step assembly and optimization of the PEN toolbox parameters, which can be useful for the research groups aiming to use this technology in their laboratories for the first time.

Secondly, we have discussed the elaboration and characterization of active surfaces, which provide loading and controllable release of DNA input, based on formation and electrochemical cleavage of Au-S bond. We have also provided a technological solution to integrate these surfaces and the PEN toolbox in microfluidics. We have showed controllable triggering of basic activation and autocatalysis PEN toolbox modules.

We have further applied our method for spatiotemporal control of autocatalytic module while still providing exponential signal amplification contrary to the activation module. This approach allows us to investigate and optimize the parameters of our technology.

Finally, we have discussed the elaboration of active surfaces with irreversibly bound DNA, which provides a higher level of the PEN toolbox spatiotemporal behavior, based on electrical polarization and tuning the shape of surface-attached patterns.

Our technological solutions were chosen for its potential to be easily transferred to laboratories without microfabrication expertise to maximize their impact. Furthermore, they are not restricted to the PEN toolbox but can also be used with, for example, the strand displacement framework developed by Winfree *et al.* [62]. The versatility with which one can produce gold microelectrodes in microfluidic channels or reservoirs makes it possible to use this approach to manage complex spatiotemporal interaction with DNA-based molecular systems. For example, it is possible to rely on multiple sets of electrodes to release different input strands at different locations or times. This could be useful to control the behaviour of the molecular program and coupled with artificial morphogenesis [82] could enable the dynamical bottom-up assembly of novel materials (*e.g.* DNA-nanoparticle crystals). Our electrochemical actuators could also be

used to reprogram molecular systems running in microfluidics by releasing templates instead of input strands.

It would be interesting to try to use our triggering approach, having DNA, assembled to the gold nanoparticles. In this case, one can potentially provide instructions for PEN toolbox reactions, which are taking place *in vivo* for medical applications.

Another possible extension of our work could be immobilisation of the enzymes on surface or on nanoparticles and, consequently, either preventing or limiting their diffusion. By doing so, one can localise in designed locations amplification and/or degradation reactions.

One can improve reaction monitoring by designing field effect transistors, to the gate electrode of which the DNA, complimentary to the molecule of interest will be attached. The hybridisation event will cause changing of current in a very sensitive manner.

Our generic tool is therefore ideally suited to significantly expand the realm of possibilities in the field of DNA-based molecular programming.

Bibliography

1. Barabási, A.-L. & Oltvai, Z. N. Network biology: understanding the cell's functional organization. *Nat. Rev. Genet.* **5,** 101–113 (2004).
2. Wilhelm, T. The smallest chemical reaction system with bistability. *BMC Syst. Biol.* **3,** 90 (2009).
3. Epstein, I. R. & Showalter, K. Nonlinear Chemical Dynamics: Oscillations, Patterns, and Chaos. *J. Phys. Chem.* **100,** 13132–13147 (1996).
4. Arkin, A. & Ross, J. Computational functions in biochemical reaction networks. *Biophys. J.* **67,** 560–578 (1994).
5. Tyson Ãy, J. J., Chen Ãz, K. C. & Novak, B. Sniffers, buzzers, toggles and blinkers: dynamics of regulatory and signaling pathways in the cell. *Curr. Opin. Cell Biol.* **15,** 221–231 (2003).
6. Wolf, D. M. & Arkin, A. P. Motifs, modules and games in bacteria. *Curr. Opin. Microbiol.* **6,** 125–134 (2003).
7. Positioning of polarity formation by extracellular signaling during asymmetric cell division. *J. Theor. Biol.* **400,** 52–64 (2016).
8. Galochkina, T. *et al.* Reaction-diffusion waves of blood coagulation. (2016).
9. Volpert, V. & Petrovskii, S. Reaction–diffusion waves in biology. *Phys. Life Rev.* **6,** 267–310 (2009).
10. Tsang, B. Patterns in reaction diffusion system. (2011).
11. Grzybowski, B. A. & Wiley InterScience (Online service). *Chemistry in motion : reaction-diffusion systems for micro- and nanotechnology*. (Wiley, 2009).
12. Turing, A. M. The Chemical Basis of Morphogenesis. *Philos. Trans. R. Soc. Lond. B. Biol. Sci.* **237,** 37–72 (1952).
13. Wolpert, L. (Lewis). *Principles of development*.
14. Kondo, S. & Miura, T. Reaction-Diffusion Model as a Framework for Understanding Biological Pattern Formation. *Science (80-.).* **329,** 1616–1620 (2010).
15. Padirac, A., Fujii, T. & Rondelez, Y. Nucleic acids for the rational design of reaction circuits. *Curr Opin Biotechnol Curr. Opin. Biotechnol.* **24,** (2012).
16. Milo, R. Network Motifs: Simple Building Blocks of Complex Networks. *Science (80-.).* **298,** 824–827 (2002).
17. Wilhelm, T. The smallest chemical reaction system with bistability. doi:10.1186/1752-

0509-3-90

18. Wong, A. S. Y. & Huck, W. T. S. Grip on complexity in chemical reaction networks. *Beilstein J. Org. Chem.* **13,** 1486–1497 (2017).
19. Bray, W. C. A PERIODIC REACTION IN HOMOGENEOUS SOLUTION AND ITS RELATION TO CATALYSIS. *J. Am. Chem. Soc.* **43,** 1262–1267 (1921).
20. VIVOS VOCO: Б.П. Белоусов, "Периодически действующая реакция" Available at: http://vivovoco.astronet.ru/VV/MISC/4/AUTO.HTM. (Accessed: 3rd October 2017)
21. ZAIKIN, A. N. & ZHABOTINSKY, A. M. Concentration Wave Propagation in Two-dimensional Liquid-phase Self-oscillating System. *Nature* **225,** 535–537 (1970).
22. Autowave processes in a distributed chemical system. *J. Theor. Biol.* **40,** 45–61 (1973).
23. Gyorgyi, L., Turanyi, T. & Field, R. J. Mechanistic details of the oscillatory Belousov-Zhabotinskii reaction. *J. Phys. Chem.* **94,** 7162–7170 (1990).
24. Thattai, M. & van Oudenaarden, A. Intrinsic noise in gene regulatory networks. *Proc. Natl. Acad. Sci. U. S. A.* **98,** 8614–9 (2001).
25. Van Roekel, H. W. H. *et al.* Programmable chemical reaction networks: emulating regulatory functions in living cells using a bottom-up approach. *Chem. Soc. Rev. Chem. Soc. Rev* **44,** 7465–7483 (2015).
26. TIME, STRUCTURE AND FLUCTUATIONS. (1977).
27. Schneider, E. D. & Sagan, D. *Into the cool : energy flow, thermodynamics, and life*. (University of Chicago Press, 2005).
28. Sorrenti, A., Leira-Iglesias, J., Sato, A. & Hermans, T. M. ARTICLE Non-equilibrium steady states in supramolecular polymerization. *Nat. Commun.* **8,** (2017).
29. Ashkenasy, G., Hermans, T. M., Otto, S. & Taylor, A. F. Systems chemistry. *Chem. Soc. Rev.* **46,** 2543–2554 (2017).
30. Maiti, S., Fortunati, I., Ferrante, C., Scrimin, P. & Prins, L. J. Dissipative self-assembly of vesicular nanoreactors. *Nat. Chem.* **8,** 725–731 (2016).
31. Boekhoven, J., Hendriksen, W. E., Koper, G. J. M., Eelkema, R. & van Esch, J. H. Transient assembly of active materials fueled by a chemical reaction. *Science* **349,** 1075–9 (2015).
32. Wilson, M. R. *et al.* An autonomous chemically fuelled small-molecule motor. *Nature* **534,** 235–240 (2016).
33. Collins, B. S. L., Kistemaker, J. C. M., Otten, E. & Feringa, B. L. A chemically powered unidirectional rotary molecular motor based on a palladium redox cycle. *Nat.*

Chem. **8,** 860–866 (2016).

34. Watson, J. & Crick, F. C. MOLECULAR STRUCTURE OF NUCLEIC ACIDS: A Structure for Deoxyribose Nucleic Acid. (1953).
35. Seeman, N. C. & Sleiman, H. F. DNA nanotechnology. *Nat. Rev. Mater.* **3,** 17068 (2017).
36. Erlich, Y. & Zielinski, D. DNA Fountain enables a robust and efficient storage architecture. *Science* **355,** 950–954 (2017).
37. Adleman, L. M. Molecular computation of solutions to combinatorial problems. *Science* **266,** 1021–4 (1994).
38. Lin, C., Liu, Y., Rinker, S. & Yan, H. DNA Tile Based Self-Assembly: Building Complex Nanoarchitectures. *ChemPhysChem* **7,** 1641–1647 (2006).
39. Seeman, N. C. Nanomaterials based on DNA. *Annu. Rev. Biochem.* **79,** 65–87 (2010).
40. Strong, M. Protein nanomachines. *PLoS Biology* (2004). doi:10.1371/journal.pbio.0020073
41. Wang, H. Proving Theorems by Pattern Recognition - II. *Bell Syst. Tech. J.* **40,** 1–41 (1961).
42. Cohen, M. F., Shade, J., Hiller, S. & Deussen, O. Wang Tiles for Image and Texture Generation.
43. Winfree, E. Algorithmic Self-Assembly of DNA. (1998).
44. Seeman, N. C., Mao, C., LaBean, T. H. & Reif, J. H. Logical computation using algorithmic self-assembly of DNA triple-crossovermolecules. *Nature* **407,** 493–496 (2000).
45. Arithmetic computation using self-assembly of DNA tiles: subtraction and division. *Prog. Nat. Sci.* **19,** 377–388 (2009).
46. Li, Y., Xiao, L. & Ruan, L. Parallel molecular computation of modular-multiplication with two same inputs over finite field GF(2n) using self-assembly of DNA tiles. *Comput. Biol. Chem.* **50,** 82–87 (2014).
47. Yan, H., LaBean, T. H., Feng, L. & Reif, J. H. Directed nucleation assembly of DNA tile complexes for barcode-patterned lattices. *Proc. Natl. Acad. Sci. U. S. A.* **100,** 8103–8 (2003).
48. Rothemund, P. W. K. Folding DNA to create nanoscale shapes and patterns. *Nature* **440,** 297–302 (2006).
49. Douglas, S. M. *et al.* Self-assembly of DNA into nanoscale three-dimensional shapes. doi:10.1038/nature08016

50. Zadegan, R. M. *et al.* Construction of a 4 Zeptoliters Switchable 3D DNA Box Origami. *ACS Nano* **6,** 10050–10053 (2012).
51. Kuzyk, A. *et al.* DNA-based self-assembly of chiral plasmonic nanostructures with tailored optical response. *Nature* **483,** 311–314 (2012).
52. Liu, W., Halverson, J., Tian, Y., Tkachenko, A. V. & Gang, O. Self-organized architectures from assorted DNA-framed nanoparticles. *Nat. Chem.* **8,** 867–873 (2016).
53. Ke, Y., Meyer, T., Shih, W. M. & Bellot, G. Regulation at a distance of biomolecular interactions using a DNA origami nanoactuator. *Nat. Commun.* **7,** 10935 (2016).
54. Derr, N. D. *et al.* Tug-of-War in Motor Protein Ensembles Revealed with a Programmable DNA Origami Scaffold. *Science (80-.).* **338,** 662–665 (2012).
55. Hernández-Ainsa, S. *et al.* DNA Origami Nanopores for Controlling DNA Translocation. *ACS Nano* **7,** 6024–6030 (2013).
56. Koirala, D. *et al.* Single-Molecule Mechanochemical Sensing Using DNA Origami Nanostructures. *Angew. Chemie* **126,** 8275–8279 (2014).
57. Perrault, S. D. & Shih, W. M. Virus-Inspired Membrane Encapsulation of DNA Nanostructures To Achieve *In Vivo* Stability. *ACS Nano* **8,** 5132–5140 (2014).
58. Douglas, S. M., Bachelet, I. & Church, G. M. A Logic-Gated Nanorobot for Targeted Transport of Molecular Payloads. *Science (80-.).* **335,** 831–834 (2012).
59. Amir, Y. *et al.* Universal computing by DNA origami robots in a living animal. *Nat. Nanotechnol.* **9,** 353–357 (2014).
60. Zenk, J. *et al.* Stable DNA-based reaction–diffusion patterns. *RSC Adv.* **7,** 18032–18040 (2017).
61. Zhang, D. Y. & Seelig, G. Dynamic DNA nanotechnology using strand-displacement reactions. *Nat. Chem.* **3,** 103–113 (2011).
62. Zhang, D. Y. & Winfree, E. Zhang, D. Y., & Winfree, E. (2009). Control of DNA Strand Displacement Kinetics Using Toehold Exchange. Journal of the American Chemical Society, 131(47), 17303–17314. https://doi.org/10.1021/ja906987sControl of DNA Strand Displacement Kinetics Using Toeh. *J. Am. Chem. Soc.* **131,** 17303–17314 (2009).
63. Yurke, B., Turberfield, A. J., Mills, A. P., Simmel, F. C. & Neumann, J. L. A DNA-fuelled molecular machine made of DNA. *Nature* **406,** 605–608 (2000).
64. Seelig, G., Soloveichik, D., Zhang, D. Y. & Winfree, E. Enzyme-free nucleic acid logic circuits. *Science* **314,** 1585–8 (2006).
65. Qian, L. & Winfree, E. A Simple DNA Gate Motif for Synthesizing Large-Scale

Circuits.

66. Qian, L. & Winfree, E. Scaling up digital circuit computation with DNA strand displacement cascades. *Science* **332,** 1196–201 (2011).
67. Qian, L., Winfree, E. & Bruck, J. Neural network computation with DNA strand displacement cascades. *Nature* **475,** 368–372 (2011).
68. Penchovsky, R. & Breaker, R. R. Computational design and experimental validation of oligonucleotide-sensing allosteric ribozymes. *Nat. Biotechnol.* **23,** 1424–1433 (2005).
69. Yoshida, W. & Yokobayashi, Y. Photonic boolean logic gates based on DNA aptamers. *Chem. Commun.* **0,** 195–197 (2007).
70. Benenson, Y. *et al.* Programmable and autonomous computing machine made of biomolecules. *Nature* **414,** 430–434 (2001).
71. Ran, T., Kaplan, S. & Shapiro, E. Molecular implementation of simple logic programs. *Nat. Nanotechnol.* **4,** 642–648 (2009).
72. Kim, J., White, K. S. & Winfree, E. Construction of an in vitro bistable circuit from synthetic transcriptional switches. *Mol. Syst. Biol.* **2,** 68 (2006).
73. Franco, E., Kim, J. & Bishop, J. Synthetic in vitro transcriptional oscillators Background: Nucleic acids and proteins. (2011).
74. Soloveichik, D., Seelig, G. & Winfree, E. DNA as a universal substrate for chemical kinetics. doi:10.1073/pnas.0909380107
75. Montagne, K., Plasson, R., Sakai, Y., Fujii, T. & Rondelez, Y. Programming an in vitro DNA oscillator using a molecular networking strategy. *Mol. Syst. Biol.* **7,** (2011).
76. Padirac, A., Fujii, T. & Rondelez, Y. Bottom-up construction of in vitro switchable memories. doi:10.1073/pnas.1212069109
77. Fujii, T. & Rondelez, Y. PredatorÀPrey Molecular Ecosystems. doi:10.1021/nn3043572
78. Srinivas, N., Parkin, J., Seelig, G., Winfree, E. & Soloveichik, D. Enzyme-Free Nucleic Acid Dynamical Systems. *doi.org* 138420 (2017). doi:10.1101/138420
79. Zadorin, A. S., Rondelez, Y., Galas, J.-C. & Estevez-Torres, A. Programmable reaction-diffusion fronts.
80. Padirac, A., Fujii, T., Estévez-Torres, A. & Rondelez, Y. Spatial Waves in Synthetic Biochemical Networks. *J. Am. Chem. Soc.* **135,** 14586–14592 (2013).
81. Zambrano, A., Zadorin, A. S., Rondelez, Y., Estévez-Torres, A. & Galas, J.-C. Pursuit-and-Evasion Reaction-Diffusion Waves in Microreactors with Tailored Geometry. *J. Phys. Chem. B* **119,** 5349–5355 (2015).

82. Zadorin, A. S. *et al.* Synthesis and materialization of a reaction–diffusion French flag pattern. *Nat. Chem.* **9,** 990–996 (2017).
83. The Electrified Interface. in *Modern Electrochemistry 2A* 771–1033 (Kluwer Academic Publishers). doi:10.1007/0-306-47605-3_1
84. Mcewen, G. D., Chen, F. & Zhou, A. Immobilization, hybridization, and oxidation of synthetic DNA on gold surface: electron transfer investigated by electrochemistry and scanning tunneling microscopy. *Anal Chim Acta. June* **8,** 26–37 (2009).
85. Adam B. Steel, *,†, Tonya M. Herne, and & Tarlov*, M. J. Electrochemical Quantitation of DNA Immobilized on Gold. (1998). doi:10.1021/AC980037Q
86. Ladik, A. V, Geiger, F. M. & Walter, S. R. Immobilization of DNA onto Gold and Dehybridization of Surface-Bound DNA on Glass Undergraduate Researcher Graduate Student Mentor. **7,** (2010).
87. Silva, M. M. S., Cavalcanti, I. T., Barroso, M. F., Sales, M. G. F. & Dutra, R. F. Gold electrode modified by self-assembled monolayers of thiols to determine DNA sequences hybridization. *J. Chem. Sci.* **122,** 911–917 (2010).
88. Anne Andrews Research Group. Available at: http://www.serotonin.ucla.edu/pages/electroanalytical. (Accessed: 30th October 2017)
89. Marras, S. A. E., Kramer, F. R. & Tyagi, S. Efficiencies of fluorescence resonance energy transfer and contact-mediated quenching in oligonucleotide probes. *Nucleic Acids Res.* **30,** 122e–122 (2002).
90. Dulkeith, E. *et al.* Fluorescence Quenching of Dye Molecules near Gold Nanoparticles: Radiative and Nonradiative Effects. doi:10.1103/PhysRevLett.89.203002
91. Acuna, G. P. *et al.* Distance Dependence of Single- Fluorophore Quenching by Gold Nanoparticles Studied on DNA Origami. **6,** 3189–3195 (2012).
92. Nazarenko, I., Pires, R., Lowe, B., Obaidy, M. & Rashtchian, A. Effect of primary and secondary structure of oligodeoxyribonucleotides on the fluorescent properties of conjugated dyes. *Nucleic Acids Res.* **30,** 2089–2195 (2002).
93. Padirac, A. Tailoring spatiotemporal dynamics with DNA circuits. (2012).
94. Baccouche, A., Montagne, K., Padirac, A., Fujii, T. & Rondelez, Y. Dynamic DNA-toolbox reaction circuits: A walkthrough. *METHODS* (2014). doi:10.1016/j.ymeth.2014.01.015
95. Wakamatsu, T. *et al.* Structure of RecJ Exonuclease Defines Its Specificity for Single-stranded DNA * □ S. (2010). doi:10.1074/jbc.M109.096487
96. Padirac, A. Tailoring spatiotemporal dynamics with DNA circuits. (2012).

97. Padirac, A., Fujii, T. & Rondelez, Y. Quencher-free multiplexed monitoring of DNA reaction circuits. doi:10.1093/nar/gks621
98. Ramirez, A. Z. Synthesis of reaction-diffusion patterns with DNA : towards Turing patterns. *http://www.theses.fr* (2016).
99. Cardelli, L., Kwiatkowska, M. & Whitby, M. Chemical Reaction Network Designs for Asynchronous Logic Circuits *.
100. Gines, G. *et al.* Microscopic agents programmed by DNA circuits. *Nat. Nanotechnol.* **12,** 351–359 (2017).
101. Soloveichik, D., Cook, M., Winfree, E. & Bruck, J. COMPUTATION WITH FINITE STOCHASTIC CHEMICAL REACTION NETWORKS.
102. Zadorin, A. S., Rondelez, Y., Galas, J.-C. & Estevez-Torres, A. Synthesis of Programmable Reaction-Diffusion Fronts Using DNA Catalyzers. doi:10.1103/PhysRevLett.114.068301
103. Kurylo, I. *et al.* Characterization of peptide attachment on silicon nanowires by X-ray photoelectron spectroscopy and mass spectrometry. *Analyst* **142,** (2017).
104. Liu, M. *et al.* Remote-Controlled DNA Release from Fe3O4@Au Nanoparticles Using an Alternating Electromagnetic Field. *J. Biomed. Nanotechnol.* **11,** 979–87 (2015).
105. Li, F., Zhang, H., Dever, B., Li, X.-F. & Le, X. C. Thermal Stability of DNA Functionalized Gold Nanoparticles. *Bioconjug. Chem.* **24,** 1790–1797 (2013).
106. Arinaga, K. *et al.* Controlling the surface density of DNA on gold by electrically induced desorption. *Biosens. Bioelectron.* **23,** 326–331 (2007).
107. Xue, Y., Li, X., Li, H. & Zhang, W. Quantifying thiol–gold interactions towards the efficient strength control. *Nat. Commun.* **5,** ncomms5348 (2014).
108. Häkkinen, H. The gold–sulfur interface at the nanoscale. *Nat. Chem.* **4,** 443–455 (2012).
109. Juan Jose Calvente, Zuzana Kováčová, M. Dolores Sanchez, Rafael Andreu, † and & Fawcett*, W. R. Desorption of Spontaneously Adsorbed and Electrochemically Readsorbed 2-Mercaptoethanesulfonate on Au(111). (1996). doi:10.1021/LA9601770
110. Ghaly, T., Wildt, B. E. & Searson, P. C. Electrochemical Release of Fluorescently Labeled Thiols from Patterned Gold Surfaces. *Langmuir* **26,** 1420–1423 (2010).
111. Yamagata, A., Masui, R., Kakuta, Y., Kuramitsu, S. & Fukuyama, K. Overexpression, purification and characterization of RecJ protein from Thermus thermophilus HB8 and its core domain. *Nucleic Acids Res.* **29,** 4617–4624 (2001).
112. Li, Z., Jin, R., Mirkin, C. A. & Letsinger, R. L. Multiple thiol-anchor capped DNA–

gold nanoparticle conjugates. *Nucleic Acids Res.* **30,** 1558–1562 (2002).

113. Borzenkov, M. *et al.* Thermal and Chemical Stability of Thiol Bonding on Gold Nanostars. *Langmuir* **31,** 8081–8091 (2015).
114. Hegner, M., Wagner, P. & Semenza, G. Immobilizing DNA on gold via thiol modification for atomic force microscopy imaging in buffer solutions. *FEBS Lett.* **336,** 452–456 (1993).
115. Steel, A. B., Levicky, R. L., Herne, T. M. & Tarlov, M. J. Immobilization of Nucleic Acids at Solid Surfaces: Effect of Oligonucleotide Length on Layer Assembly.
116. Moores, B., Simons, J., Xu, S. & Leonenko, Z. AFM-assisted fabrication of thiol SAM pattern with alternating quantified surface potential. (2011). doi:10.1186/1556-276X-6-185
117. Laibinis, P. E. & Whitesides, G. M. Self-Assembled Monolayers of n-Alkanethiolates on Copper Are Barrier Films That Protect the Metal against Oxidation by Airr.
118. Yee, C. K. *et al.* Novel One-Phase Synthesis of Thiol-Functionalized Gold, Palladium, and Iridium Nanoparticles Using Superhydride. doi:10.1021/la990015e
119. Arinaga, K. *et al.* Controlling the surface density of DNA on gold by electrically induced desorption. *Biosens. Bioelectron.* **23,** 326–331 (2007).
120. Damodaran, S. & Razumovsky, L. Role of surface area-to-volume ratio in protein adsorption at the air–water interface. *Surf. Sci.* **602,** 307–315 (2008).
121. Fischer, T. & Hess, H. Materials chemistry challenges in the design of hybrid bionanodevices: supporting protein function within artificial environments. *J. Mater. Chem.* **17,** 943 (2007).
122. Adsorption of proteins on glass surfaces and pertinent parameters for the immobilization of enzymes in the pores of inorganic carriers. *J. Non. Cryst. Solids* **19,** 277–283 (1975).
123. Hua, B. *et al.* An improved surface passivation method for single-molecule studies. *Nat. Methods* **11,** 1233–6 (2014).
124. Park, J. H. *et al.* Controlling adsorption and passivation properties of bovine serum albumin on silica surfaces by ionic strength modulation and cross-linking. *Phys. Chem. Chem. Phys.* **19,** 8854–8865 (2017).
125. Ogura, K., Haruyama, S. & Nagasaki, K. The Electrochemical Oxidation and Reduction of Gold. *J. Electrochem. Soc.* **118,** 531 (1971).
126. Qiao, W., Chiang, H.-C., Xie, H. & Levicky, R. Surface vs Solution Hybridization: Effects of Salt, Temperature, and Probe Type. doi:10.1039/c5cc06674c

127. Impact of spacers on the hybridization efficiency of mixed self-assembled DNA/alkanethiol films. *Biosens. Bioelectron.* **24,** 72–77 (2008).
128. Demers, L. M. *et al.* A fluorescence-based method for determining the surface coverage and hybridization efficiency of thiol-capped oligonucleotides bound to gold thin films and nanoparticles. *Anal. Chem.* **72,** 5535–41 (2000).
129. Edwardson, T. G. W., Lau, K. L., Bousmail, D., Serpell, C. J. & Sleiman, H. F. Transfer of molecular recognition information from DNA nanostructures to gold nanoparticles. *Nat. Chem.* **8,** 162–70 (2016).
130. Gaur, R., Mishra, L. & Sen Gupta, S. K. Diffusion and Transport of Molecules In Living Cells. in 27–49 (2014). doi:10.1007/978-3-319-05657-9_2
131. Zipper, H., Brunner, H., Bernhagen, J. € U. U. & Vitzthum, F. Investigations on DNA intercalation and surface binding by SYBR Green I, its structure determination and methodological implications. doi:10.1093/nar/gnh101
132. Tymoczko, J., Schuhmann, W. & Gebala, M. Electrical Potential-Assisted DNA Hybridization. How to Mitigate Electrostatics for Surface DNA Hybridization. *ACS Appl. Mater. Interfaces* **6,** 21851–21858 (2014).